Scanning Tunneling Microscopy

掃描穿隧顯微術

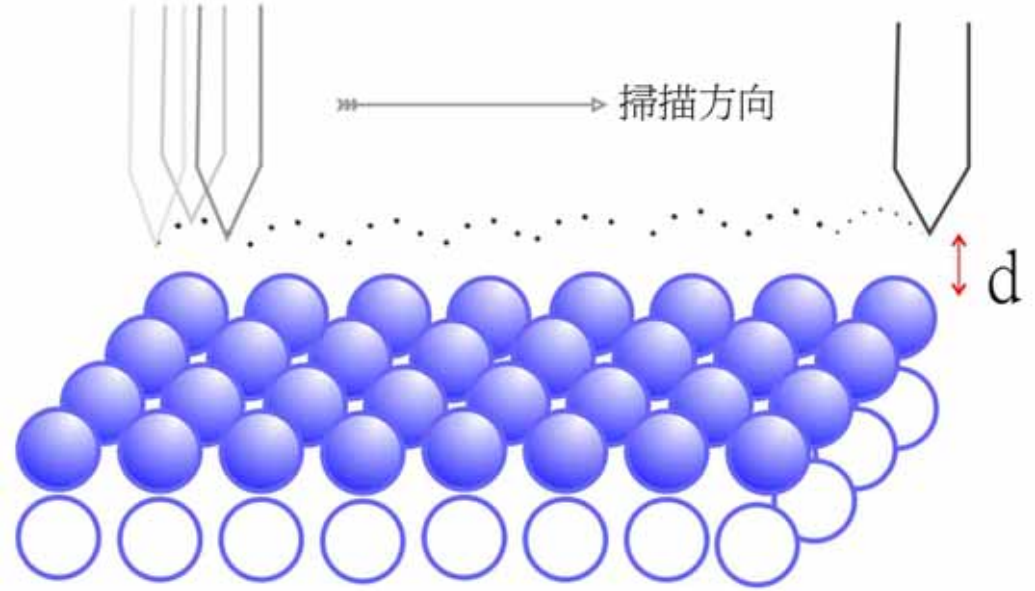

References

1. G. Binnig, H. Rohrer, C. Gerber, and Weibel, Phys. Rev. Lett. **49**, 57(1982); and ibid **50**, 120(1983).

2. J. Chen, *Introduction to Scanning Tunneling Microscopy*, New York, Oxford Univ. Press (1993).

3. 黃英碩，科儀新知95，18 (3), 4 (1996)。

4. 黃英碩，科儀新知144，26 (4), 7 (2005)。

Tunneling

Classical

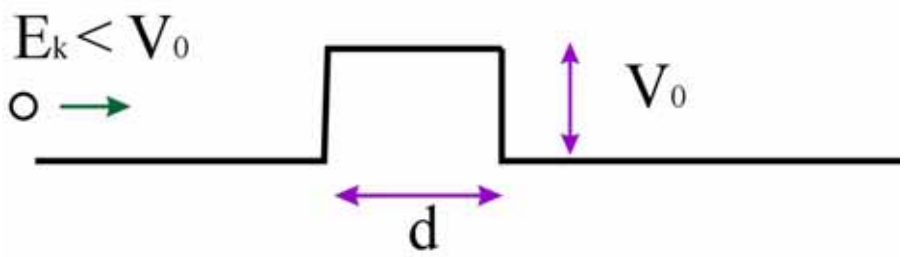

Quantum Mechanics

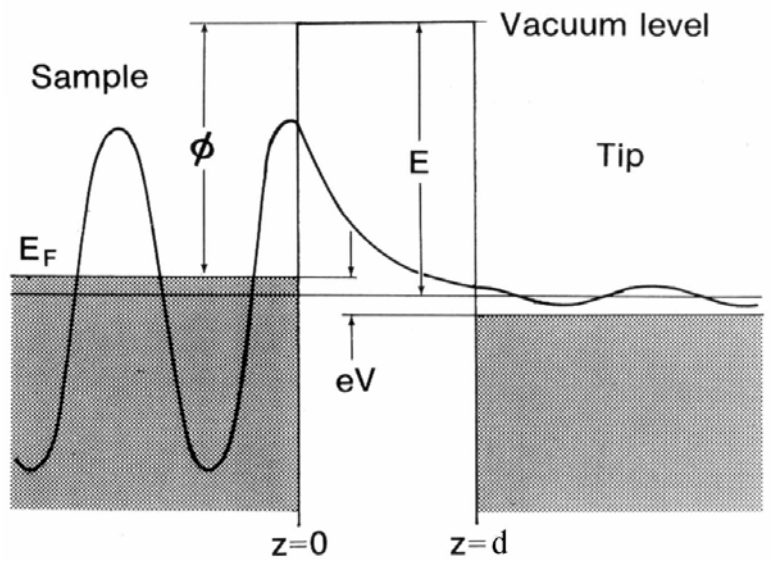

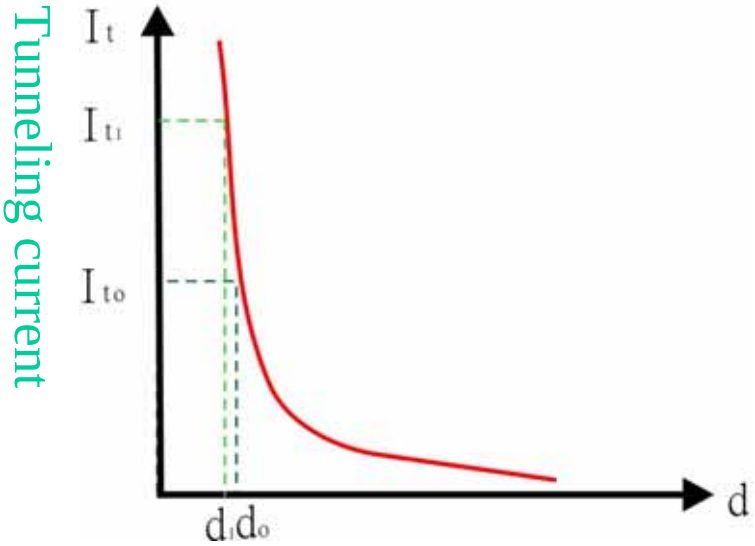

Tunneling current I_t

$I_t \propto (V/d)\exp(-A\phi^{1/2}d)$

$A = 1.025\ (eV)^{-1/2}Å^{-1}$

I_t = 10 pA~10nA

V = 1mV ~ 3V

d decreases by 1Å, I_t increases by about one order of magnitude.

Schematics of STM

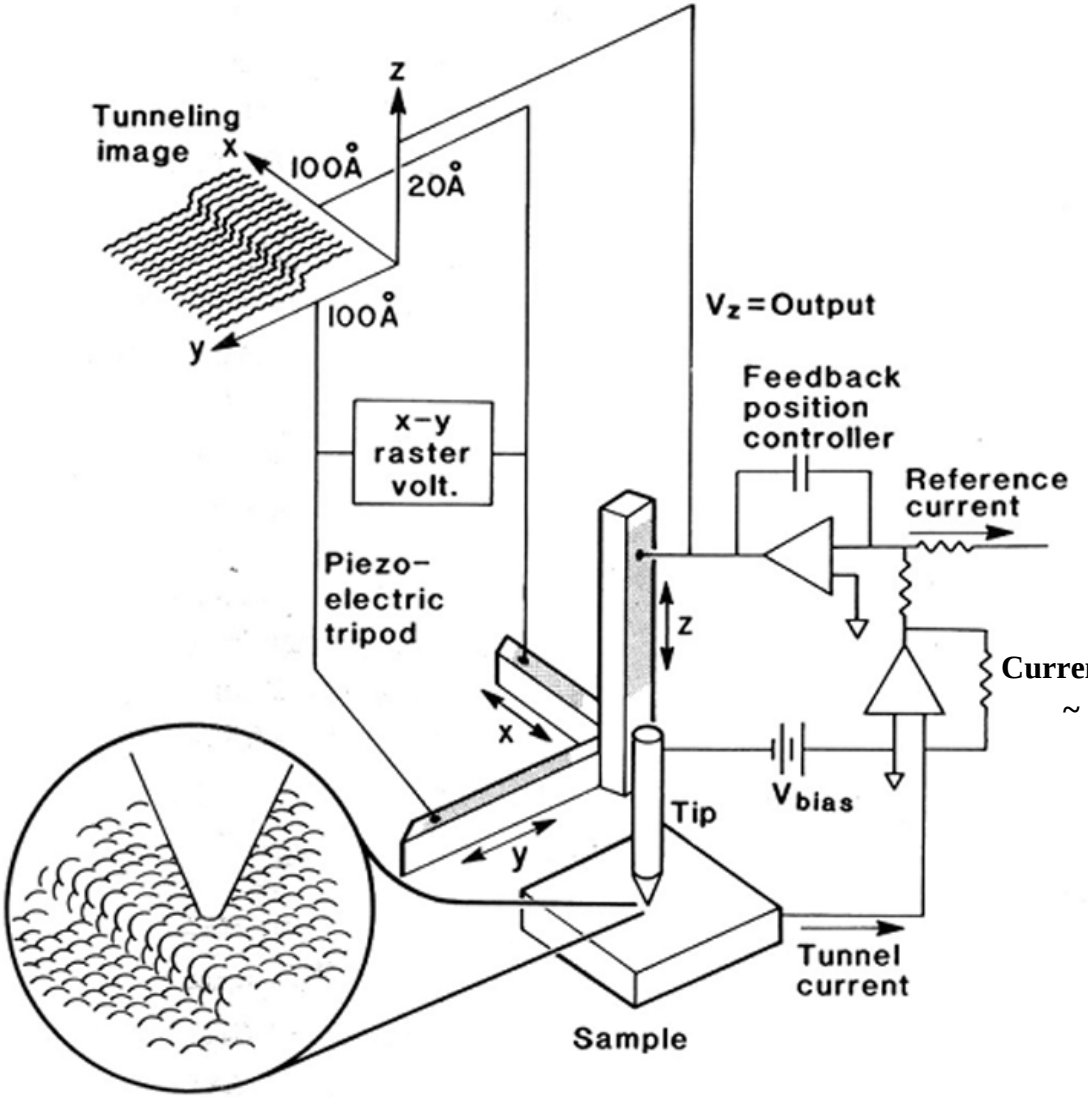

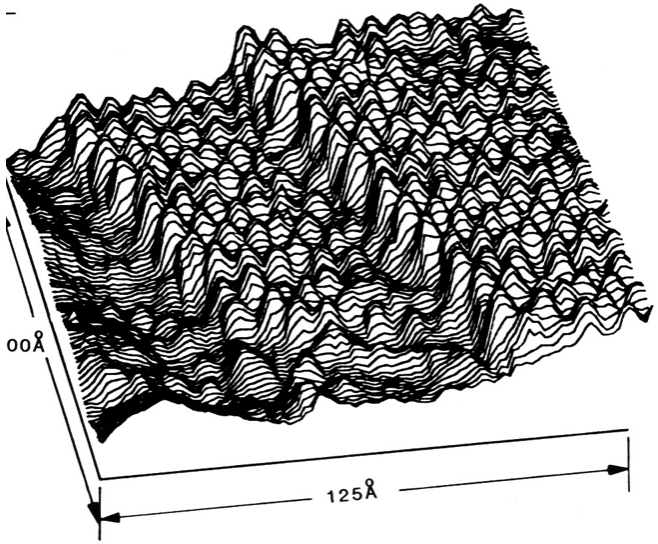

Current pre-amp
~ 1 V/nA

STM Images of Si(111)-(7×7)

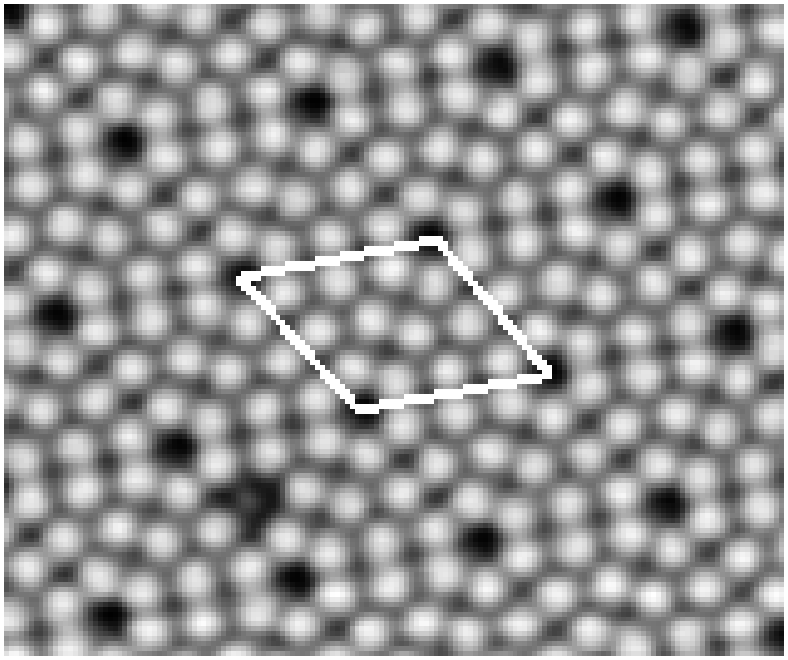

Empty-state image

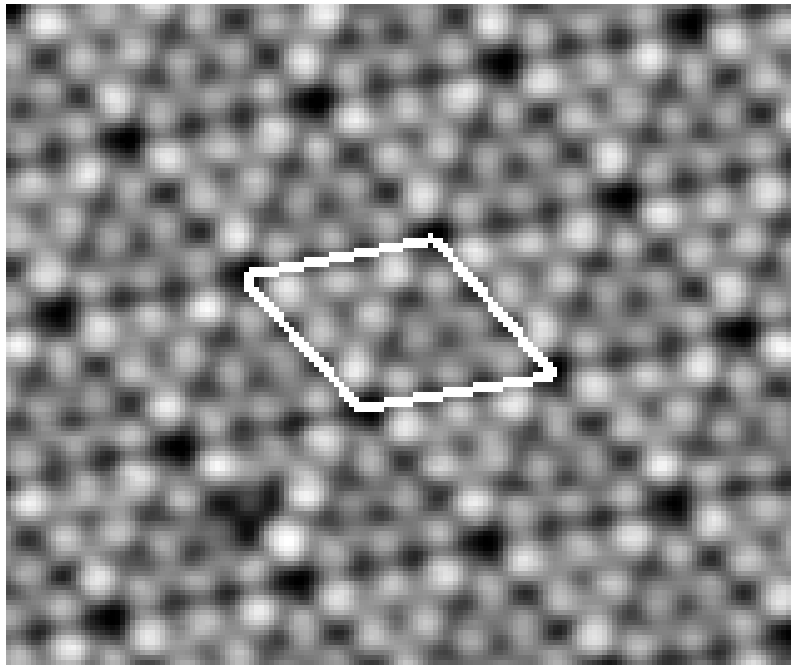

Filled-state image

Atomic Model of Si(111)-(7×7)

Top view

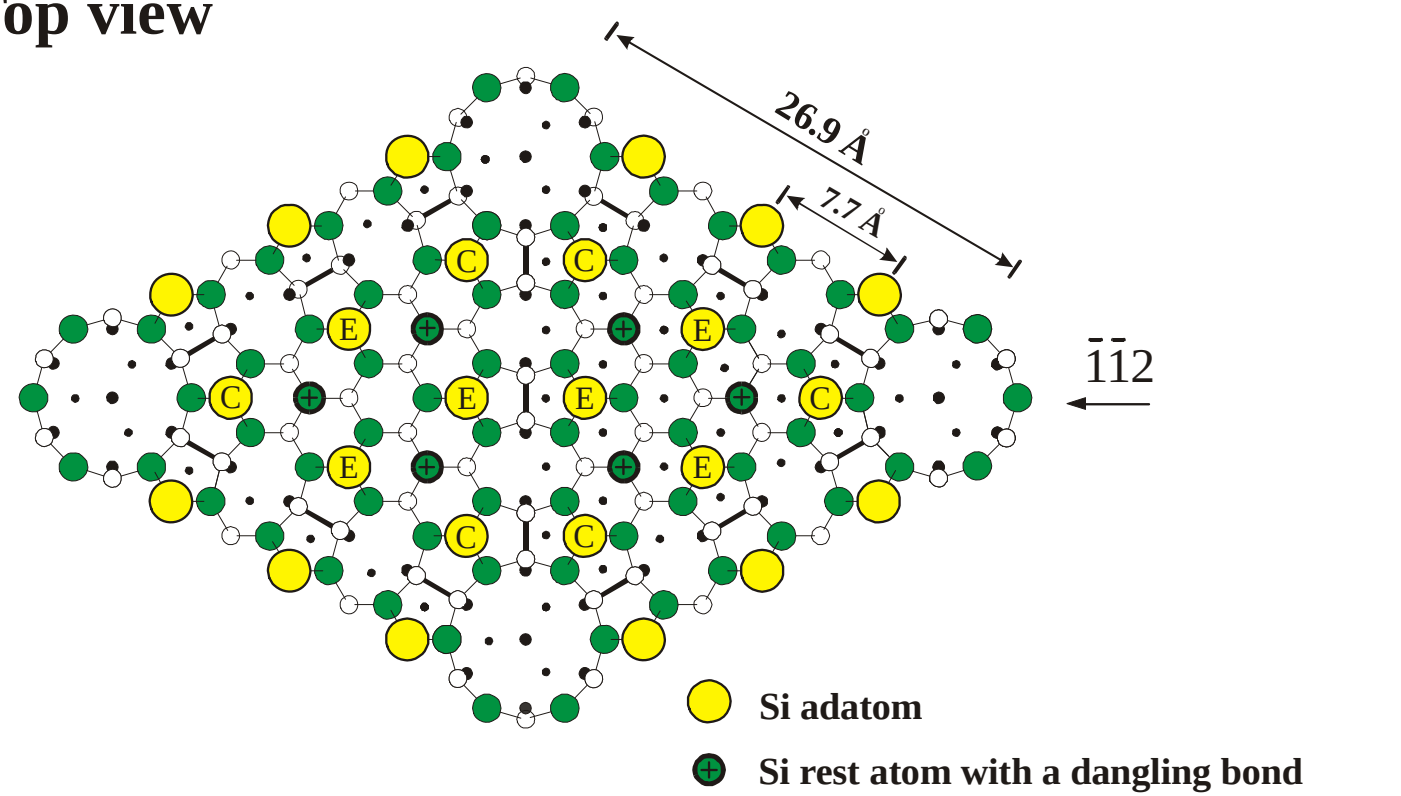

Side view

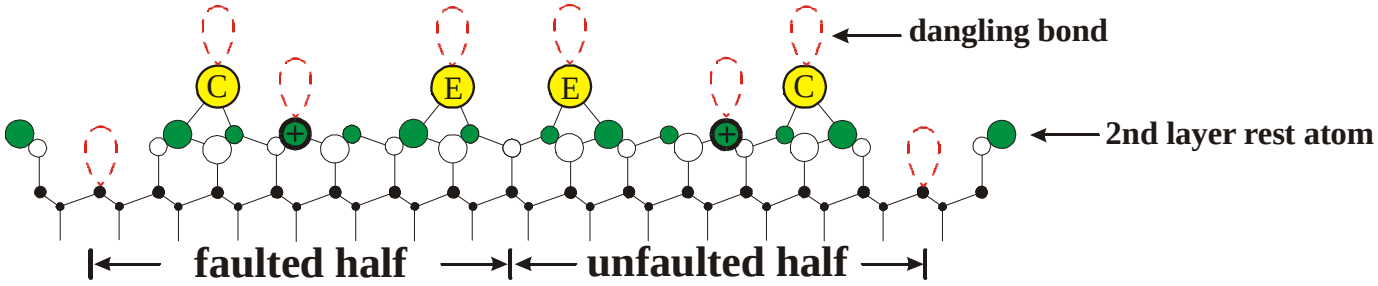

Atomic Structure of the Si(001) Surface

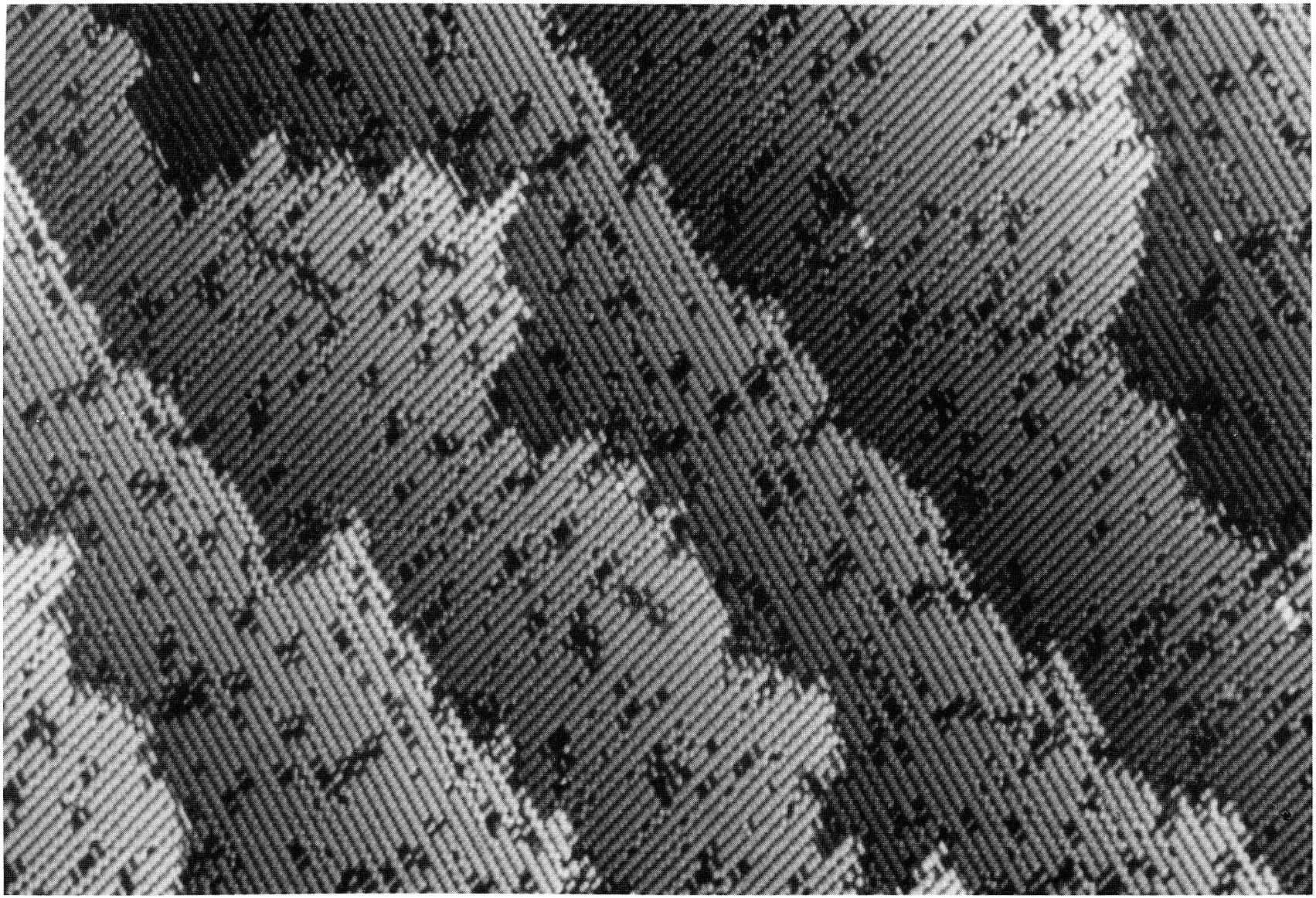

Atomic Structure of the Pt(001) Surface

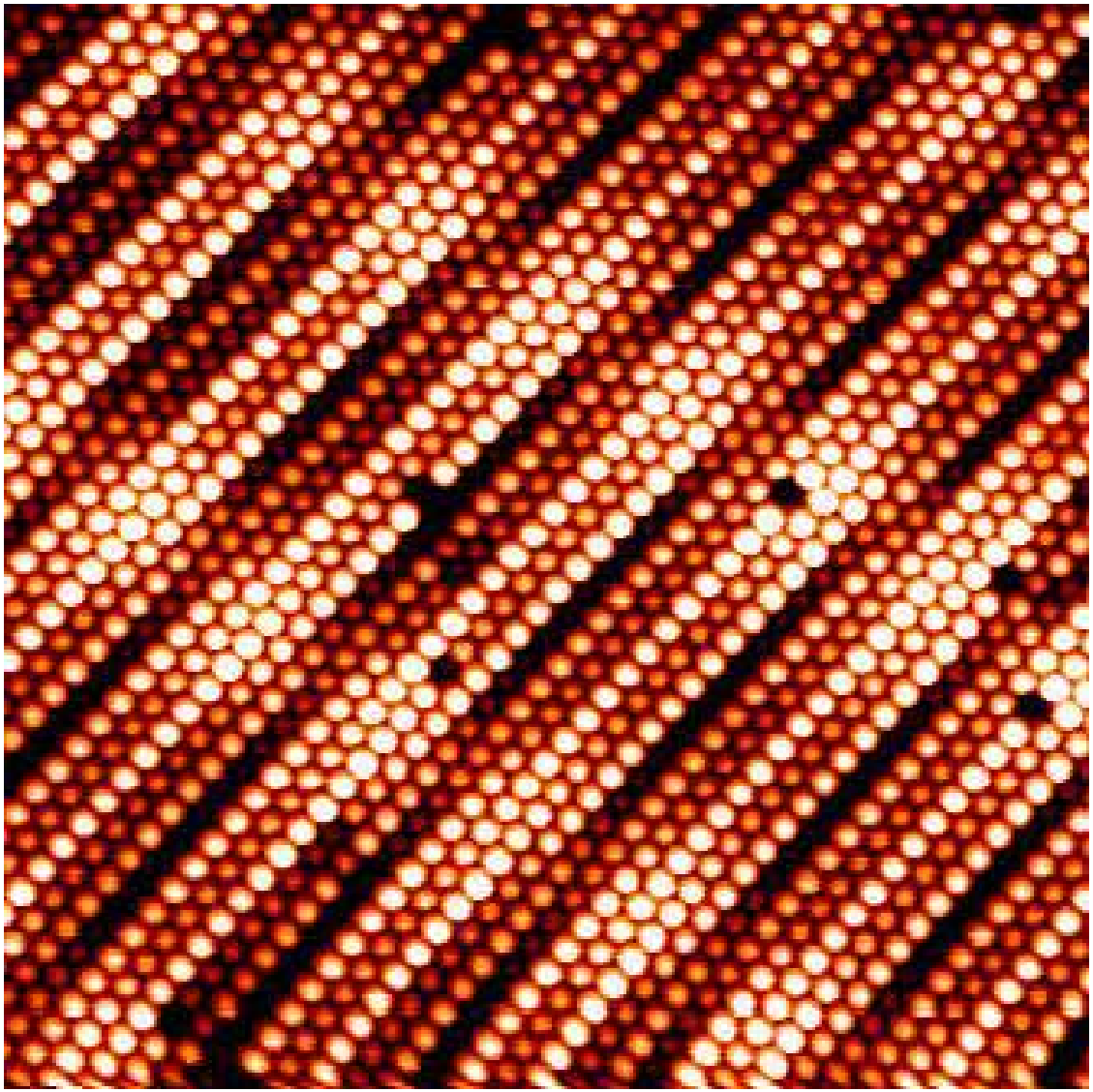

Surface Science **306**, 10 (1994).

Si Magic Clusters

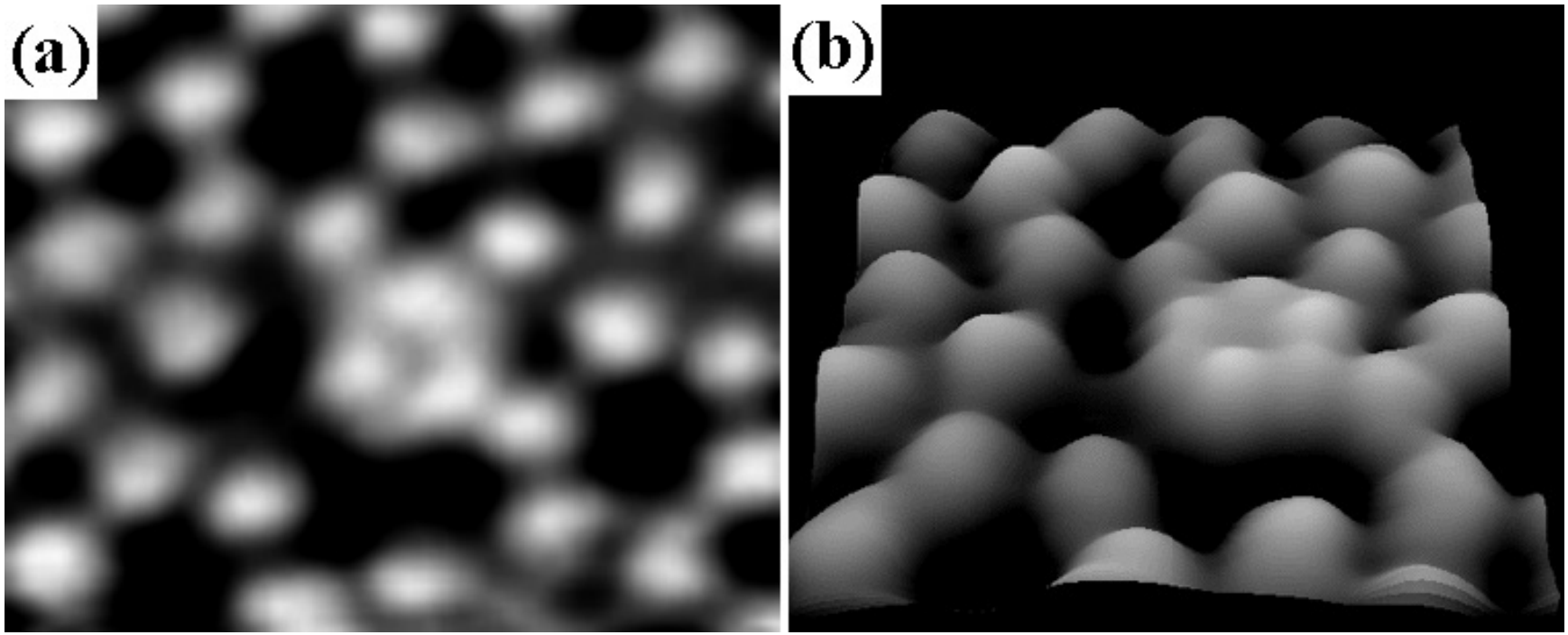

Physical Review Letters **83**, 120 (1999).

Nucleation and Growth of Ge at Pb/Si(111)

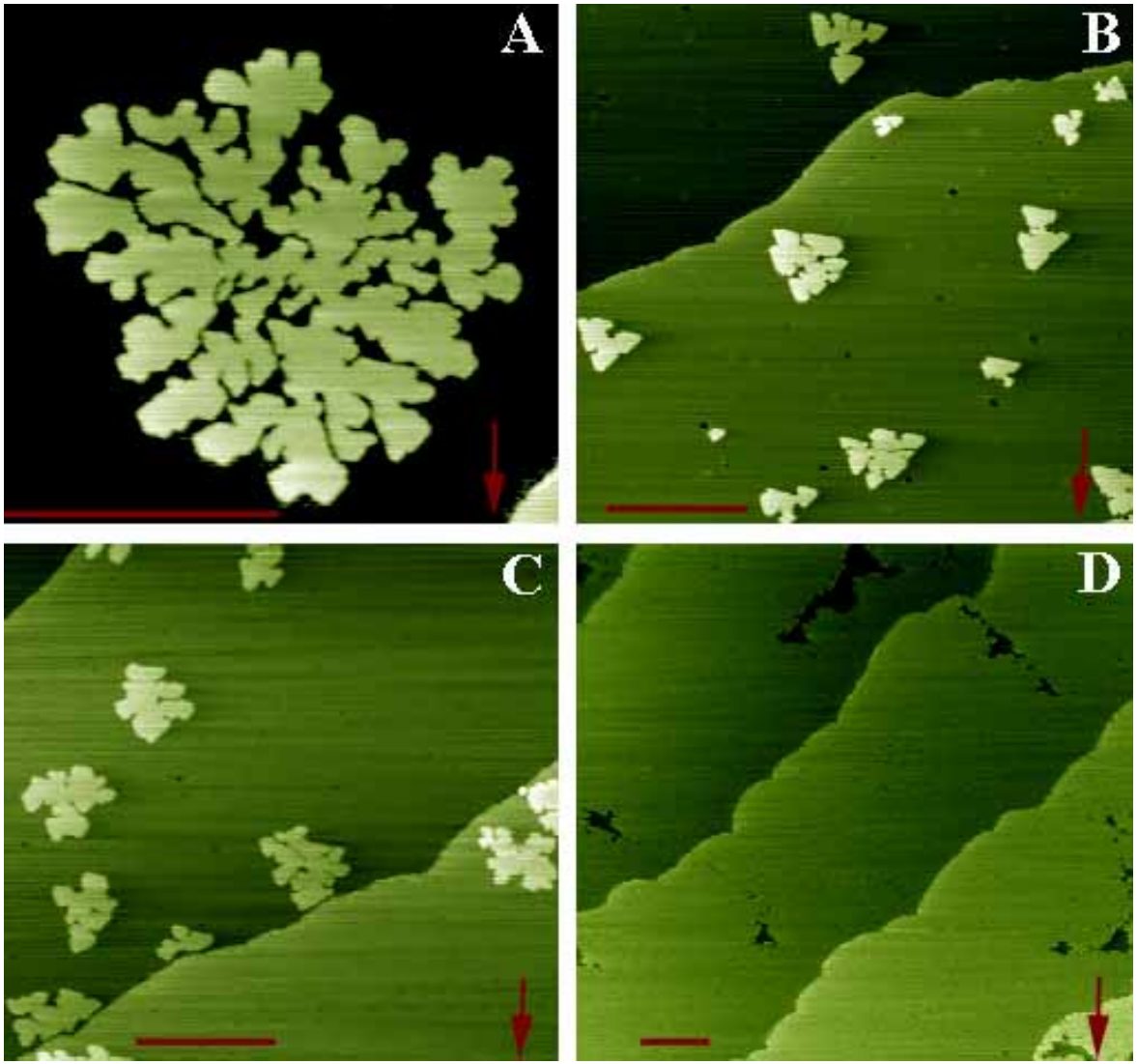

Physical Review Letters **83**, 1191 (1999).

Japanese Journal of Applied Physics **39**, Part 1, No. 7A, 4100 (2000).

Ultra-High Vacuum Scanning Tunneling Microscope

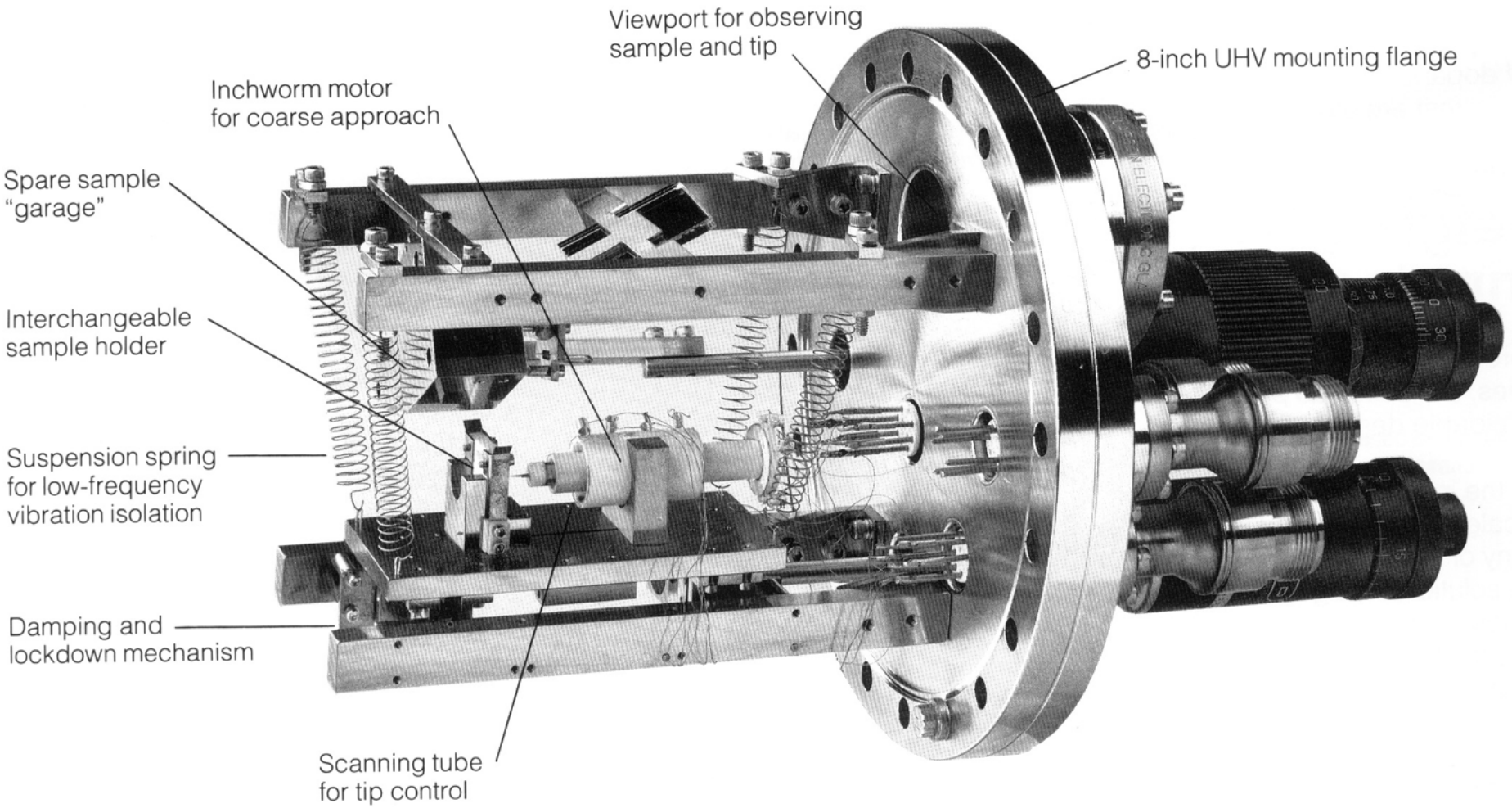

Inchworm-Type Linear Motor

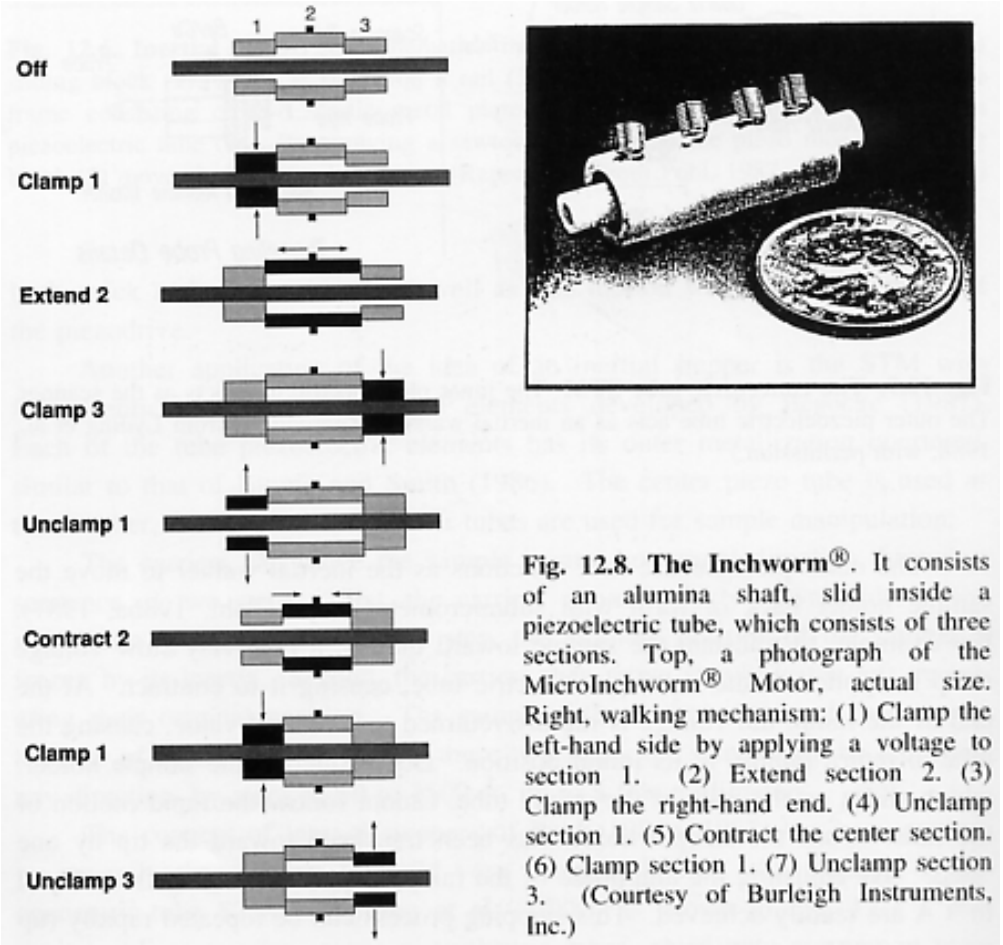

Fig. 12.8. The Inchworm®. It consists of an alumina shaft, slid inside a piezoelectric tube, which consists of three sections. Top, a photograph of the MicroInchworm® Motor, actual size. Right, walking mechanism: (1) Clamp the left-hand side by applying a voltage to section 1. (2) Extend section 2. (3) Clamp the right-hand end. (4) Unclamp section 1. (5) Contract the center section. (6) Clamp section 1. (7) Unclamp section 3. (Courtesy of Burleigh Instruments, Inc.)

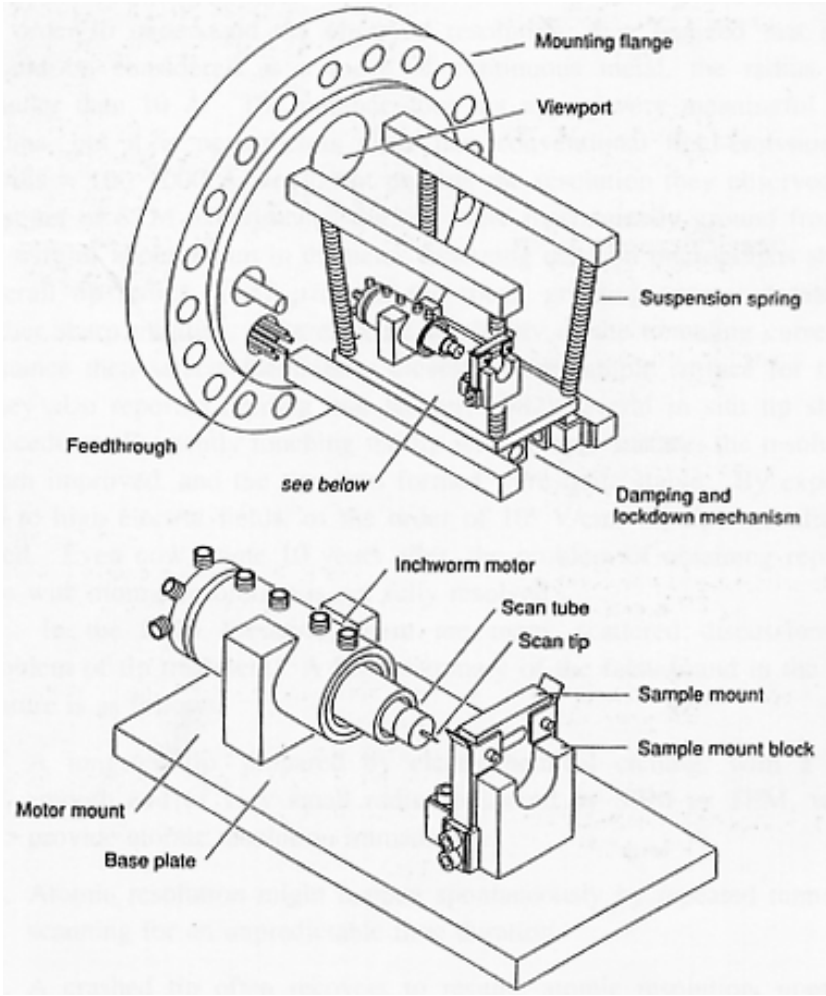

Piezoelectric Scanners

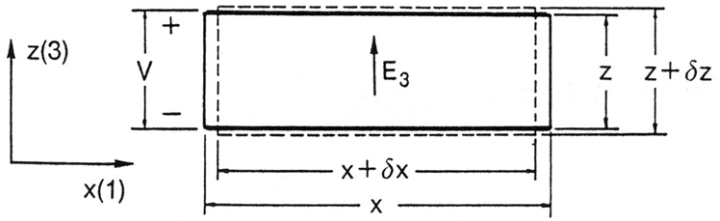

$d_{31} = S_1/E_3$, $S_1 = \delta x/x$, $E_3 = V/z$

$d_{33} = S_3/E_3$, $S_3 = \delta z/z$

Tripod scanner

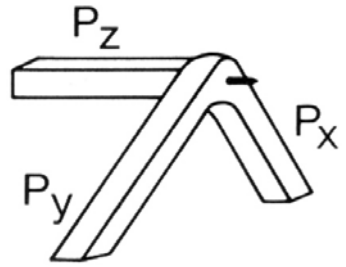

Variation of piezoelectric coefficient with temperature.

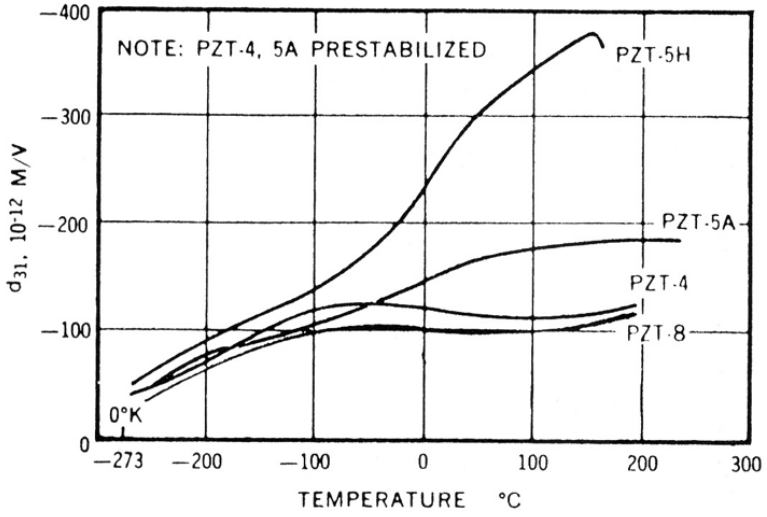

Tube scanner

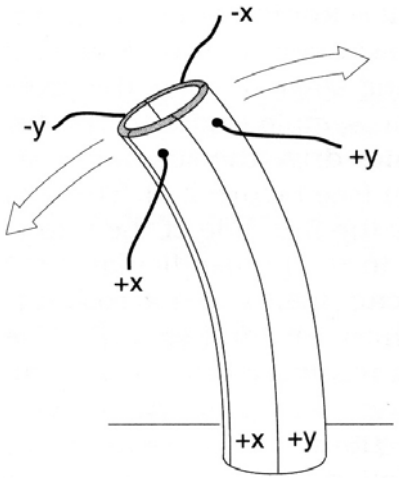

Tube Scanners

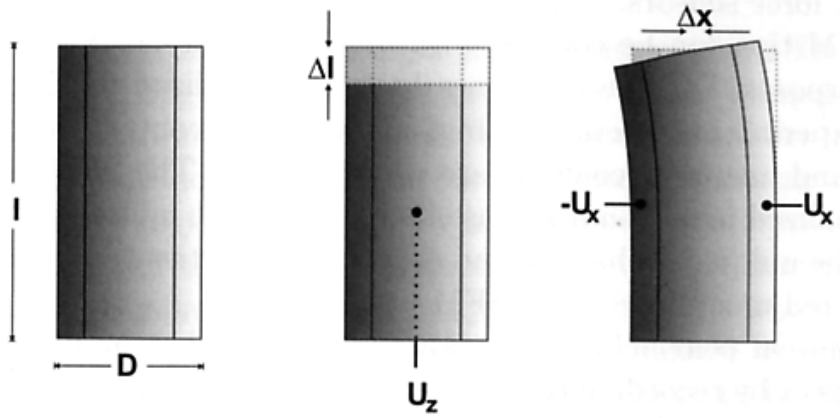

Fig. 1.4. Schematic side view of tube scanning. The outside electrode is divided into four parts. When a voltage U_z is applied to the inner electrode, the length of the tube is changed. When a pair of voltages U_x and $-U_x$ is applied to opposite electrodes outside the tube, the tube is bent and a lateral movement is realized. Note that the bending of the tube is largely exaggerated in order to visualize the effect. However, one should keep in mind that lateral displacements by tube scanners are always accompanied by height changes

$$\Delta l = \frac{d_{31} l U_z}{h} \qquad \Delta x = \frac{2\sqrt{2} d_{31} l^2 U_x}{\pi D h}$$

where l is the length of the tube

and h the wall thickness of the tube.

PZT Materials

1. The piezoelectric effect was discovered by Pierre Curie and Jacques Curie in 1880.
2. The piezo materials used in STM are various kinds of lead zirconate titanate ceramics (PZT) --- a mixture of $PbZrO_3$ and $PbTiO_3$. It consists of small ferroelectric crystals in random orientations.
3. An advantage for PZT ceramics over single crystal materials is that it can be shaped easily and poled at a desired direction.
4. PZT scanners are widely used in SPM because they have excellent resolution in displacement, high stiffness, and fast response. A major drawback of PZT materials is its lack of accuracy due to many nonlinear characteristics, such as hysteresis, creep, and recoil-generated ringing, which often cause distortion in SPM images. The positioning error of a PZT scanner can be as much as 10-15% of the full scanning range.
5. The piezoelectric constants vary with temperature in a complicated manner, and also with the particular batch of materials by the manufacturer and time (the aging effect).
6. Displacement calibration or compensation is needed for accurate measurement of length or size.

Hysteresis of a PZT Actuator

Hysteresis curves of an open-loop piezo actuator for various peak voltages

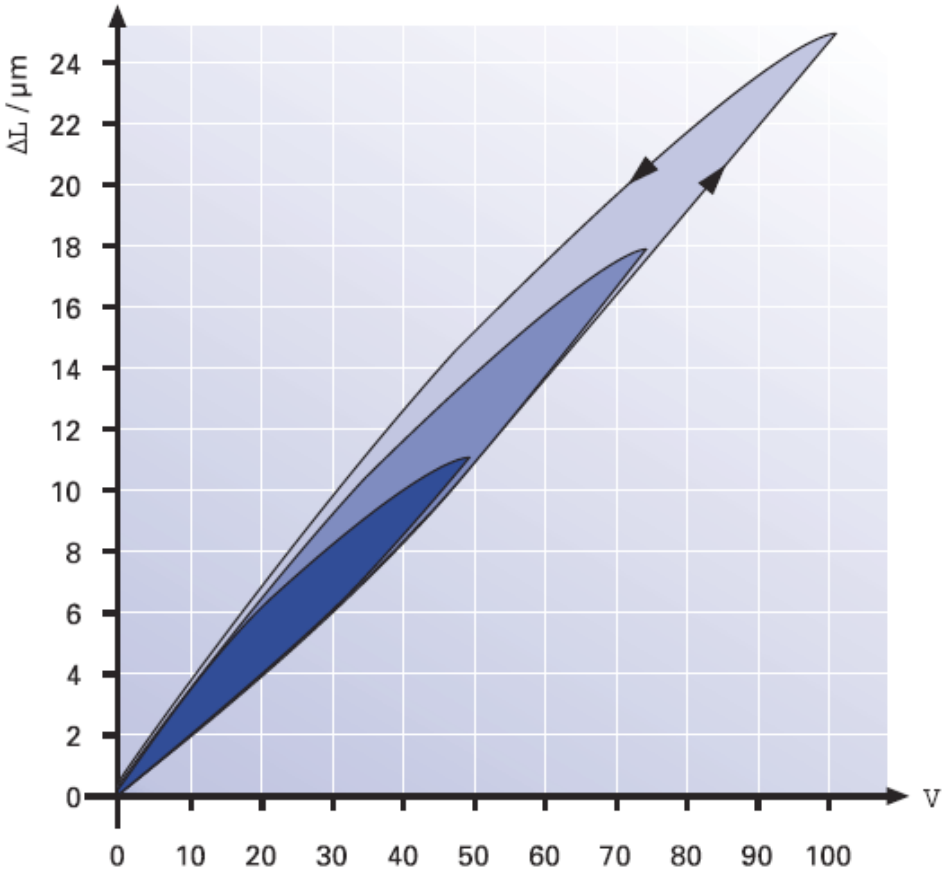

Response of a PZT translator to a 1 V, 200 Hz triangular drive signal

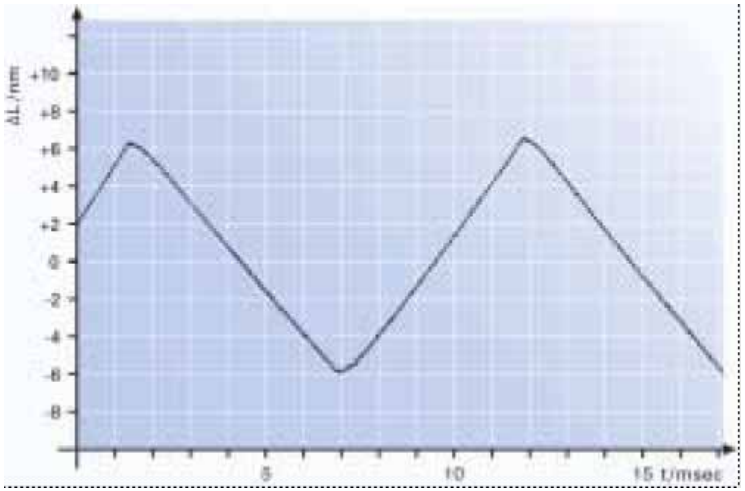

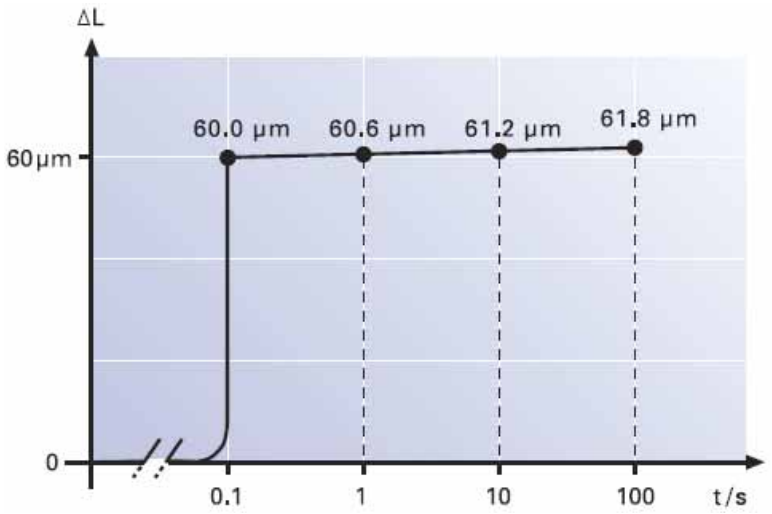

Creep of open-loop PZT motion

Topographic Images of AFM Square Grating

Without correction

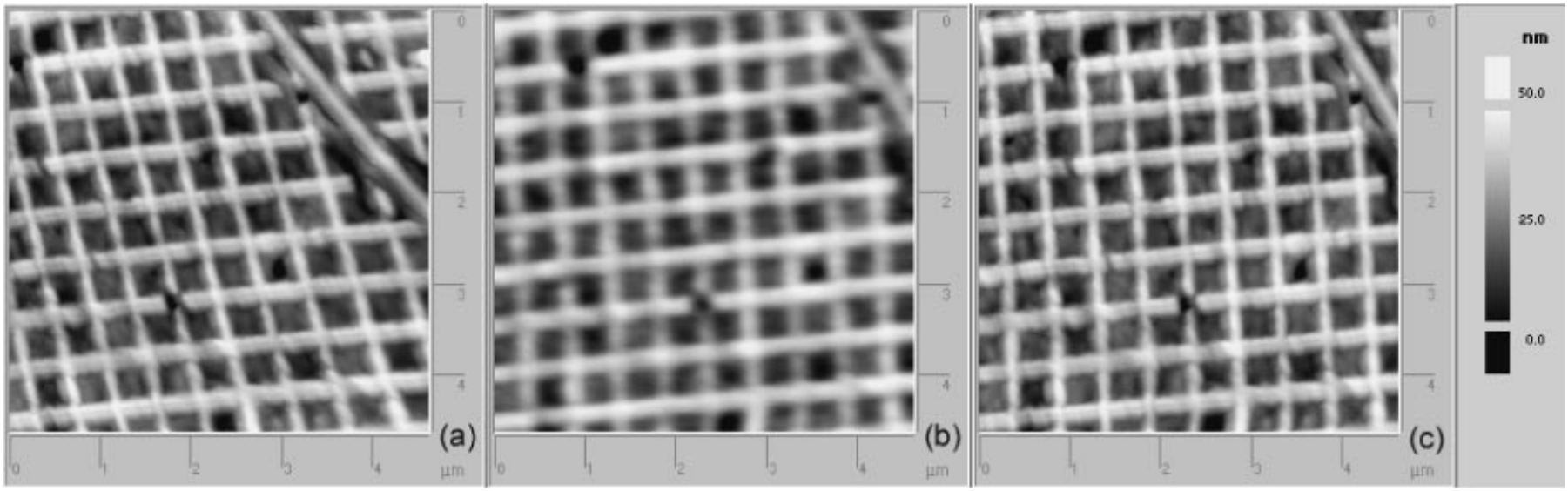

With correction in the x-direction

Jap. J. of Appl. Phys. **45**, 3B, 1917-1921.

Vibration Isolation

Power spectra of a tunneling signal

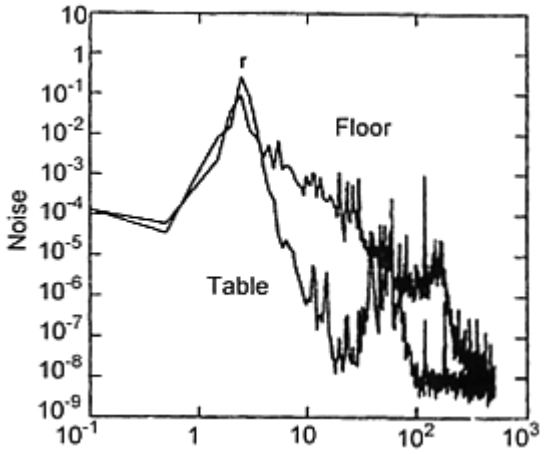

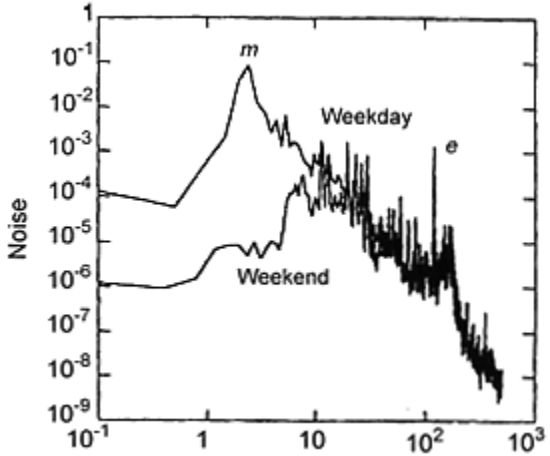

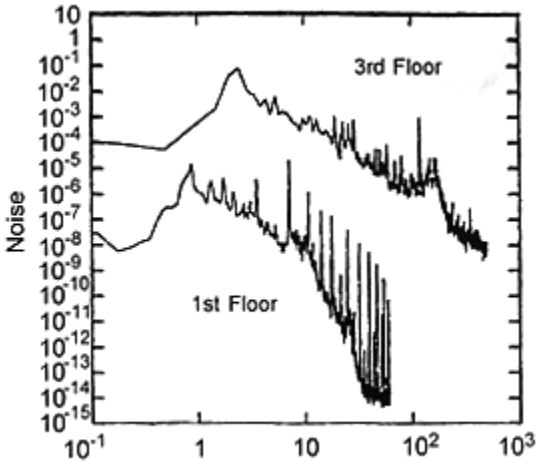

Calculated transfer function

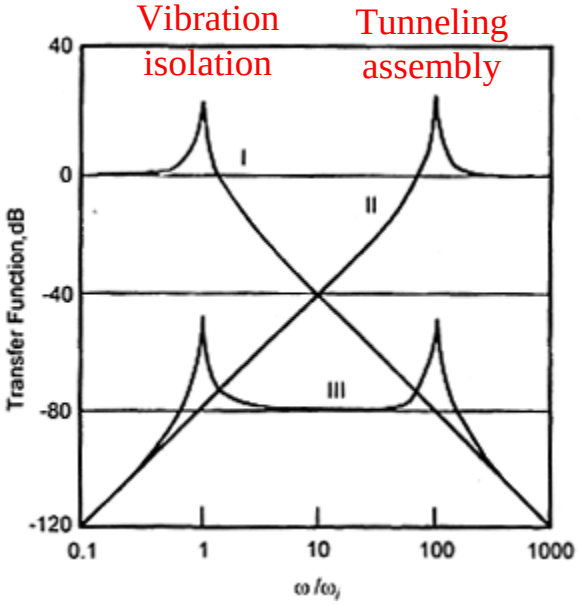

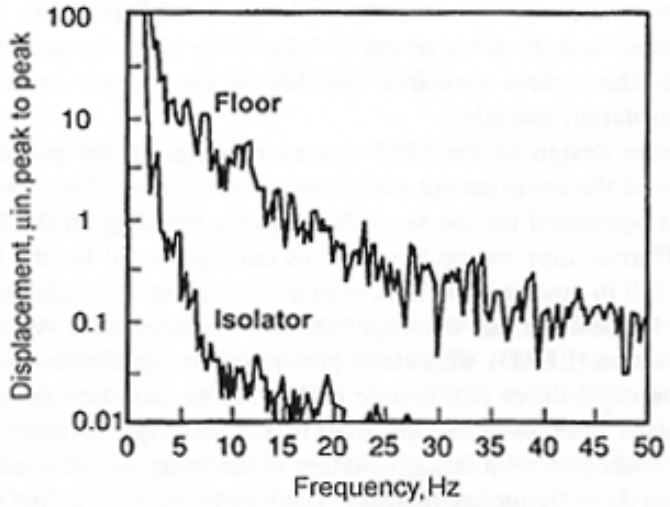

Vibration Isolation

Requirement in vibrational noise: < 0.01Å in z, and < 0.1Å in x and y.

1. Building vibrations 5-100 Hz.
2. Acoustic noise 10-10k Hz
3. Table/chamber resonances 30-100 Hz
4. The design strategy is to reduce the resonance frequency of the vibration isolation system as low as possible, increase the resonance frequency of the tunneling assembly.
5. An effective way to damp the low-frequency vibrations is to suspend the microscope on long tension wires or levitate the table/chamber system on air legs. The performance can further be improved by increasing the mass of the system.
6. The microscope itself can be suspended with tension spring.
7. Vibrations in the medium-frequency can be damped by mounting the scanner assembly on a stack of materials of different elastic moduli or to suspend the scanner on tension springs with eddy current damping.

Tip Shape Effects

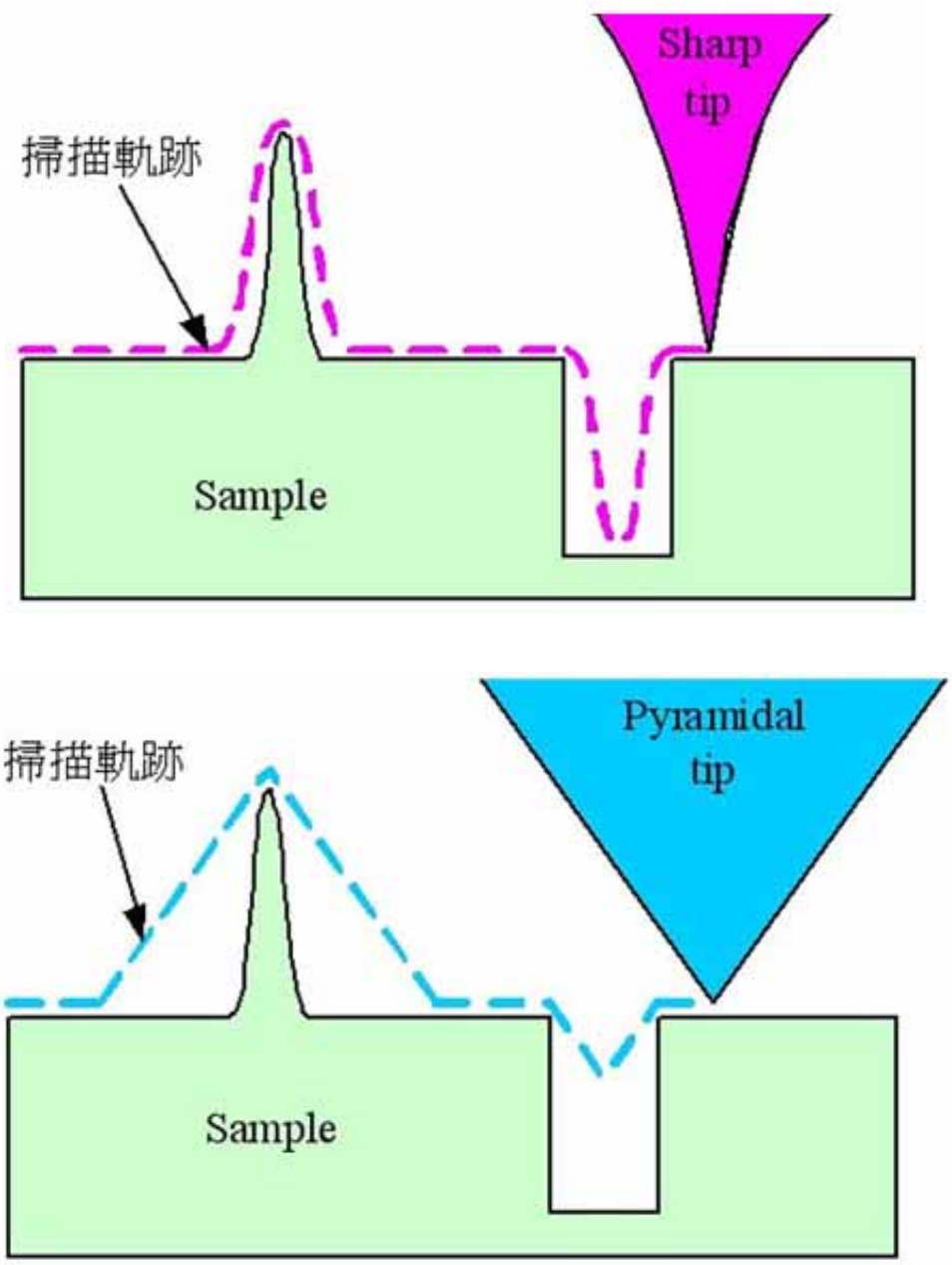

Artifacts of the Tip

Si(111)-(7x7)

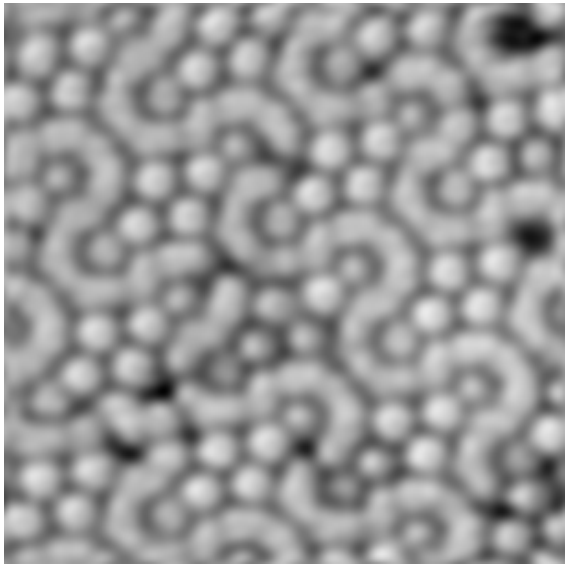

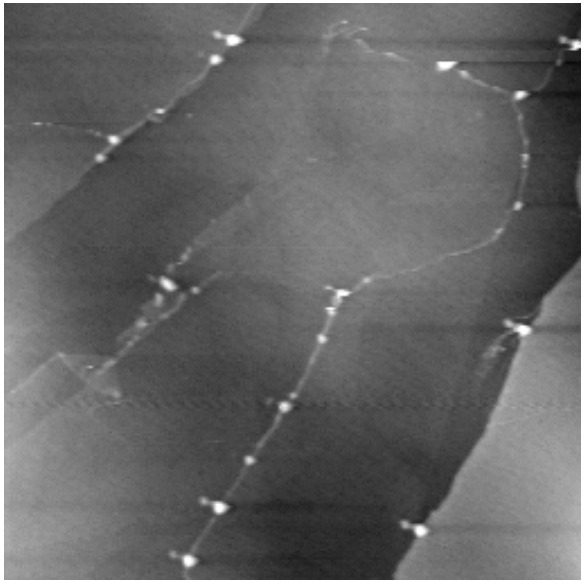

Pb/Si(111)

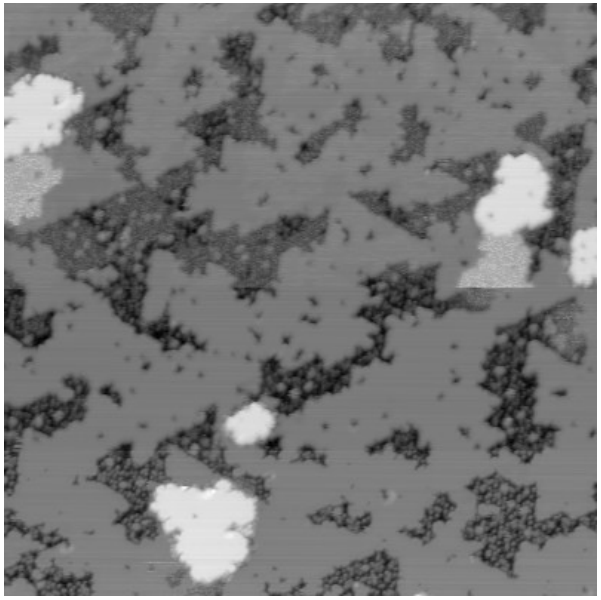

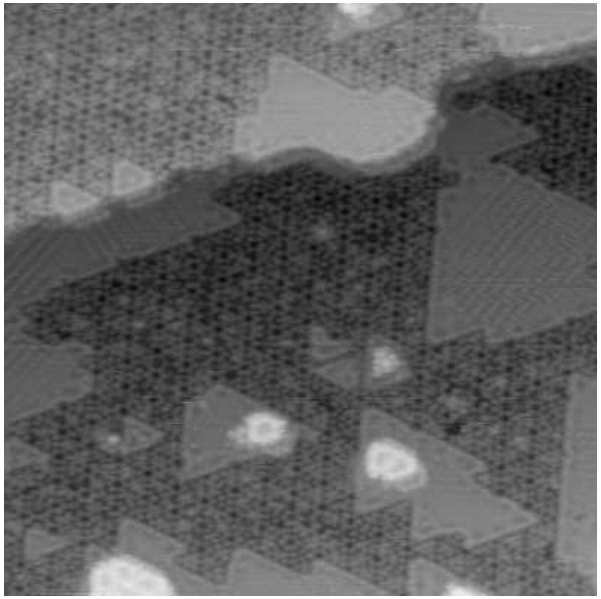

Artifacts of the Tip

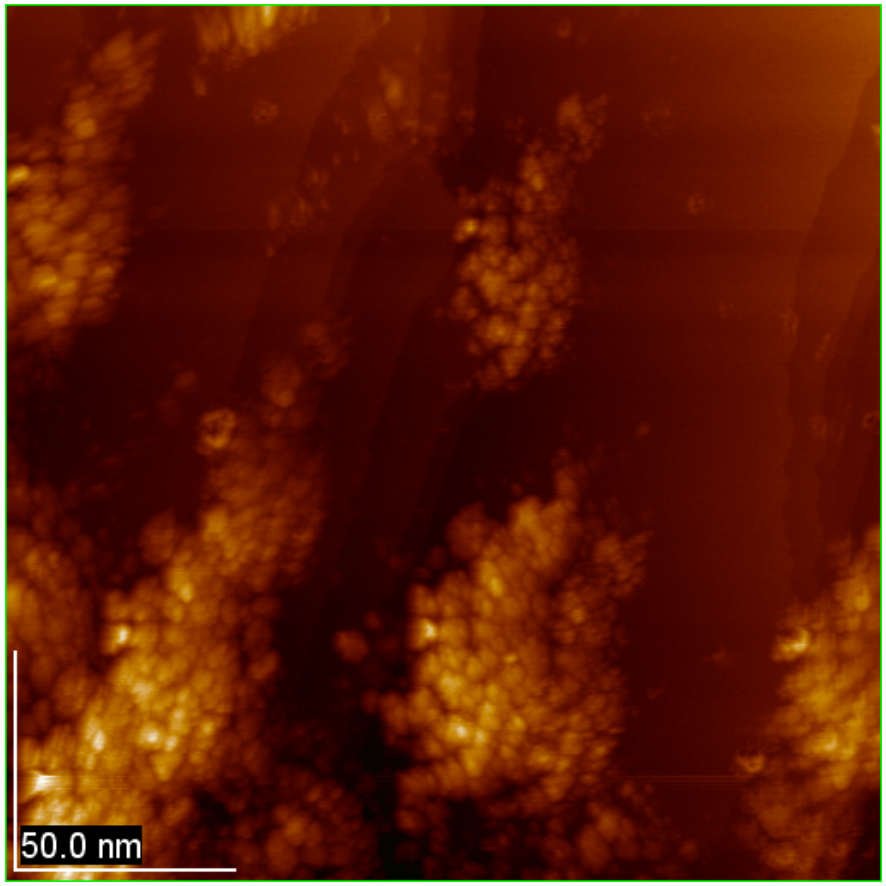

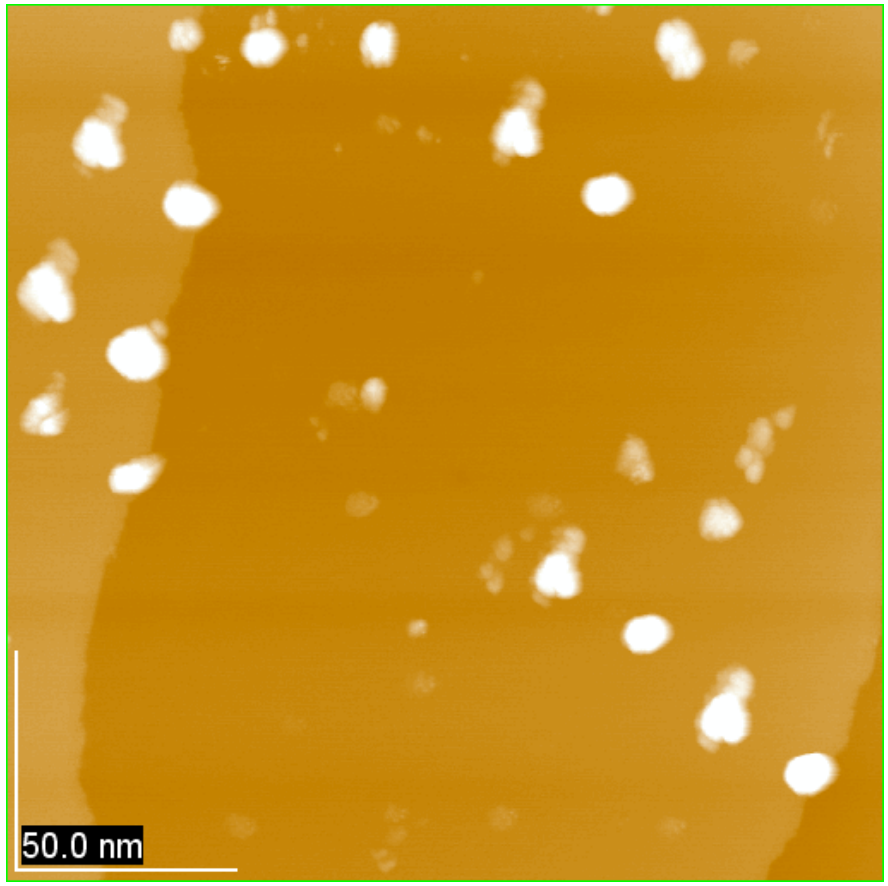

STM Feedback Control

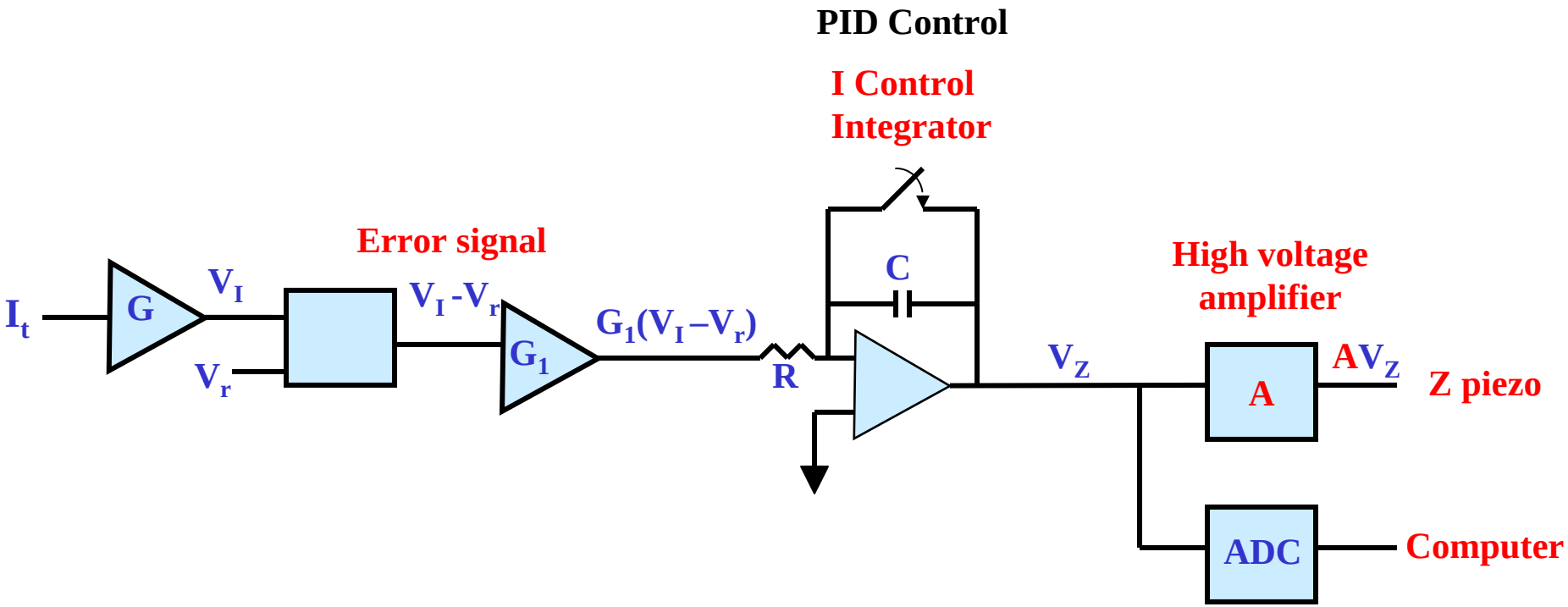

1. When values of the gain are too high, feedback oscillations may occur; when values are too low, details can be lost due to slow reaction of the feedback.
2. Use of high integral and proportional gains can reduce the error signal, but it increases the noise level in the feedback loop and in the height data.

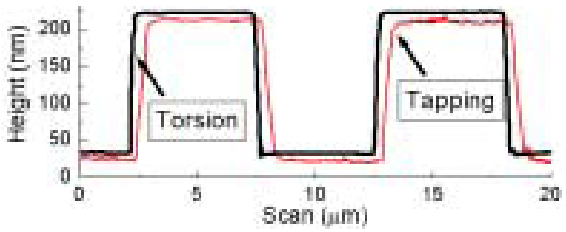

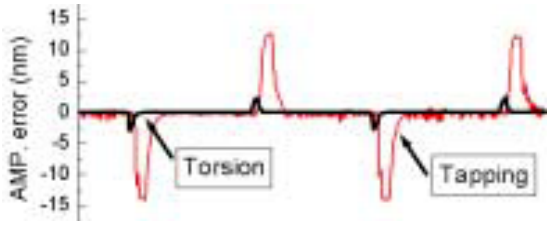

Electronic Surface States

*** Many macroscopic effects and phenomena on surfaces are related to the change in electronic structure.**
*** The electronic structure near to the surface is markedly different from that in the bulk.**

1. An ideal surface with its atoms at bulk-like positions (called truncated bulk) displays new electronic levels --- the periodicity perpendicular to the surface breaks down.
2. Surface relaxations and reconstructions frequently occur.

One-dimensional semi-infinite lattice model potential (solid curve) and an associated surface state (dashed curve).

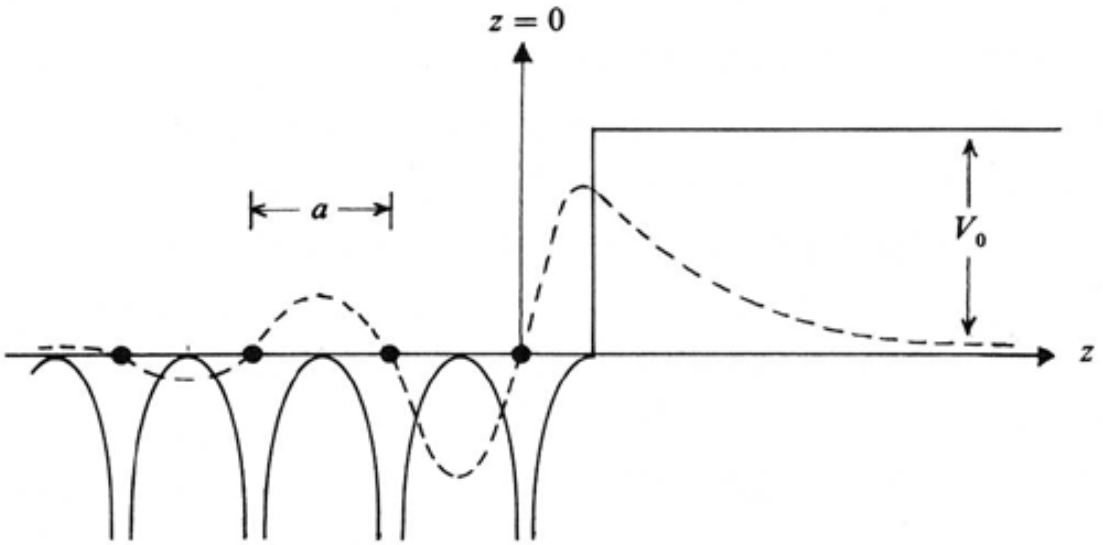

A. Electrons in surface states are localized within a few Å of the surface plane.

B. Some electronic surface states may located somewhere in the gap of the bulk states.

Surface States

1.Impurities, defects, etc.

2.Termination of periodic arrangement

Tamm's model --- modified Kronig-Penney model

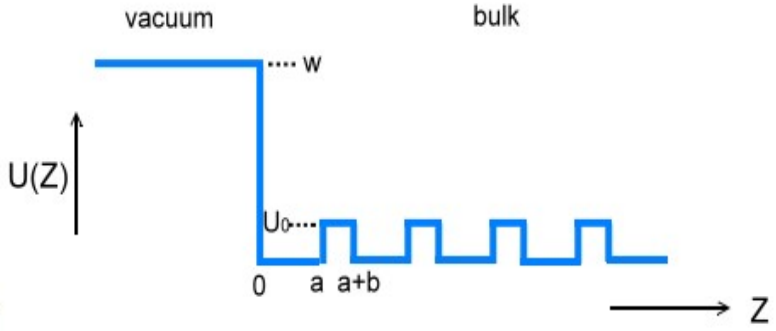

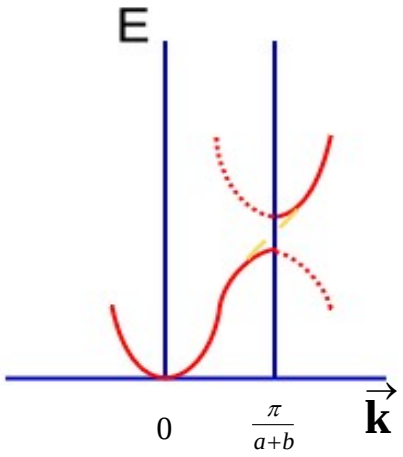

One-dimensional periodic potential of lattice constant a+b (Kronig-Penney)

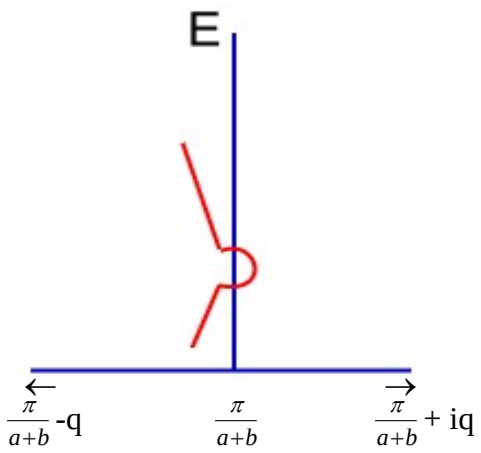

Tamm's model

Bloch form $\varphi(z) = e^{ikz}u(z) = e^{i\frac{\pi}{a+b}z}e^{-qz}u(z)$

The surface states are localized near the surface (z=0).

Hans Lüth, "Surfaces and Interfaces of Solids", Springer-Verlag, 1993, Chap 6.

Coupling between Surface States and Bulk states

1. A surface state

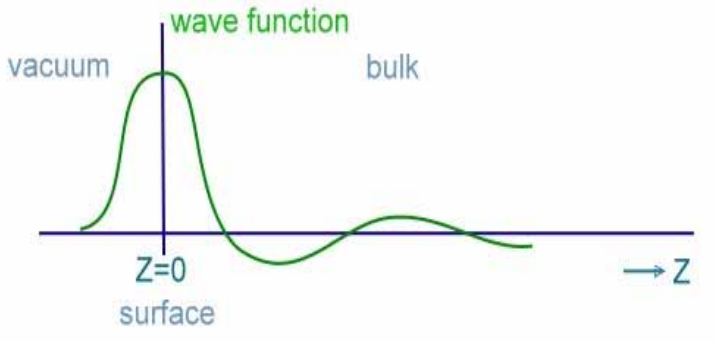

2. A bulk state

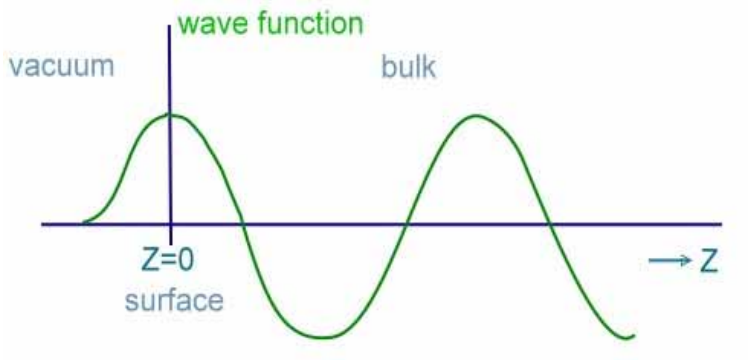

3. A quasi-stationary surface which resonates with the bulk continuum

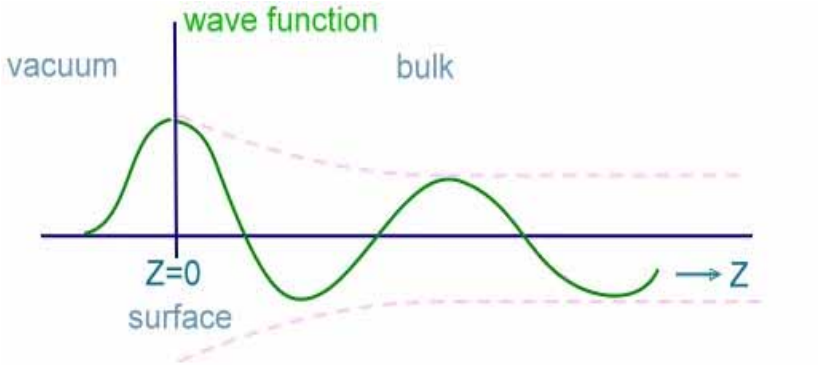

Theory of STM

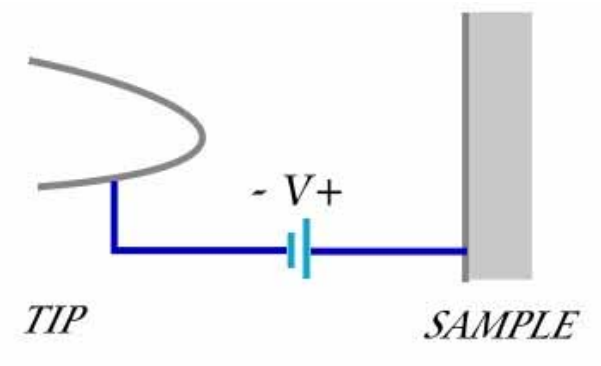

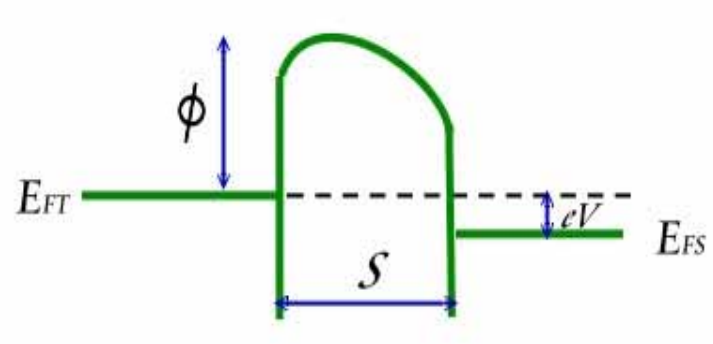

From one-dimensional tunneling problem

tunneling current (eV<< ϕ)

$$I \propto \frac{V}{S}\exp\left(-A\phi^{\frac{1}{2}}S\right)$$

$$A = 1.025(eV)^{-\frac{1}{2}}\ {}^{0}A^{-1}$$

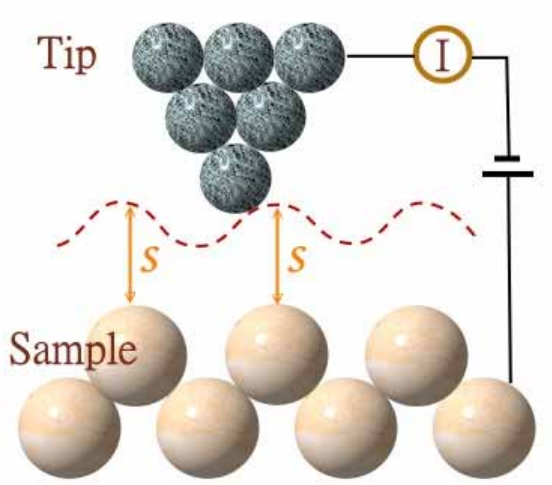

Constant Current Mode

Tunneling Current

$$I_{T\to S} = \frac{2\pi e}{\hbar}\sum_{\mu\nu} f\left(E_\mu\right)\left[1- f\left(E_\nu + eV\right)\right]\left|M_{\mu\nu}\right|^2 \delta\left(E_\mu - E_\nu - eV\right)$$

where $f(E)$ is Fermi function

E_μ is the energy of state μ ,where μ and ν run over all the states of the tip and surface , respectively.

$M_{\mu\nu}$ is tunneling matrix element

$$M_{\mu\nu} \equiv \frac{\hbar^2}{2m}\int d\vec{s}\left(\psi_\mu * \nabla\psi_\nu - \psi_\nu \nabla\psi_\mu *\right)$$

where ψ_μ is the wave function, and the integral is over any plane in the barrier region.

$$I = I_{T\to S} - I_{S\to T}$$
$$= A'\int_{-\infty}^{\infty} \rho_T\left(E\right)\rho_S\left(E+eV\right)\left|M\left(E\right)\right|^2\left[f\left(E\right)- f\left(E+eV\right)\right]dE$$

where ρ_S and ρ_T are the densities of states in the sample and the tip, respectively.

Electronic Structures at Surfaces

Not Tunneling

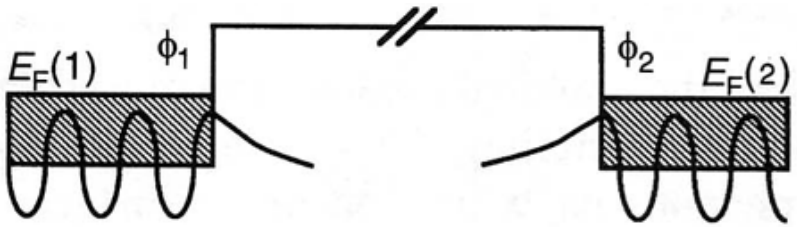

Empty-State Imaging

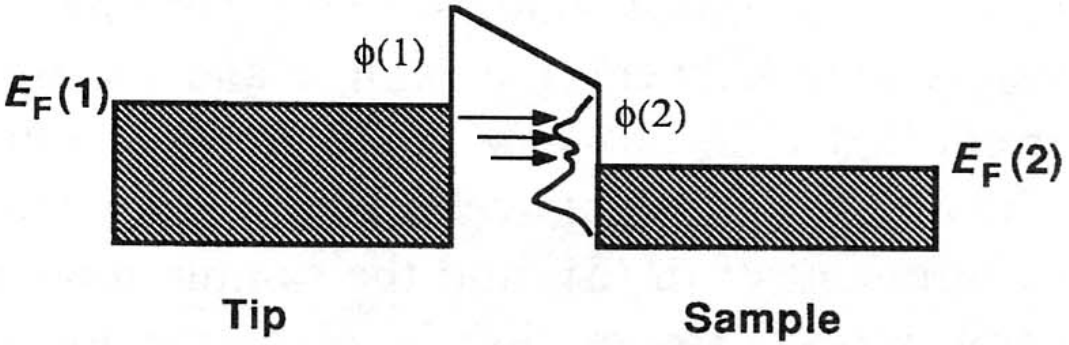

Tunneling

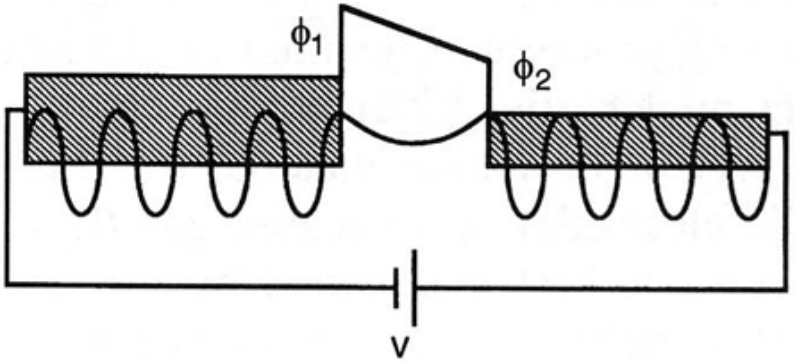

Filled-State Imaging

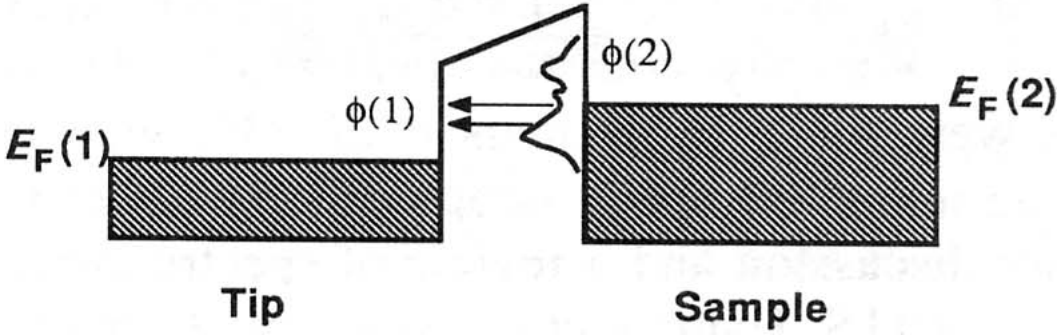

Tunneling Current

$$I \equiv A' \int_{-\infty}^{\infty} \rho_T(E)\rho_S(E+eV)\left|M(E)\right|^2 \left[f(E) - f(E+eV)\right]dE$$

Transmission probability of the electron

$$M(E) = \exp\left[-A\phi^{\frac{1}{2}}S\right]$$

Usually, we assume ρ_T is featureless (ie. $\rho_T \approx const.$), and the sample electronic states dominate the tunnel spectra.

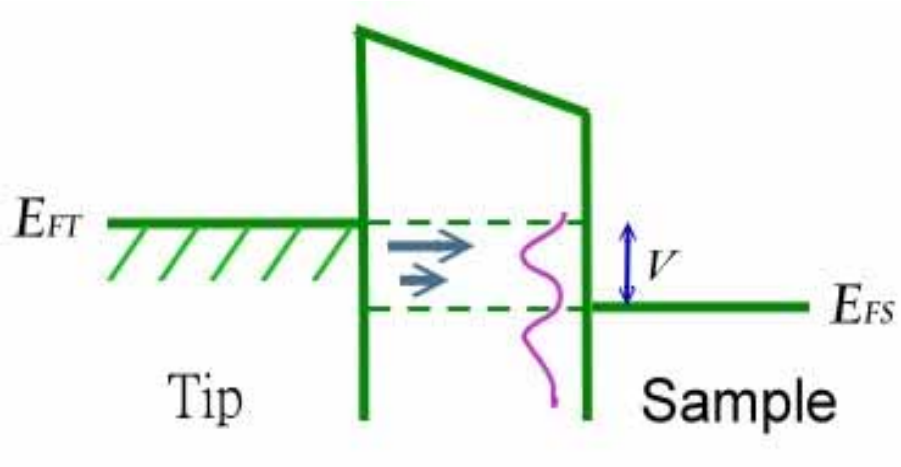

However, the tips might have effect on the tunnel spectra, if

1. we have atomically sharp tips ,or
2. the tip has picked up a foreign atom.

Tunneling Barrier

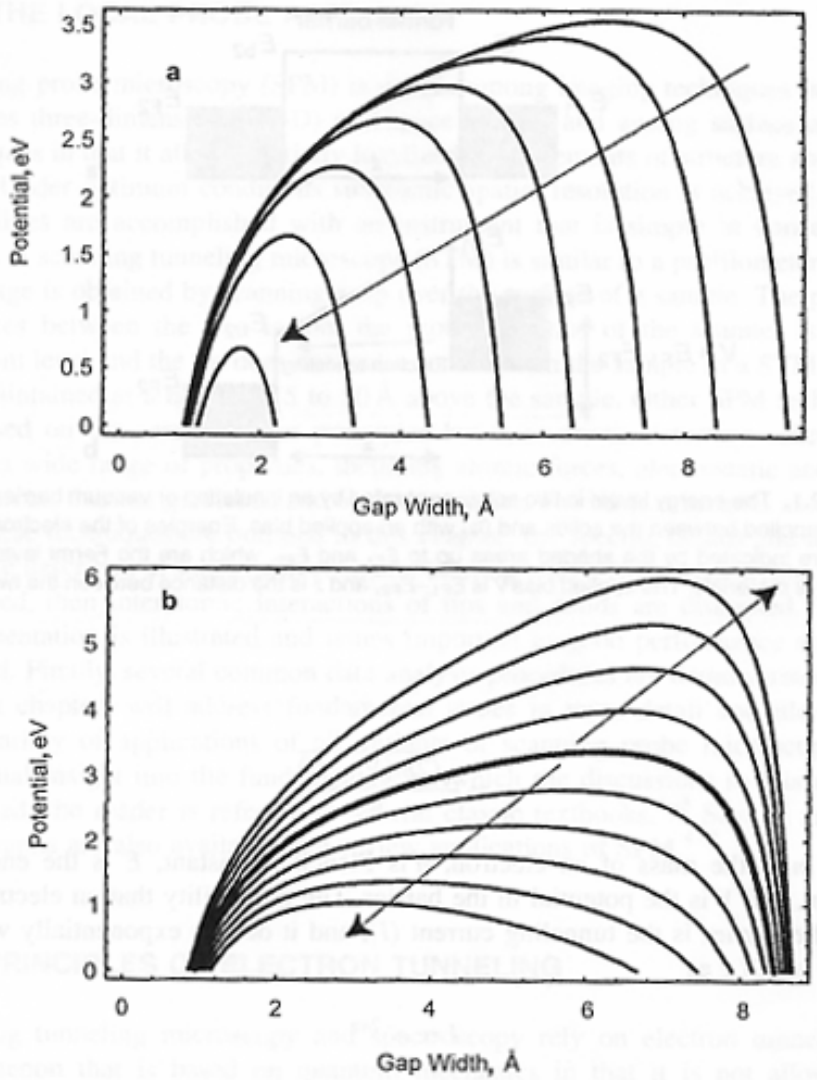

Figure 2.2. A more realistic depiction of the tunneling barrier, including the effect of image charge on the shape of the barrier. **a**, As the distance between the solids is decreased (*arrow*), the size and shape of the barrier change. **b**, The barrier also changes when a voltage is applied, the arrows show the response to opposite signs of bias.[25]

Case Ⅰ -----metals

In the low-voltage limit

$$I \propto V\rho_S(\tilde{r}_t;E_F)\rho_t(E_F)$$

where $\rho_S(\tilde{r}_t;E_F)$ is the surface density of states of the sample at the center of the tip($\tilde{r}_t$),

$$\rho_S(\tilde{r};E) \equiv \sum_\nu |\psi_\nu(\tilde{r})|^2 \delta(E_\nu - E)$$

$\rho_t(E_F)$ is the density of states of the tip at the Fermi level and is often regarded as a constant.

The contour followed by the tip is a contour of constant Fermi-level density of states of the sample, measured at the center of curvature of the tip.

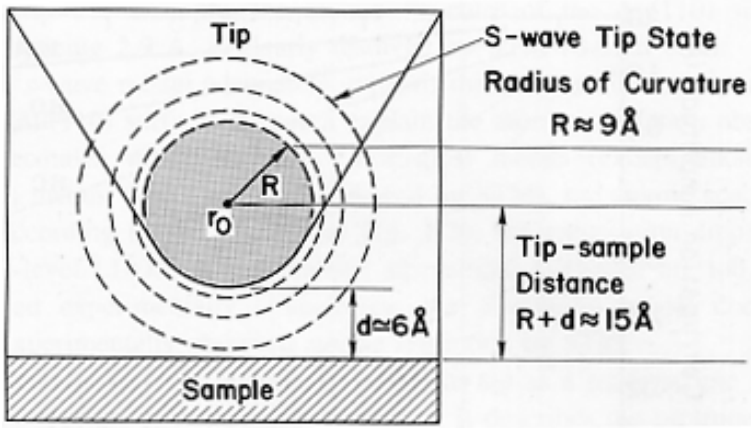

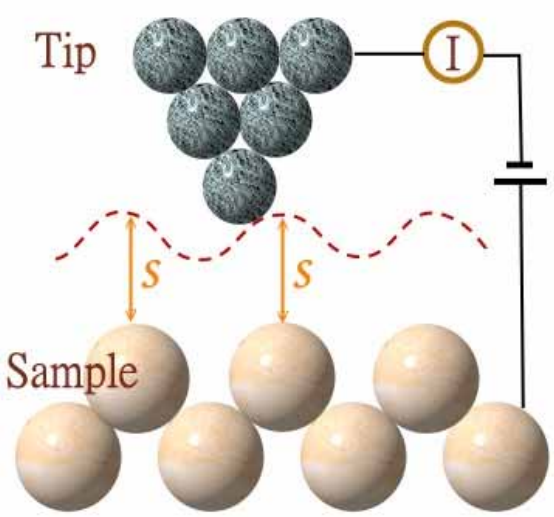

Constant Current Mode

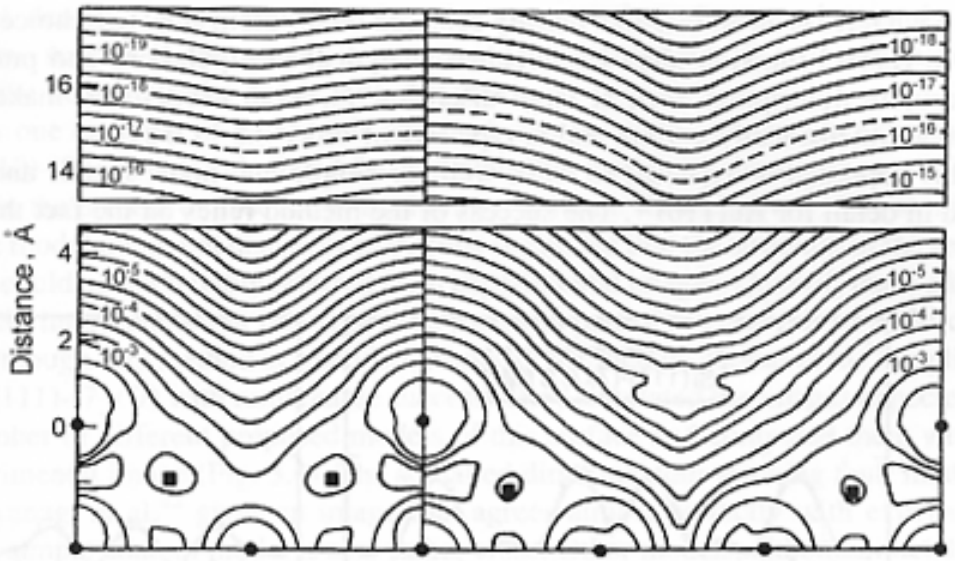

Figure 3.3. Calculated $\rho(\boldsymbol{r}, E_F)$ for Au (110)-(2 × 1) (*left*) and (3 × 1) (*right*) surfaces. The figure shows the (1$\bar{1}$0) plane through outermost atoms. Positions of nuclei are indicated by *solid circles* (in plane) and *solid squares* (out of plane). Contours of constant ρ are labeled in units of a.u.$^{-3}$ eV^{-1}. Note the break in the vertical distance scale. Assuming a 0.9-nm tip radius in the *s*-wave tip model, the center of curvature of the tip is calculated to follow the dashed line. (Reprinted with

Example -----Semiconductor

1.Tip-negative

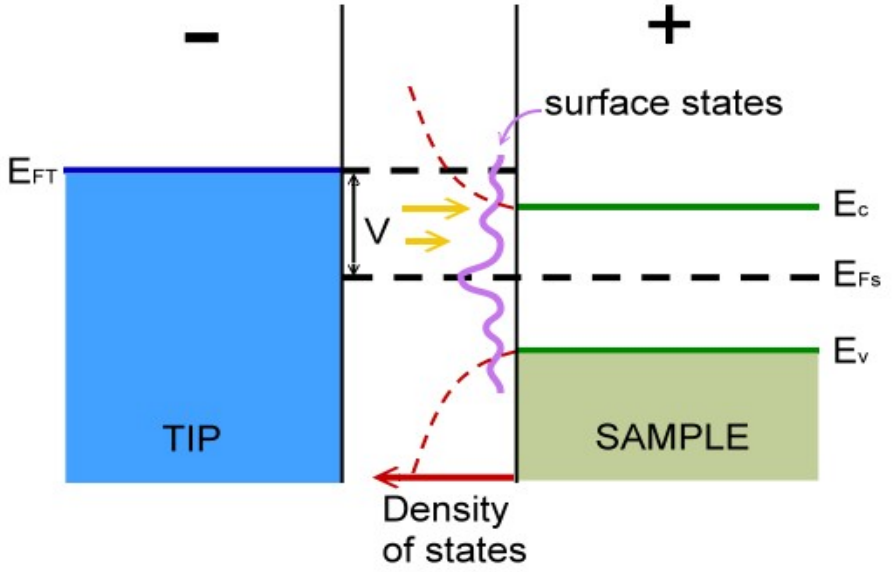

2.Tip -positive

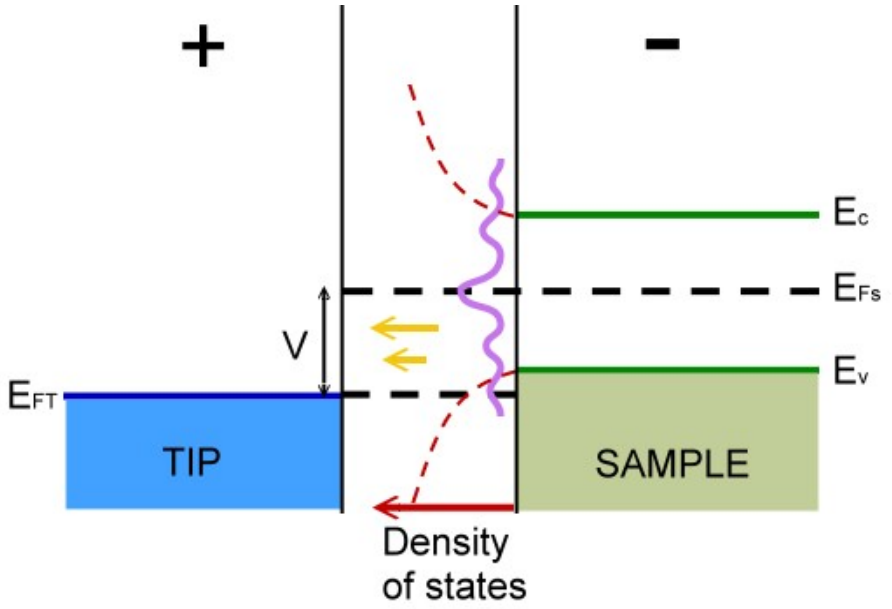

Science **234**, 304 (1986).

Scanning Tunneling Spectroscopy

STM provides atomic-scale topographic information, and atomic-scale electronic information. However, the mixture of geometric and electronic structure information often complicates interpretation of observed feature.

Several spectroscopic modes:

1. **Voltage-dependent STM imaging.**
2. **Tunneling I-V curves, dI/dV.**

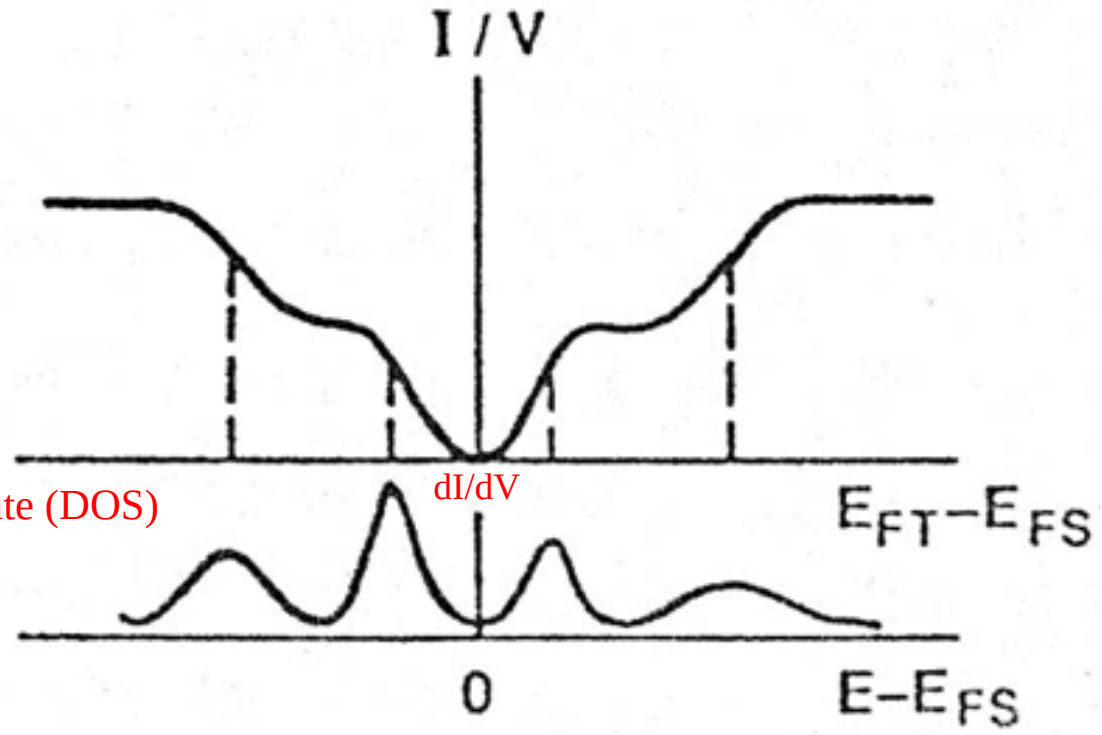

Pb/Si(111)

+1.8 V

+2.4 V

-1.8 V

Filled-state

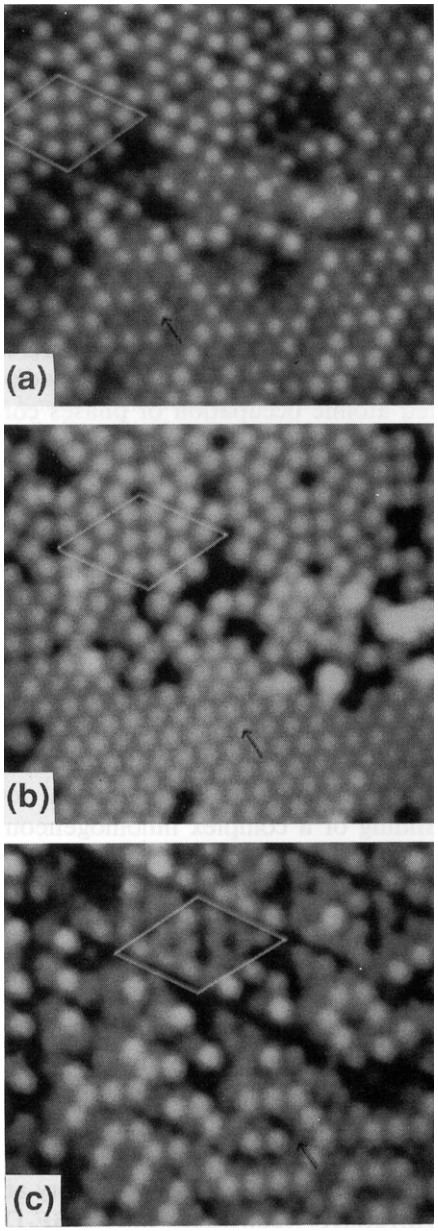

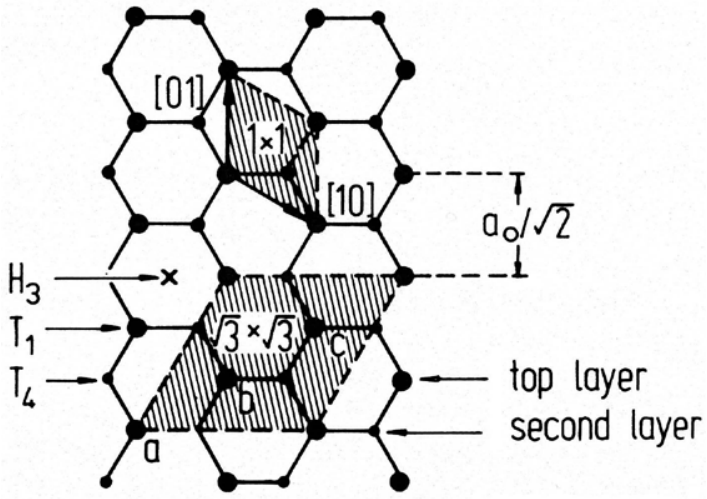

T_4 site

$\sqrt{3}\times\sqrt{3}$

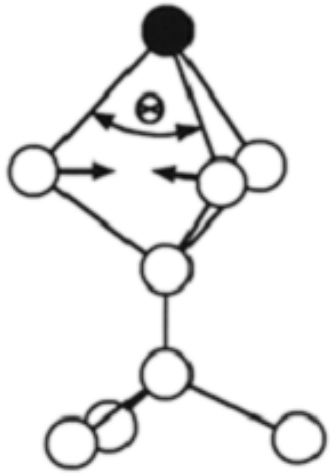

Surface Science **257**, 259 (1991)

Scanning Tunneling Spectroscopy (STS)

$$\frac{dI}{dV} = \rho_s(r, eV)\rho_t(r, 0)T(eV, eV, r) + \int_0^{eV} \rho_s(r, E)\rho_t(r, E - eV)\,\frac{dT(E, eV, r)}{dV}\,dE$$

1. The tunneling transmission probablility T is a smooth, monotonically increasing function of V. Thus dT/dV contributes a smooth background. Therefore, structure in dI/dV can usually be assigned to changes in the state density.
2. Extracting quantitative information about the sample density of states is difficult because the density of states of the tip and the tunneling transmission probability T are almost unknown.
3. Normalization of dI/dV by I/V was proposed to minimize the distance dependence of the tunneling probability (or the voltage dependence of the tunneling barrier).

Single-Wall Carbon Nanotubes

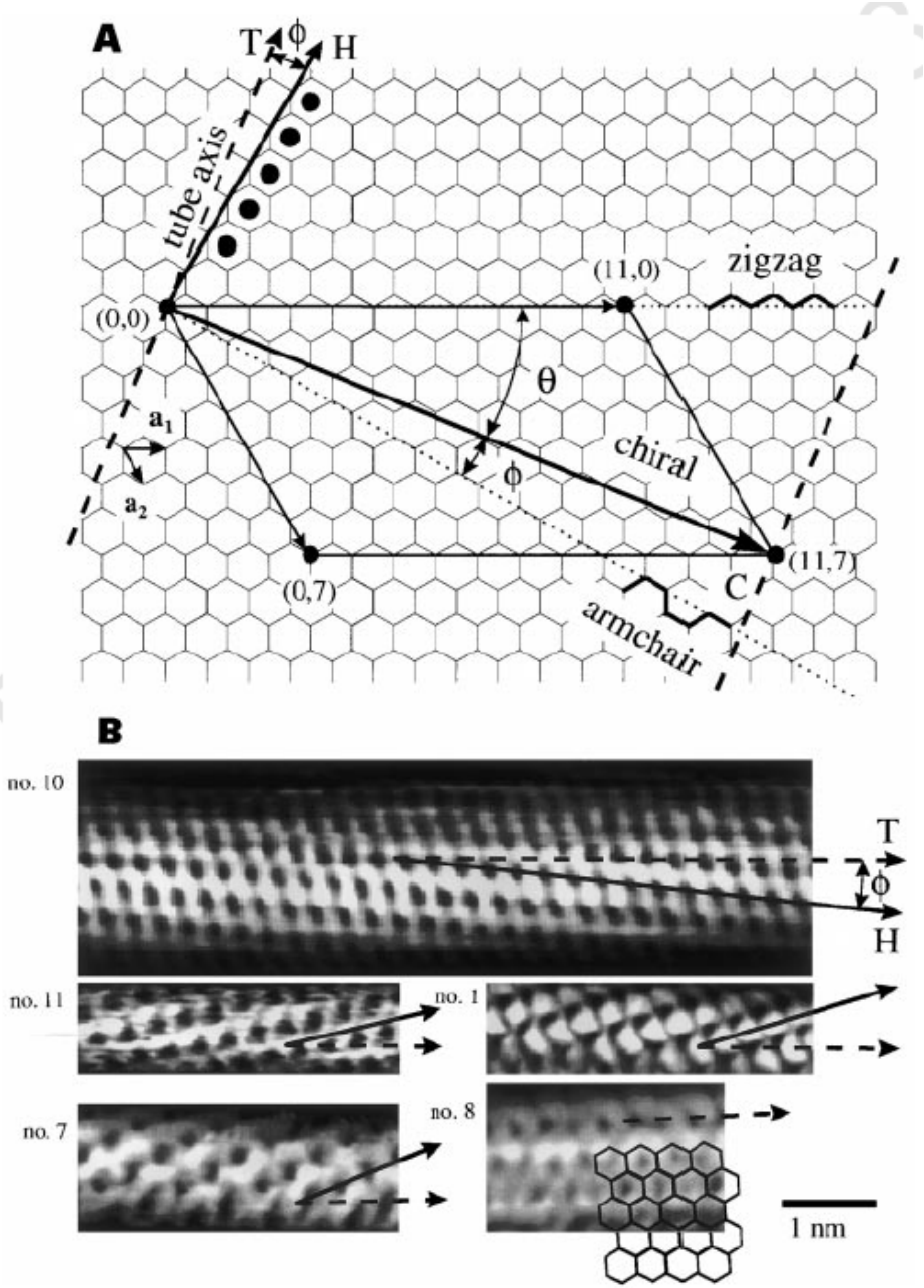

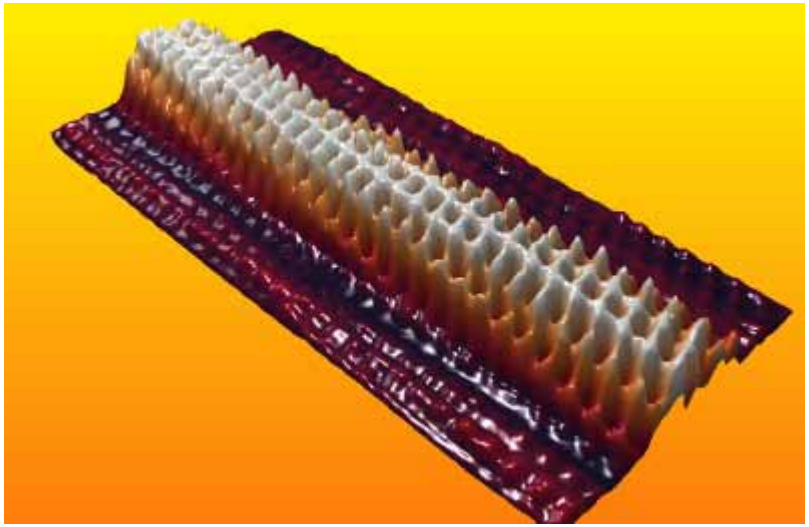

Electronic Structure of Single-Wall Nanotubes

1. Armchair nanotubes (n,n) → metallic

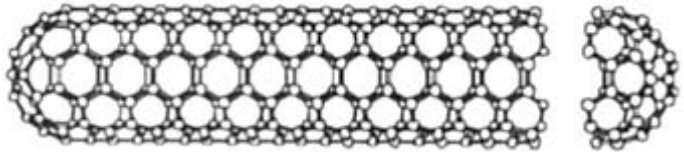

2. Zigzag nanotubes (n,0) → metallic, when n=3q

   → semiconducting, otherwise

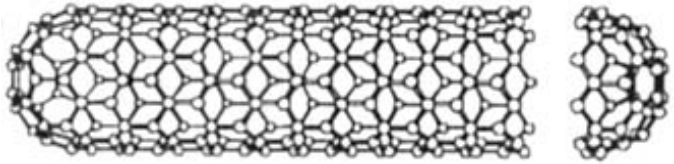

3. Chiral nanotubes (n,m) → metallic, when m=n+3q

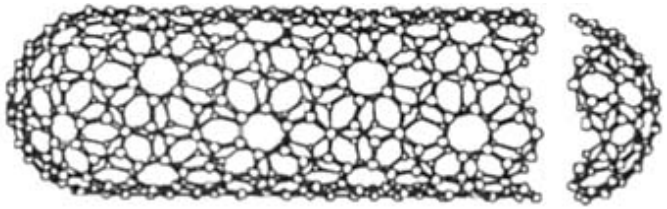

Electronic Structure of Single-wall Nanotubes

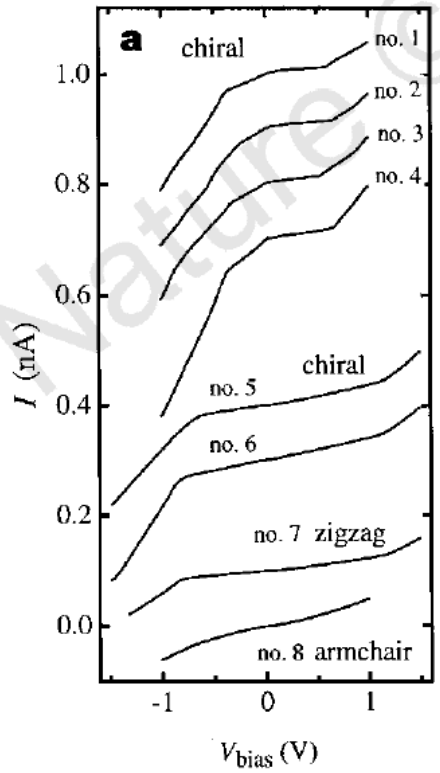

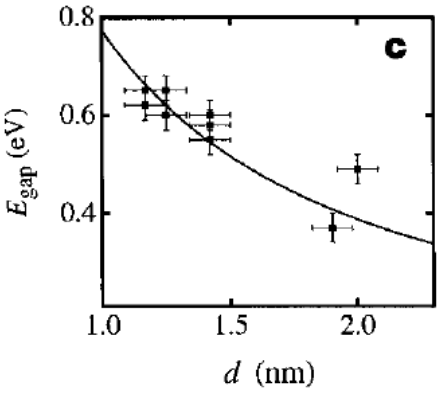

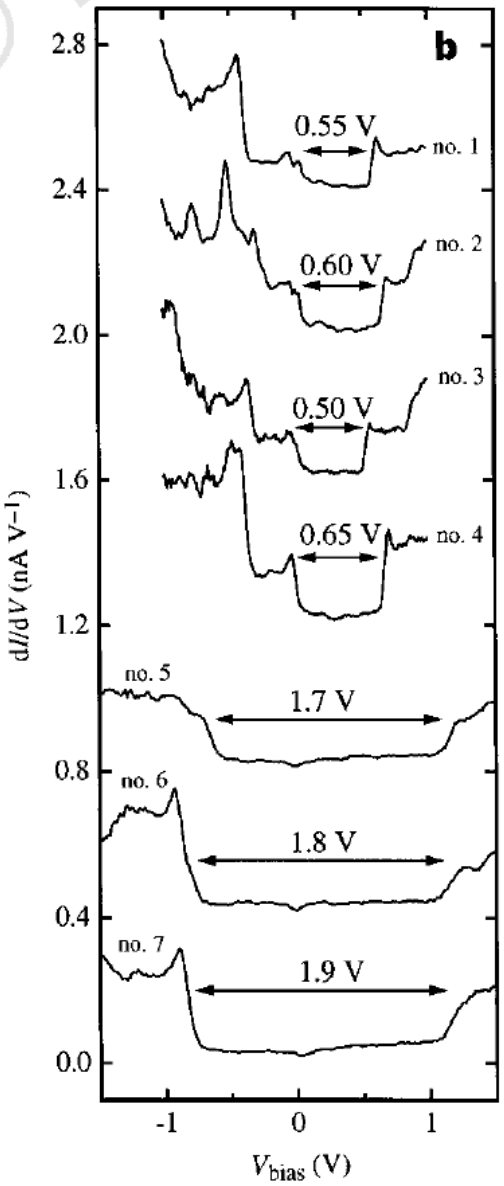

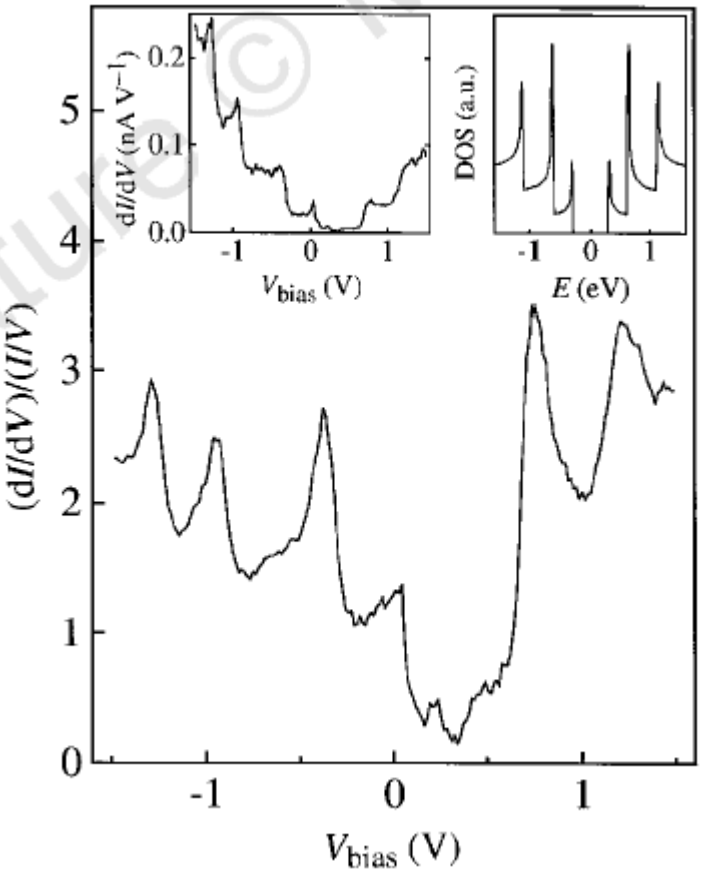

Nature **391**, 59 (1998).

Atomic Manipulation with STM

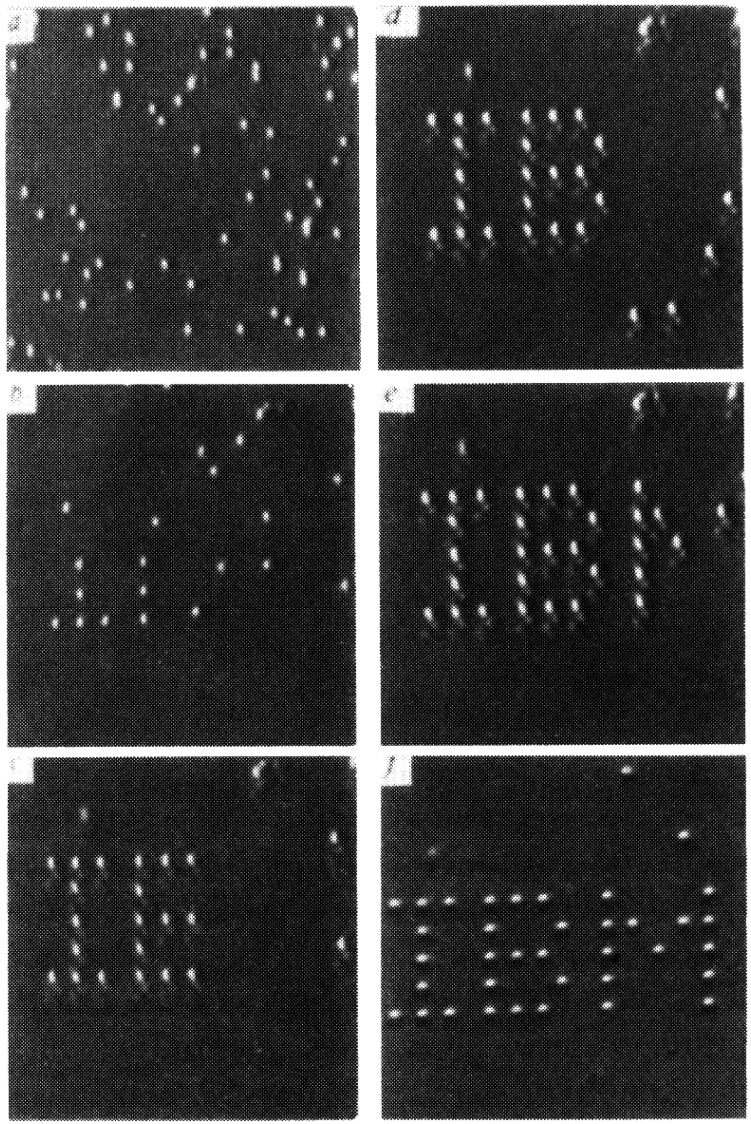

Nature **344**, 524 (1990)

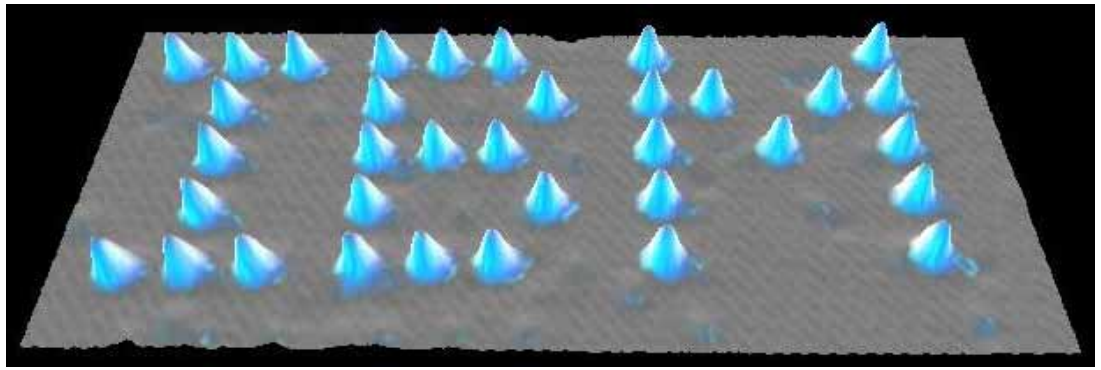

Xe on a Ni surface

Positioning Atoms with an STM

D.M. Eigler & E.K. Schweizer Nature **344** 524 (1990)

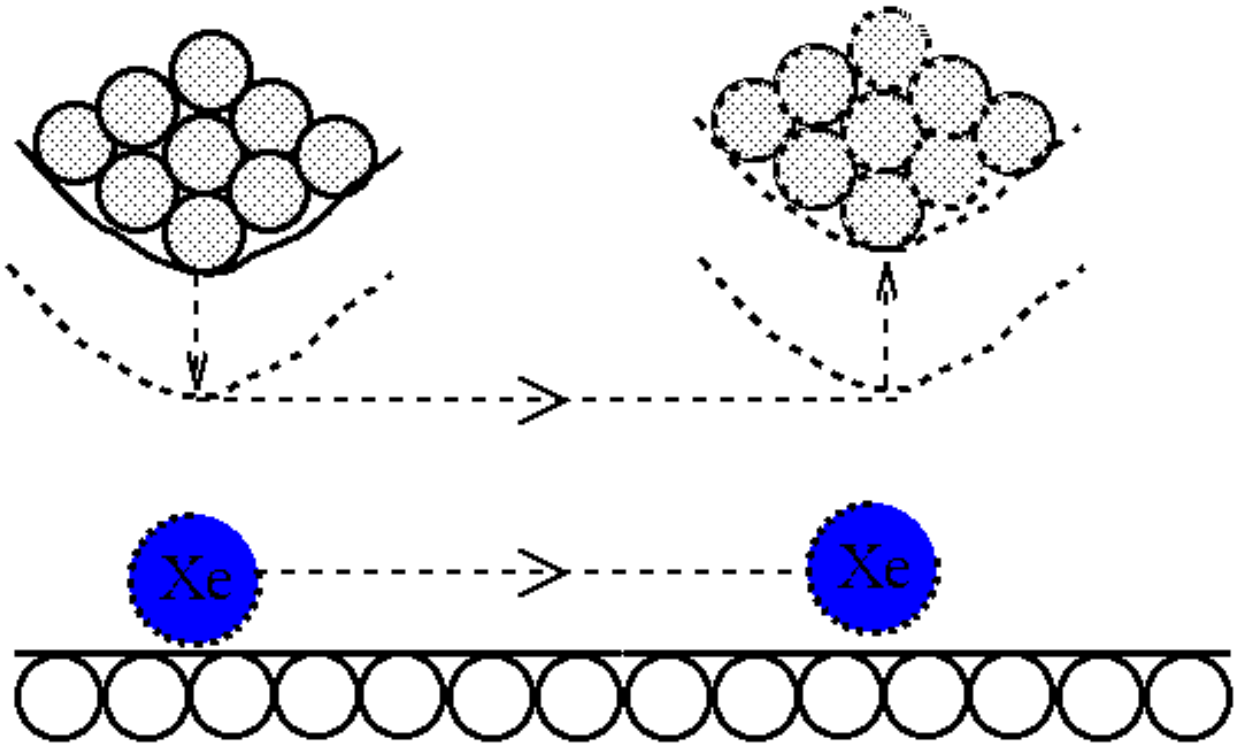

The STM tip is brought down near the atom, until the attraction is enough to hold it as the atom is dragged across the surface to a new position.

Quantum Correl

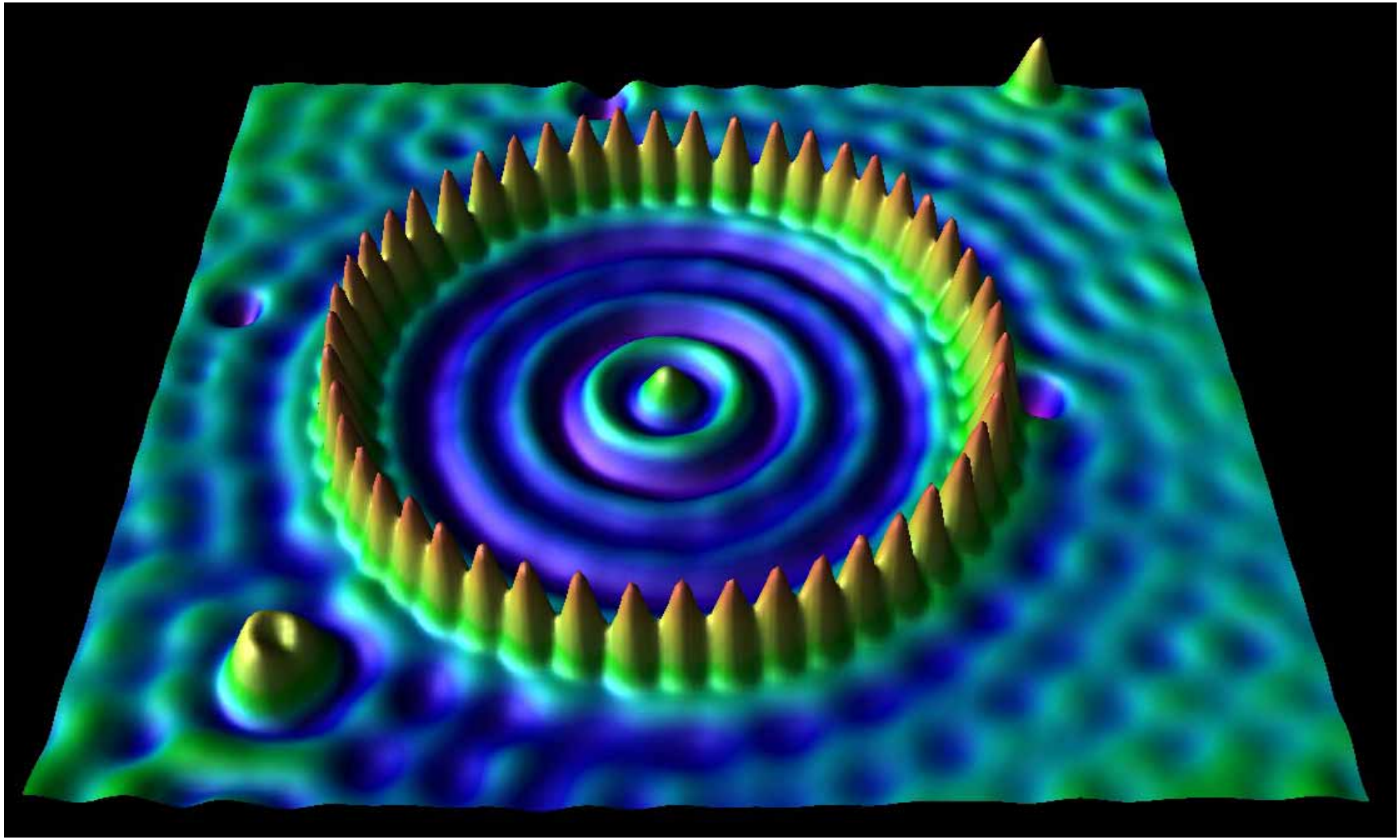

M.F. Crommie *et al., Science* 262, 218 (1993).

Energy-Dependent Friedel Oscillations

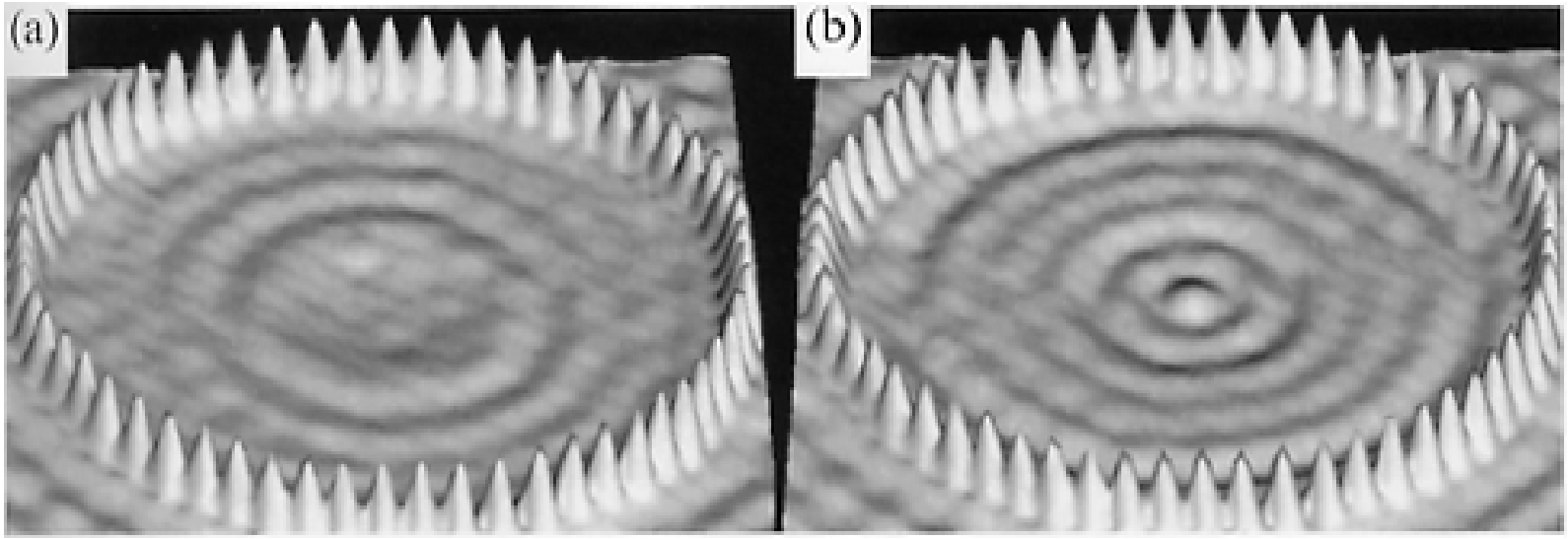

V_t = + 10 mV

V_t = - 10 mV

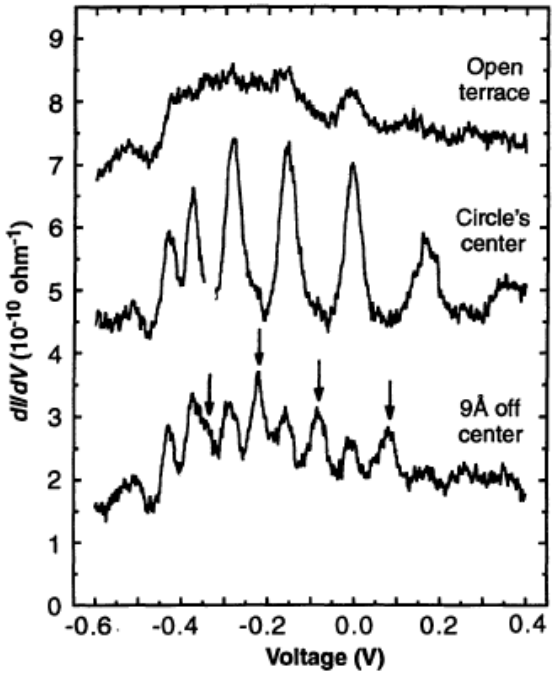

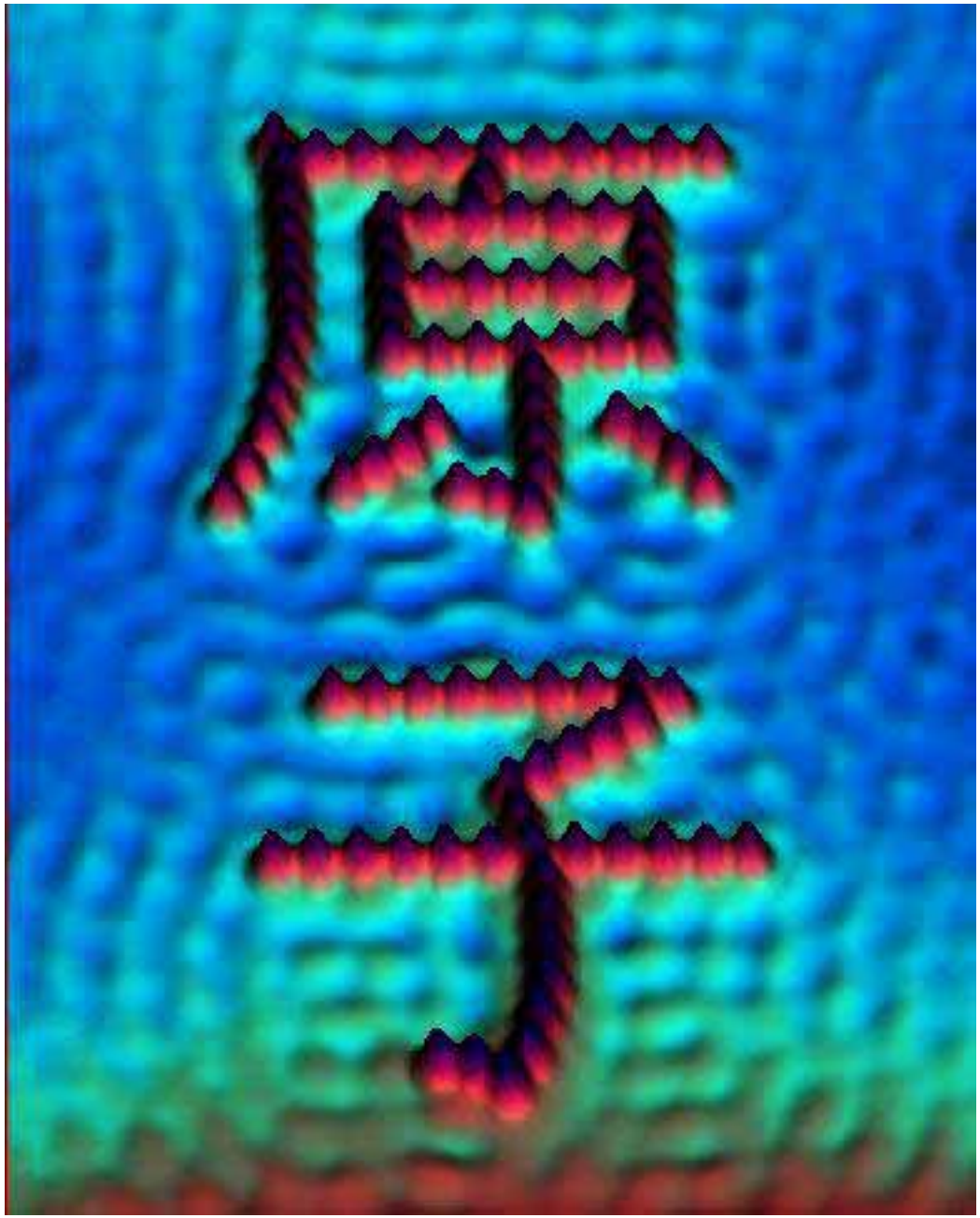

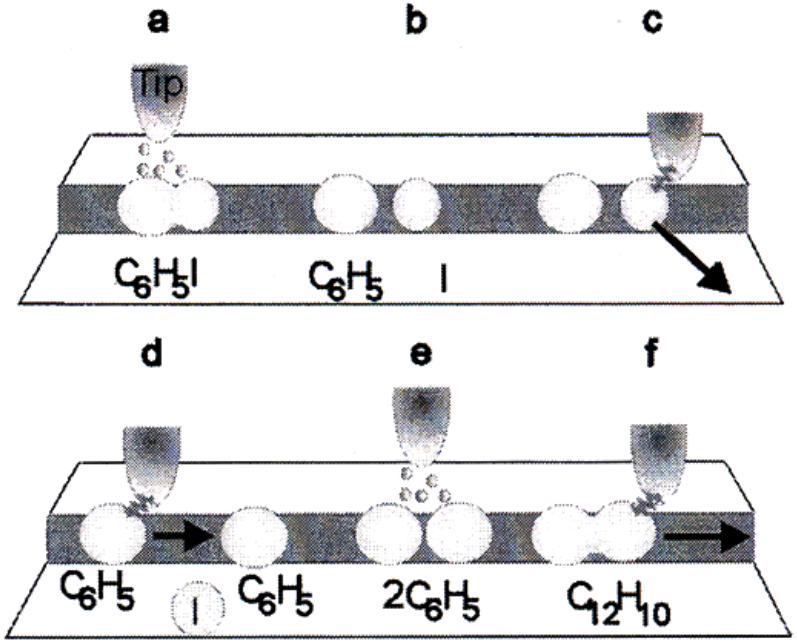

FIG. 1. Schematic illustration of the STM tip-induced synthesis steps of a biphenyl molecule. (a),(b) Electron-induced selective abstraction of iodine from iodobenzene. (c) Removal of the iodine atom to a terrace site by lateral manipulation. (d) Bringing together two phenyls by lateral manipulation. (e) Electron-induced chemical association of the phenyl couple to biphenyl. (f) Pulling the synthesized molecule by its front end with the STM tip to confirm the association.

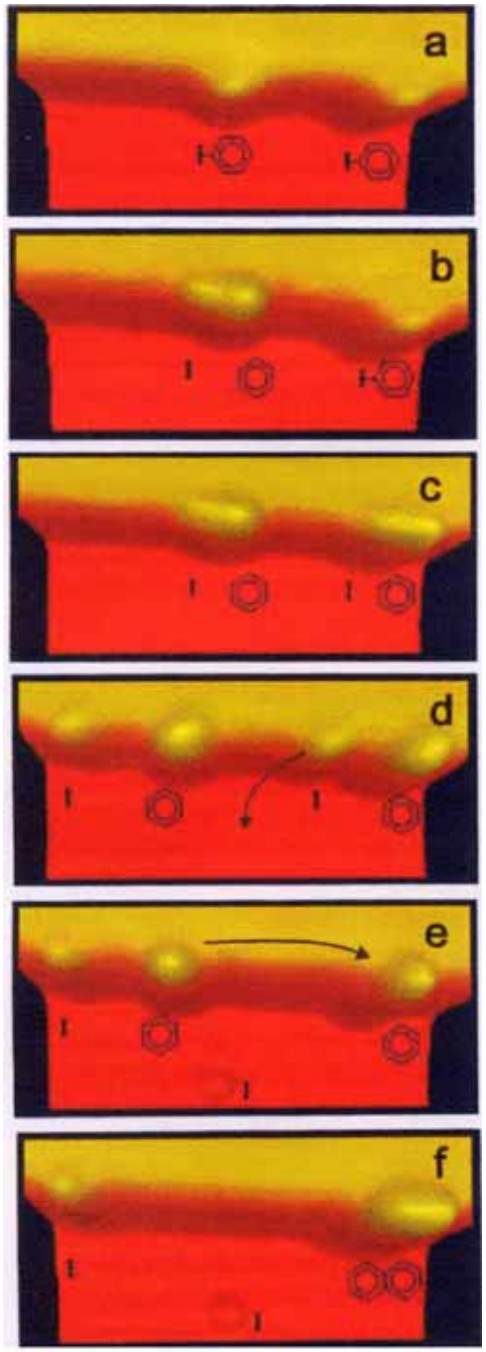

Phys. Rev. Lett. 85, 2777 (2000)

Site Hopping of O_2 on Si(111)-7x7

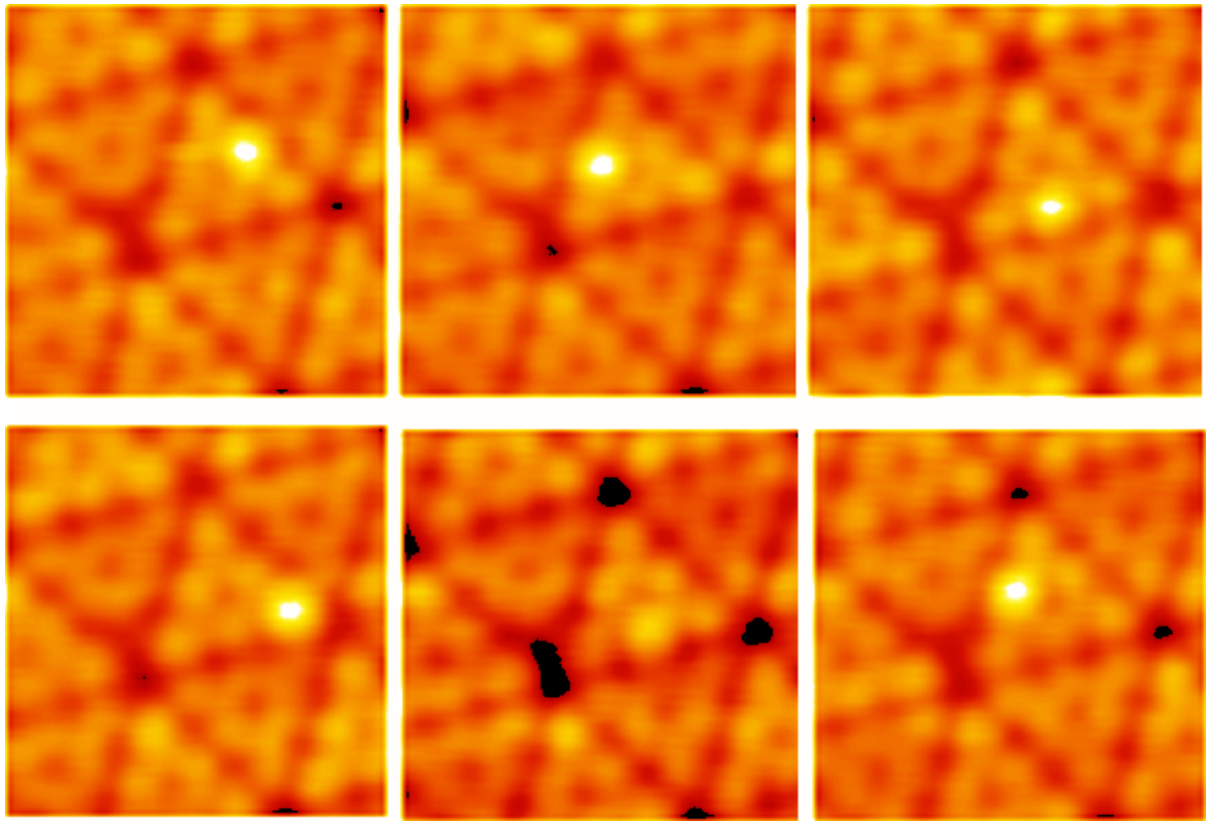

O_2 molecule starts to hop between neighboring adatom sites at temperature about 300ºC.

1. I.-S. Hwang, R.-L. Lo, and T.T. Tsong, Physical Review Letters **78**, 4797 (1997).
2. I.-S. Hwang, R.-L. Lo, and T.T. Tsong, Surface Science **399**, 173 (1998).

Arrhenius Plot for the Hopping from a Center Site to an Adjacent Center Site

Jumping rate

$R = N/t = R_o \exp(-E_a/k_B T)$

Arrhenius relation

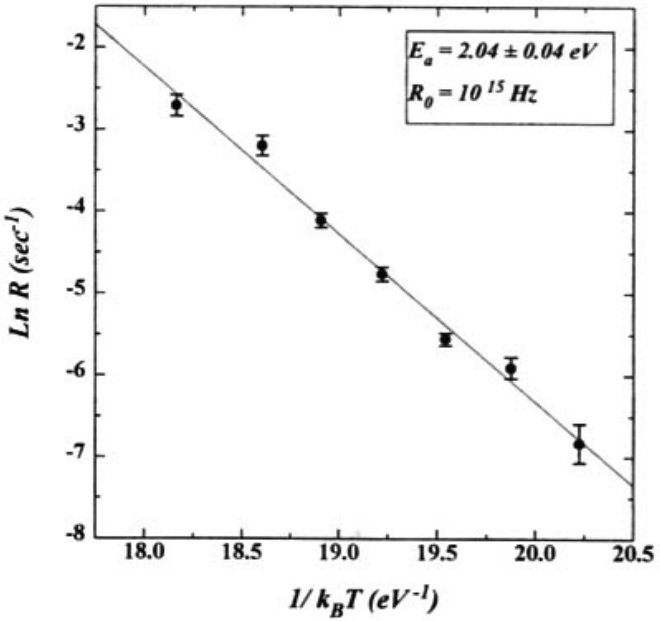

TABLE I. Parameters for site hopping of O_2 on Si(111)-(7 × 7).

Hopping	Activation energy	Frequency factors
FE to FE	2.04 ± 0.04 eV	$10^{15.0}$ s^{-1}
FE to FO	2.29 ± 0.06 eV	$10^{16.2}$ s^{-1}
FO to FE	2.13 ± 0.11 eV	$10^{15.6}$ s^{-1}
UE to UE	2.16 ± 0.04 eV	$10^{15.9}$ s^{-1}
UE to UO	2.01 ± 0.10 eV	$10^{14.6}$ s^{-1}
UO to UE	1.96 ± 0.13 eV	$10^{14.1}$ s^{-1}

Continuous-Time Scanning

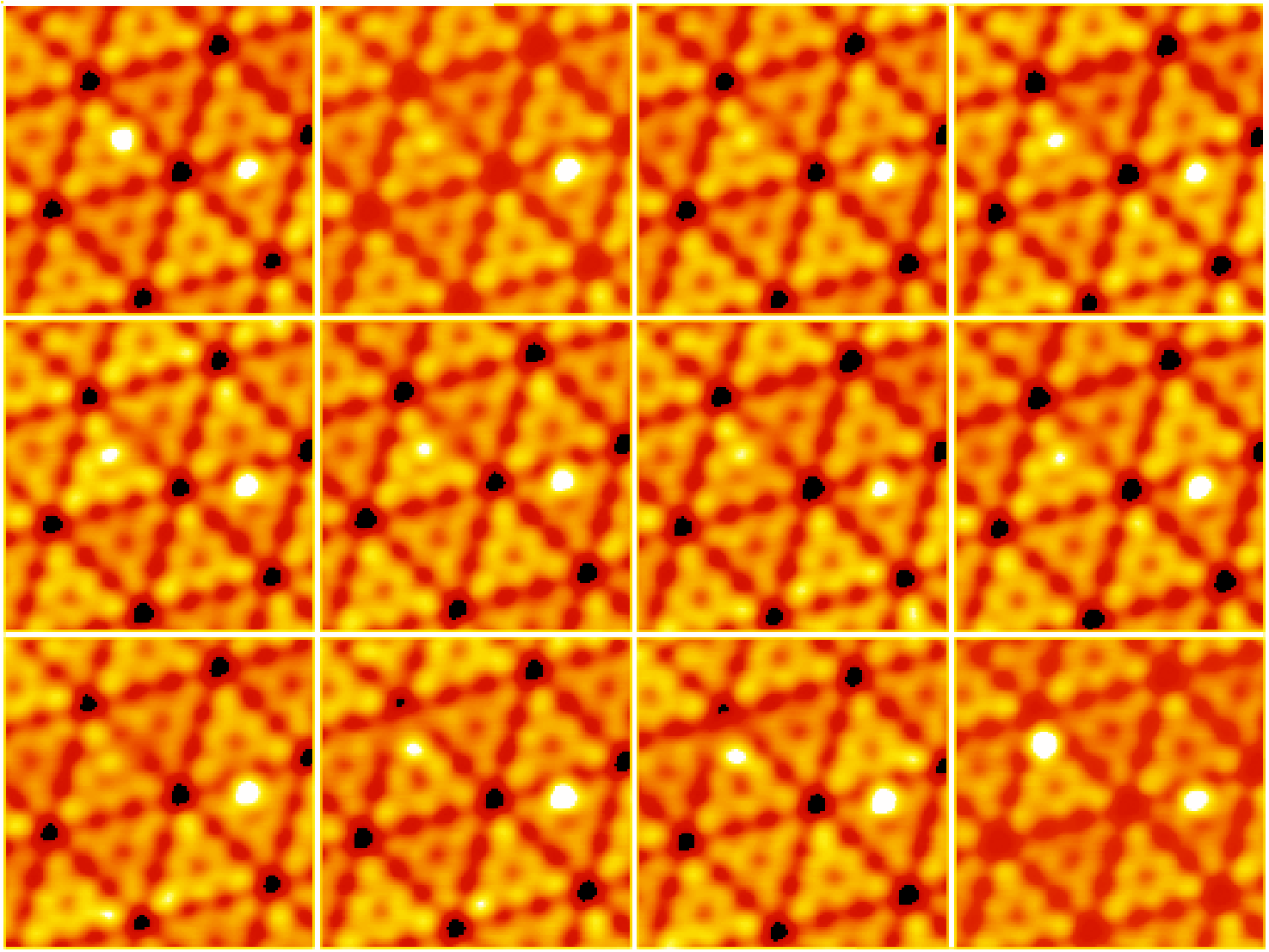

300 C, 1V(filled-state), 0.2 nA, 2.4 sec per image

Site Hopping of O_2 Molecule on Si(111)-(7x7)

STM images

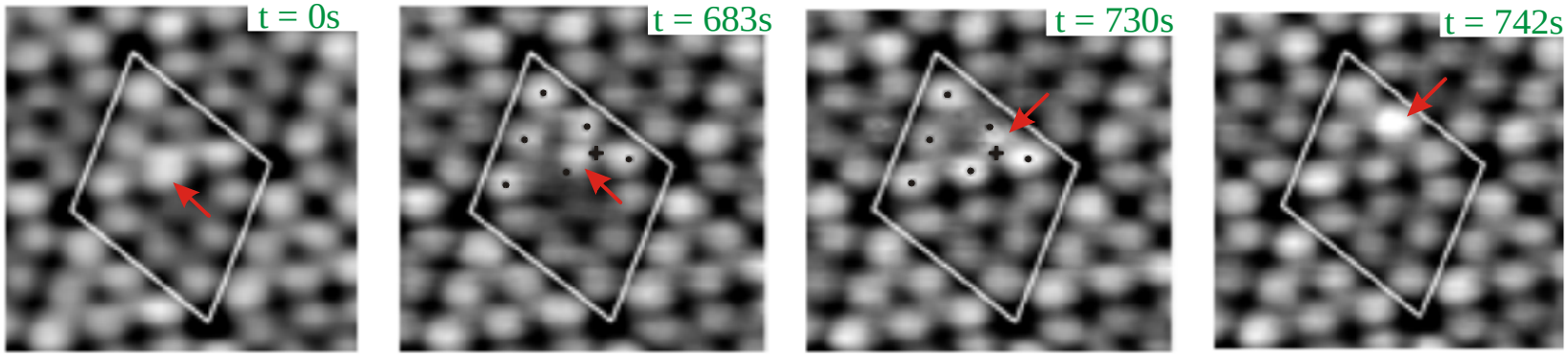

B_i I^*_i I^*_f B_f

Atomic model

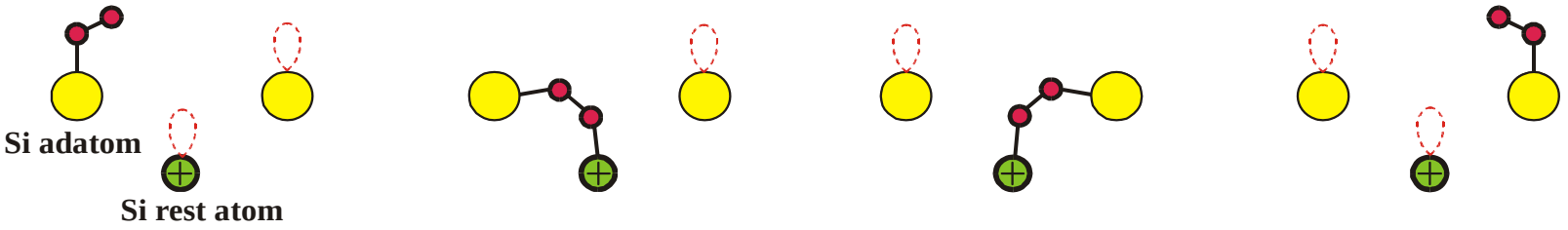

Potential diagram

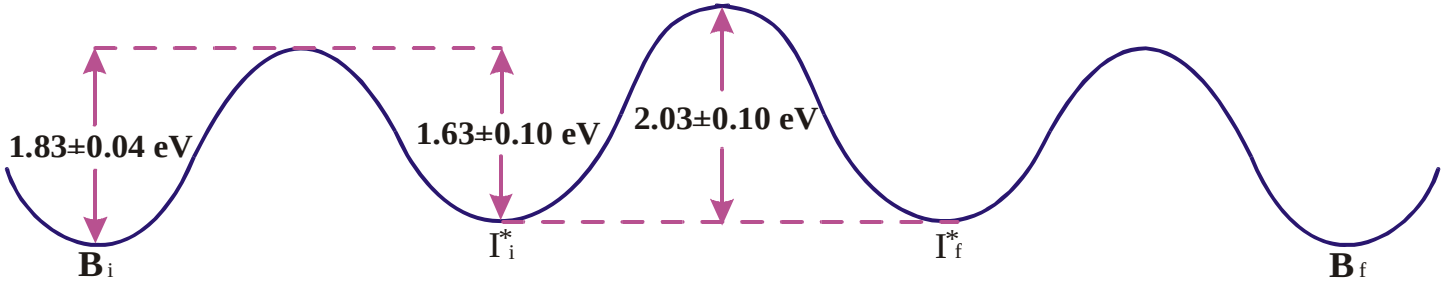

I.-S. Hwang, et al., Phys. Rev. Lett. **78**, 4797 (1997)

Silicon Magic Clusters on Si(111) Surfaces

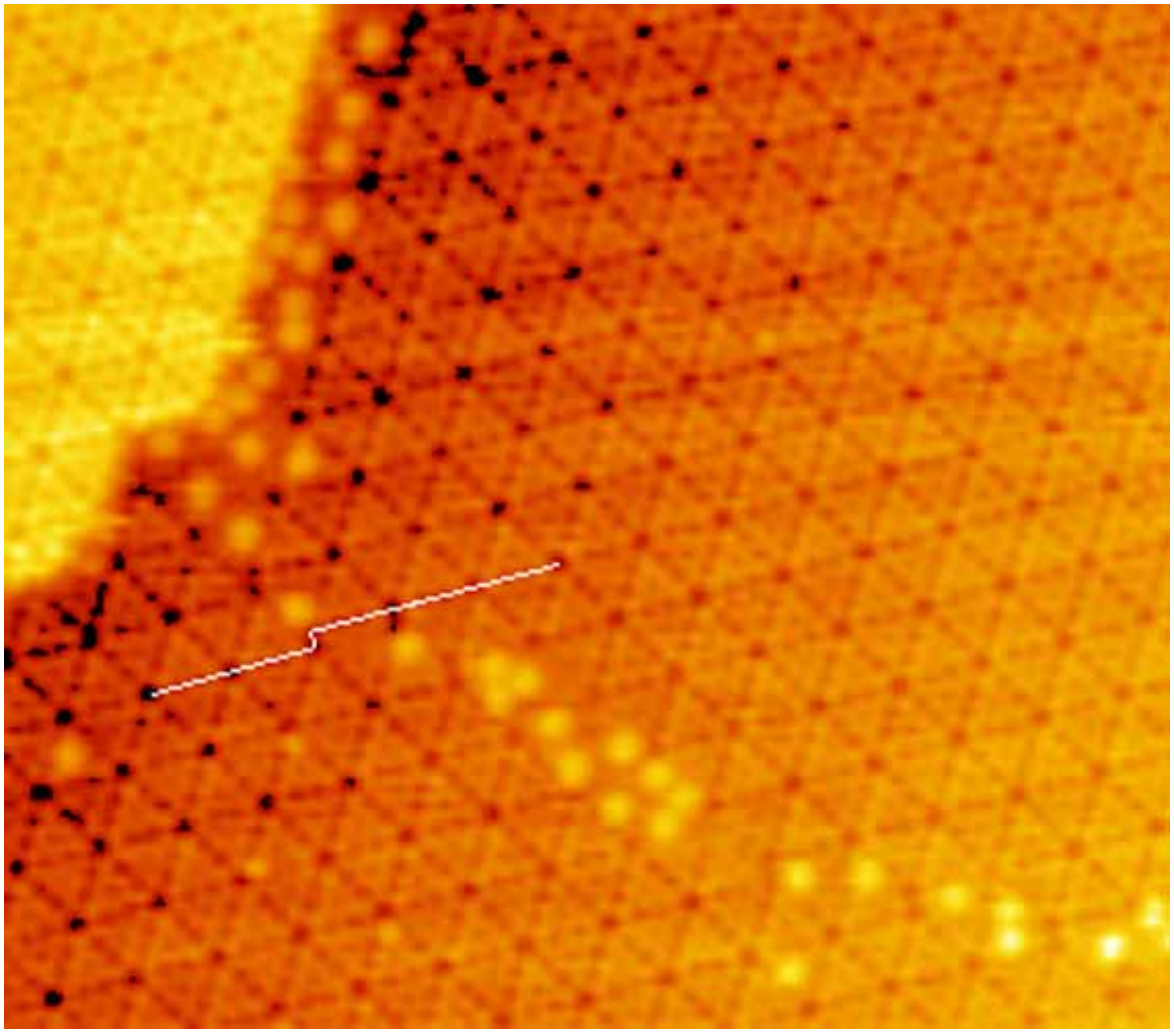

480℃

Sample bias of –1.5V

1. I. -S. Hwang, M. -S. Ho, and T. T. Tsong, Phys. Rev. Lett. **83**, 120 (1999).
2. M. -S. Ho, I. -S. Hwang, and T. T. Tsong, Phys. Rev. Lett. **84**, 5792 (2000).
3. I. -S. Hwang, M. -S. Ho, and T. T. Tsong, J. Phys. Chem. Solids **62**, 1655 (2001).

Si Magic Clusters on Si(111)-(7×7)

1. The concentration of Si magic clusters is very low for samples cooled down slowly to room temperature.
2. The concentration increases with temperature, ~2×10^{-7}Å^{-2} at 450℃.
3. Deposition of Si atoms can increases the concentration of magic clusters.

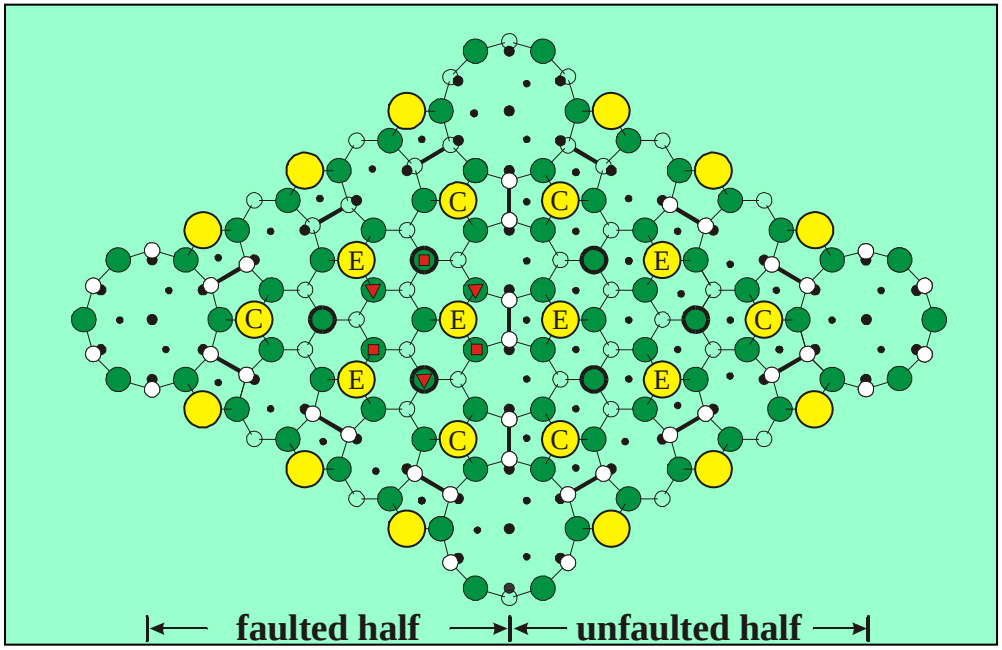

The spacing between the protrusions is ~3.8Å, which is much larger than the Si-Si bond length (2.3Å).

The magic number is estimated to be 9 to 15.

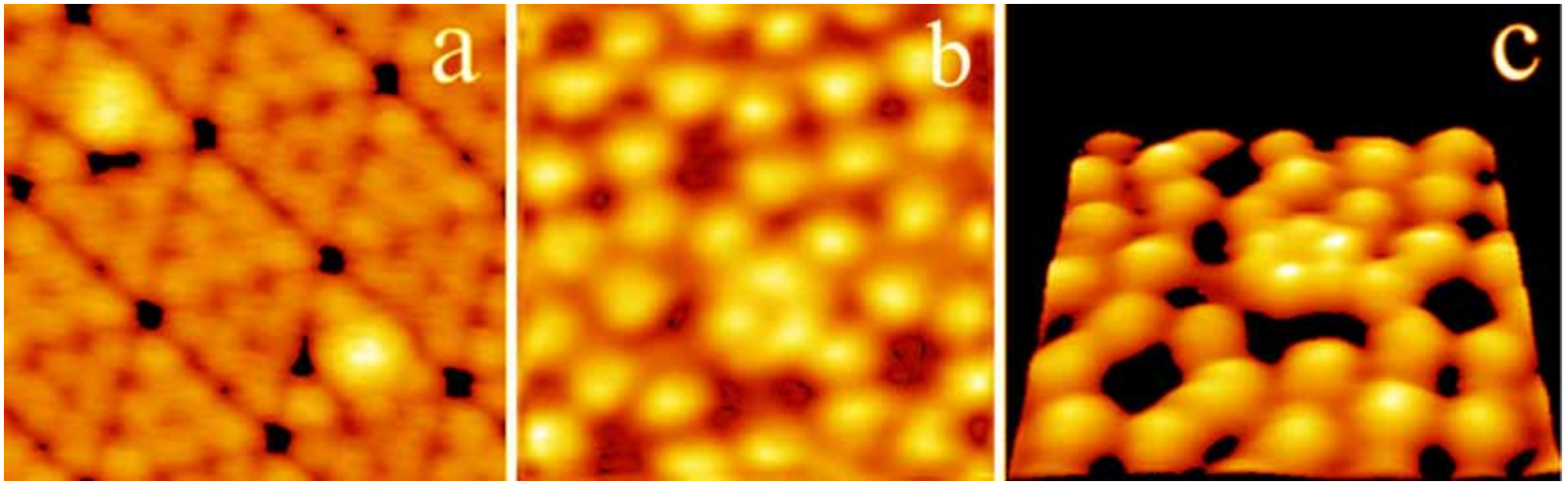

sample bias –1.5 V +1.8 V +1.2 V

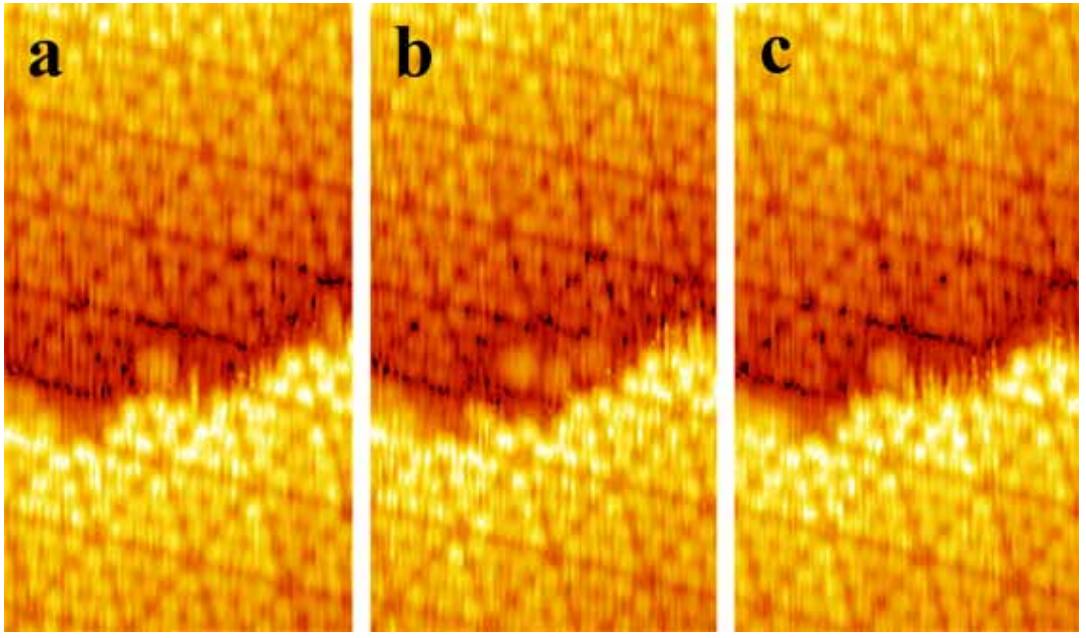

Time interval 4.6 s

Sample bias of –1.5V

450℃

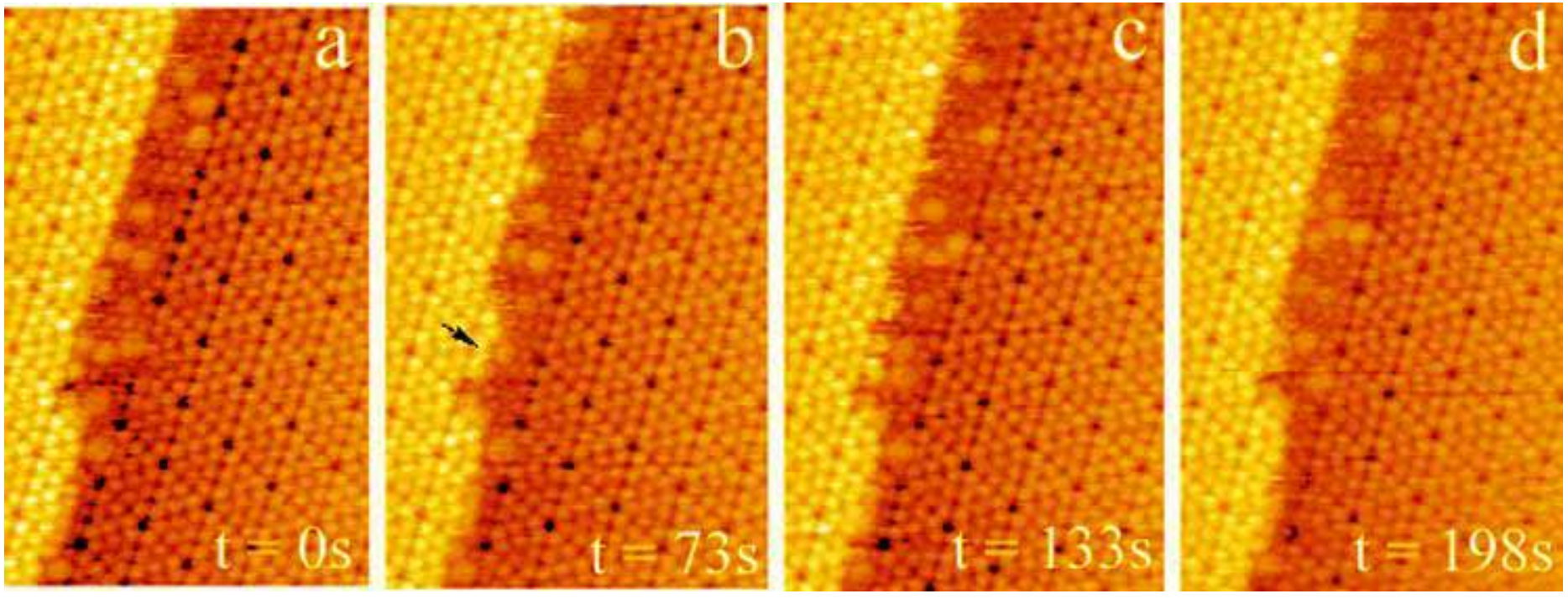

The Decay Processes of 2D Islands

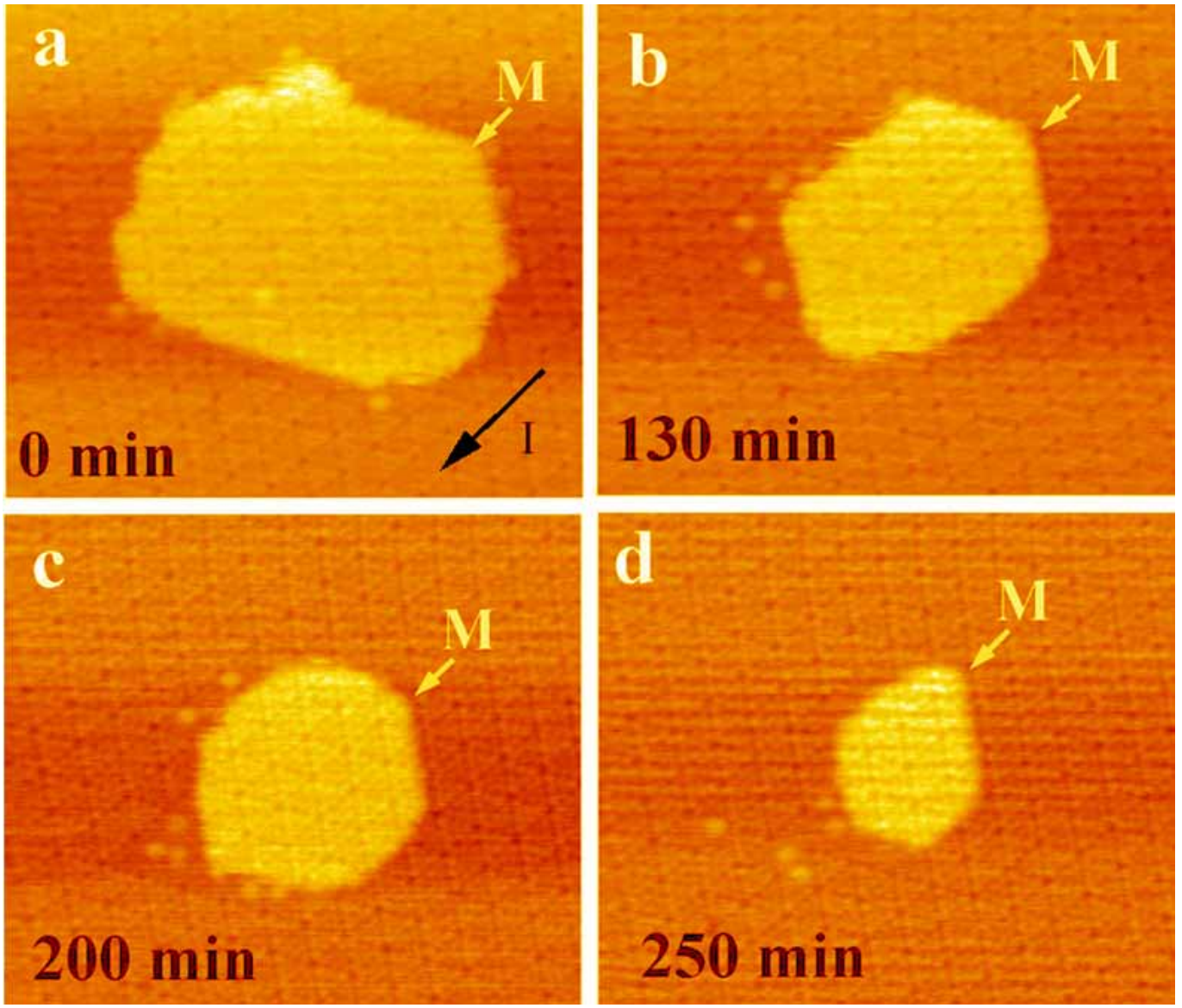

450Å ⅹ 380Å Sample bias -2V 450℃

Decomposition of a Si Island into Magic Clusters

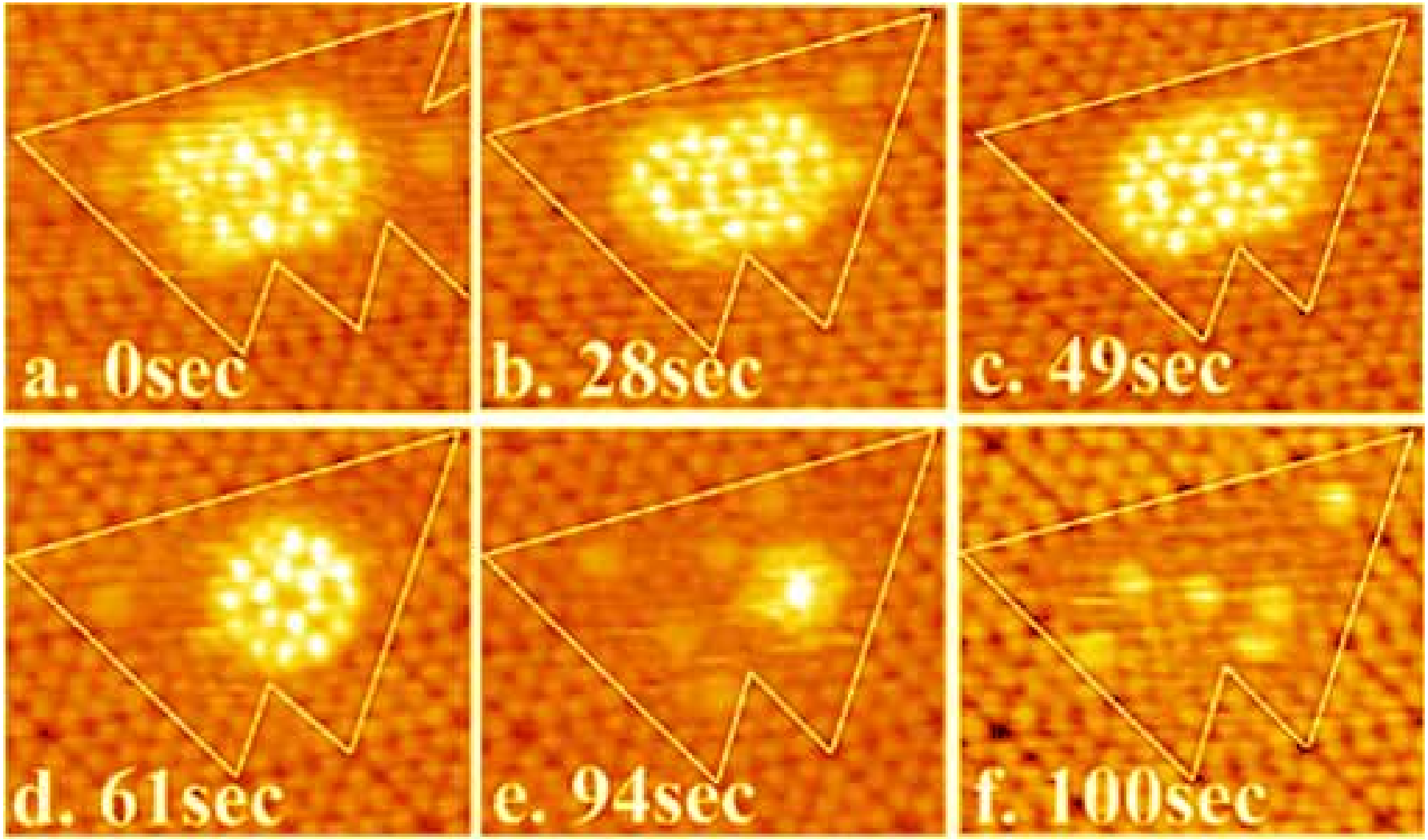

Sample bias –1.5V

460℃

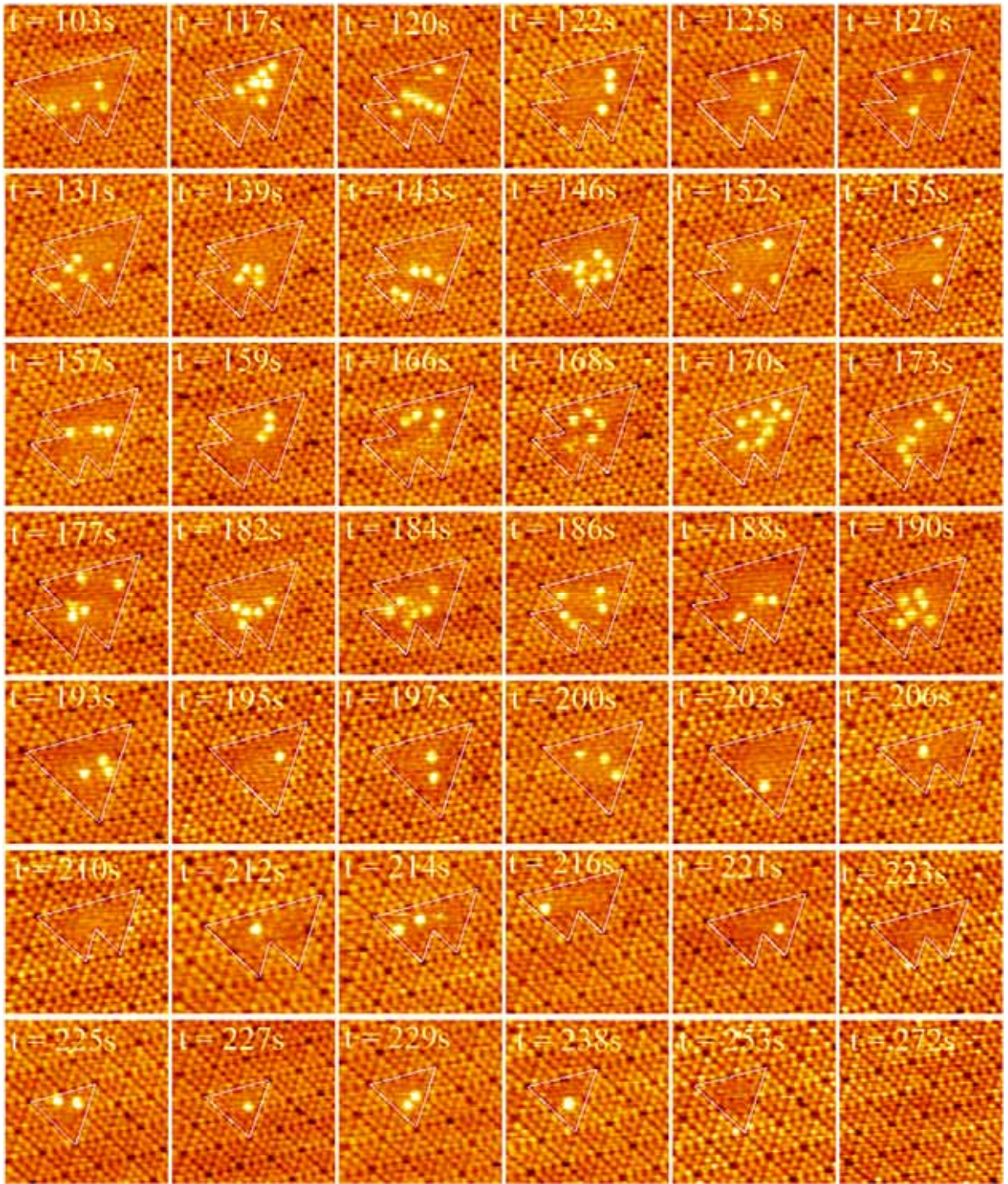
t = 103s
t = 117s
t = 120s
t = 122s
t = 125s
t = 127s
t = 131s
t = 139s
t = 143s
t = 146s
t = 152s
t = 155s
t = 157s
t = 159s
t = 166s
t = 168s
t = 170s
t = 173s
t = 177s
t = 182s
t = 184s
t = 186s
t = 188s
t = 190s
t = 193s
t = 195s
t = 197s
t = 200s
t = 202s
t = 206s
t = 210s
t = 212s
t = 214s
t = 216s
t = 221s
t = 223s
t = 225s
t = 227s
t = 229s
t = 238s
t = 253s
t = 272s

Pb islands on Pb/Si(111)

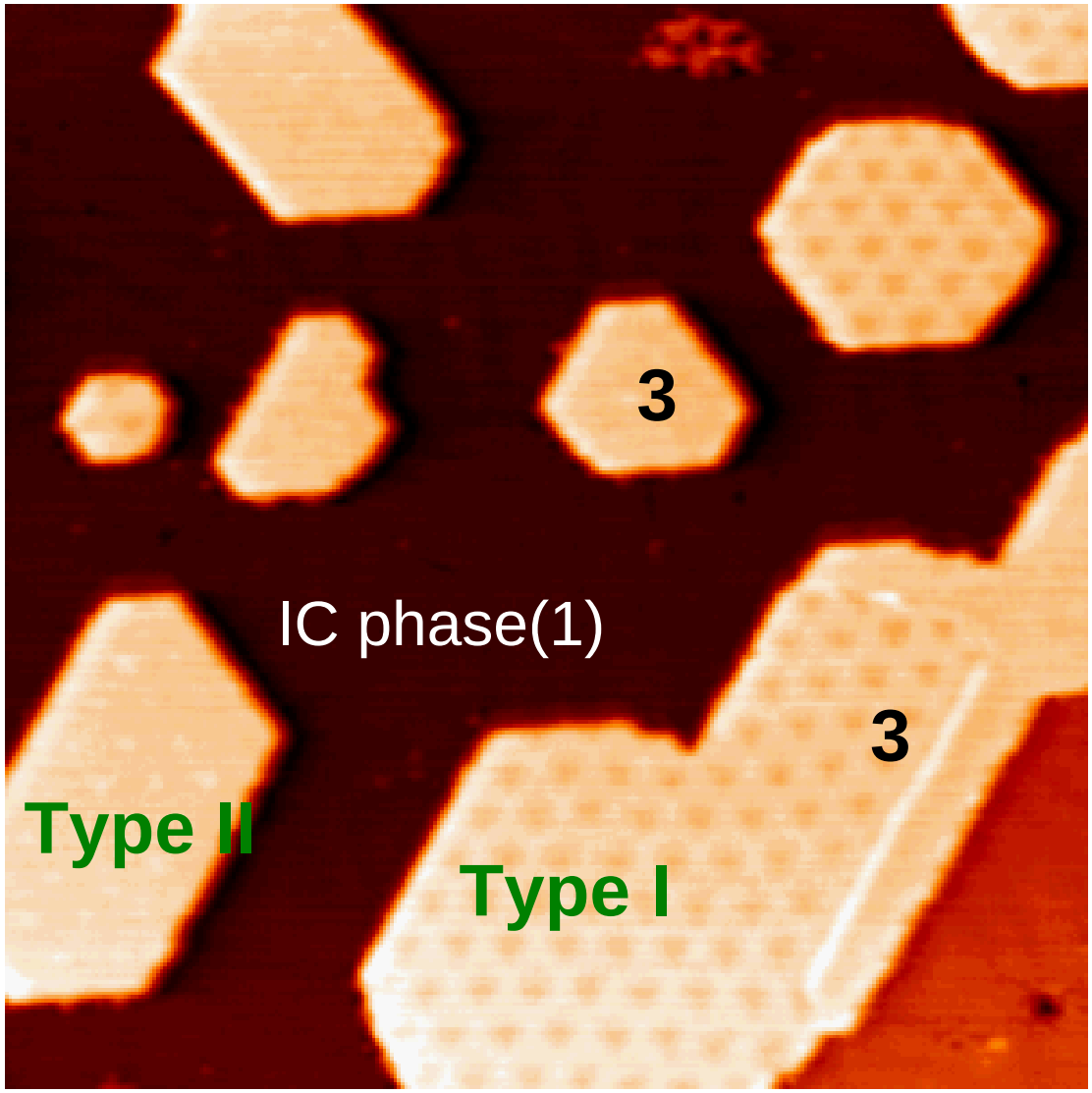

Deposit Pb on Pb/Si(111) at **T~200K**

---Single thickness

Sample bias : +2V

Ref : PRL 90 (2003) 196603

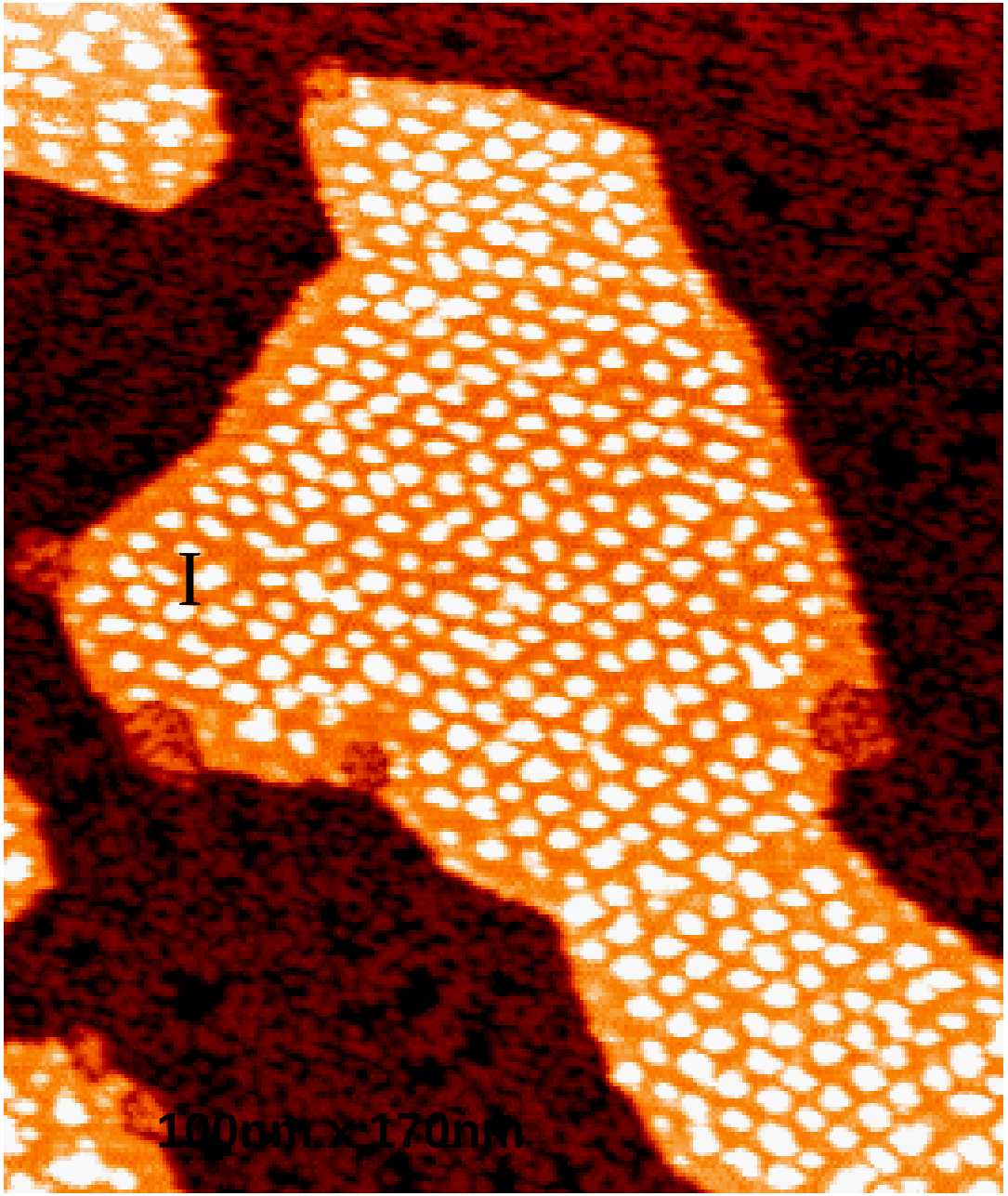

Two-dimensional

Ag cluster arrays

on quantum Pb

islands

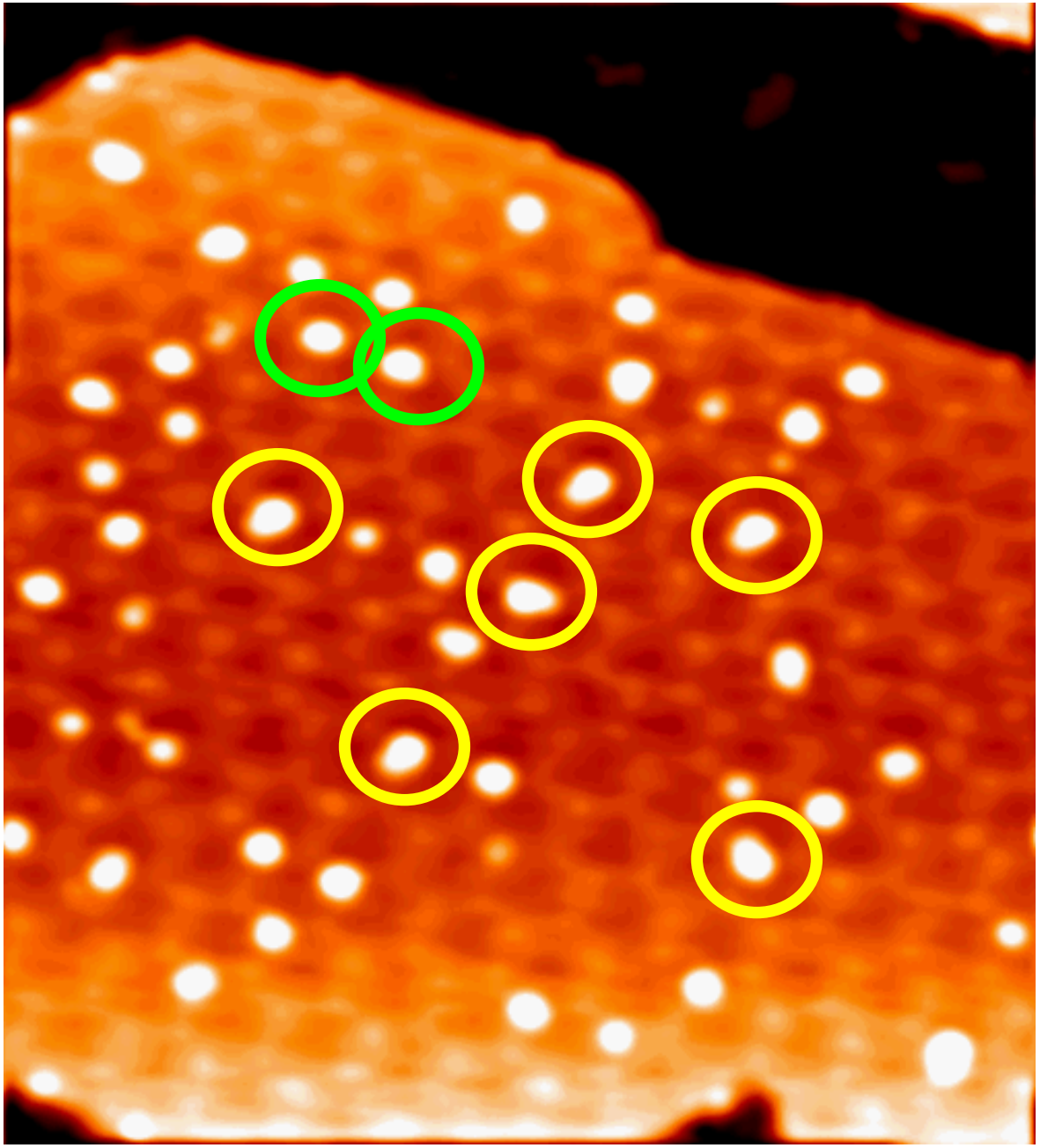

Deposit Ag
on Pb islands
at ***T~175K***

The size of the nanopucks

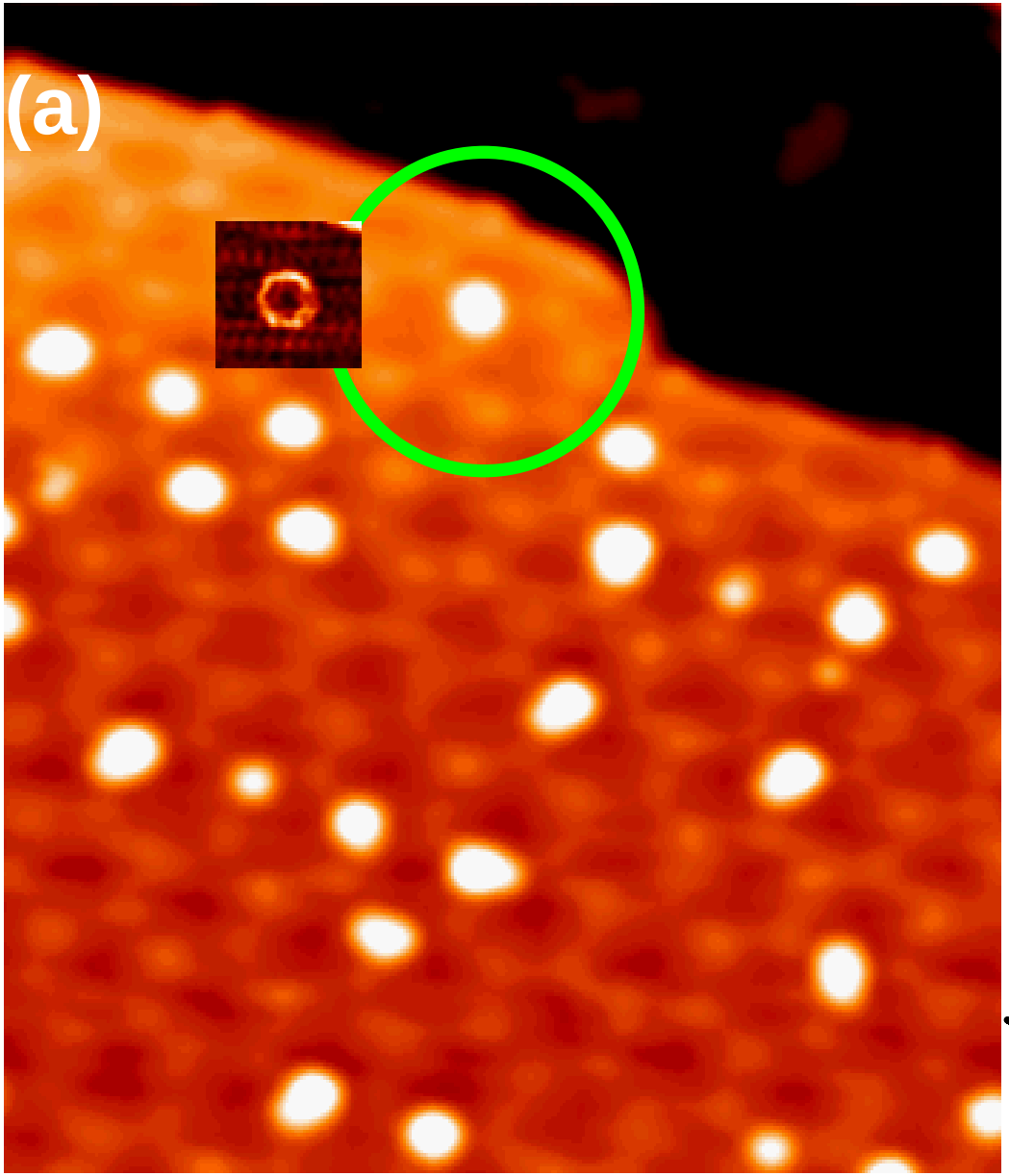

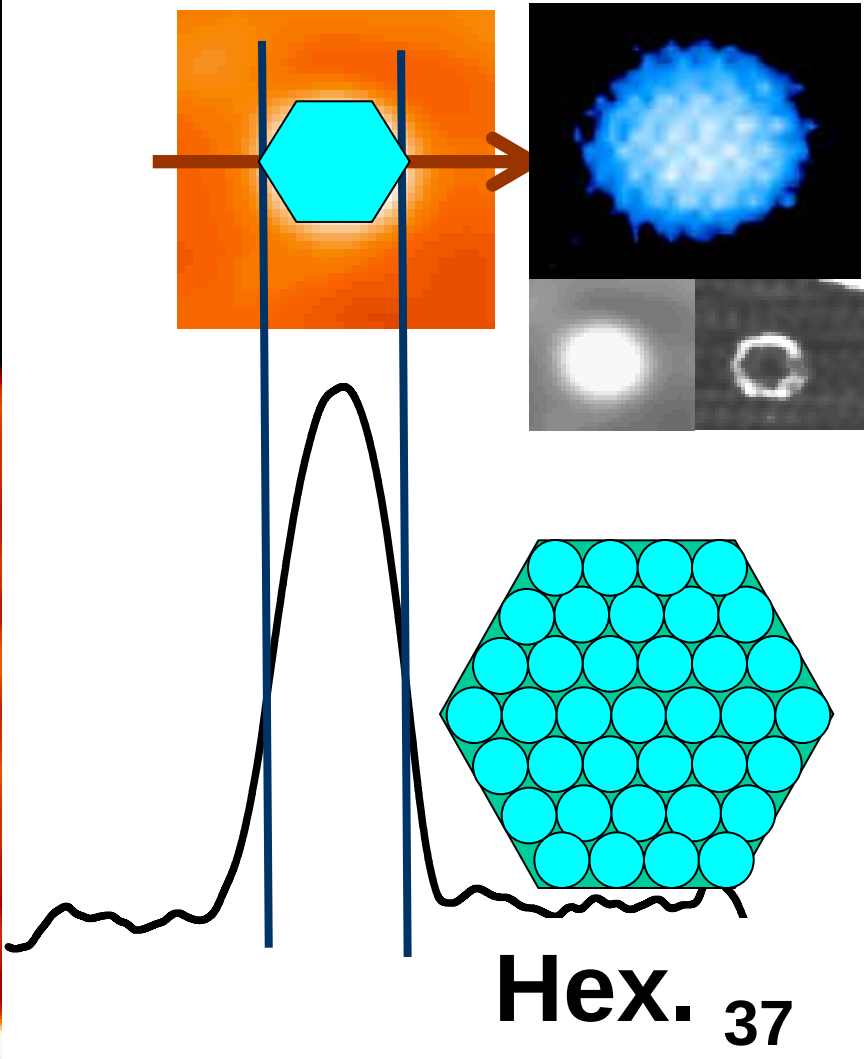

Size distribution of Ag nanopucks

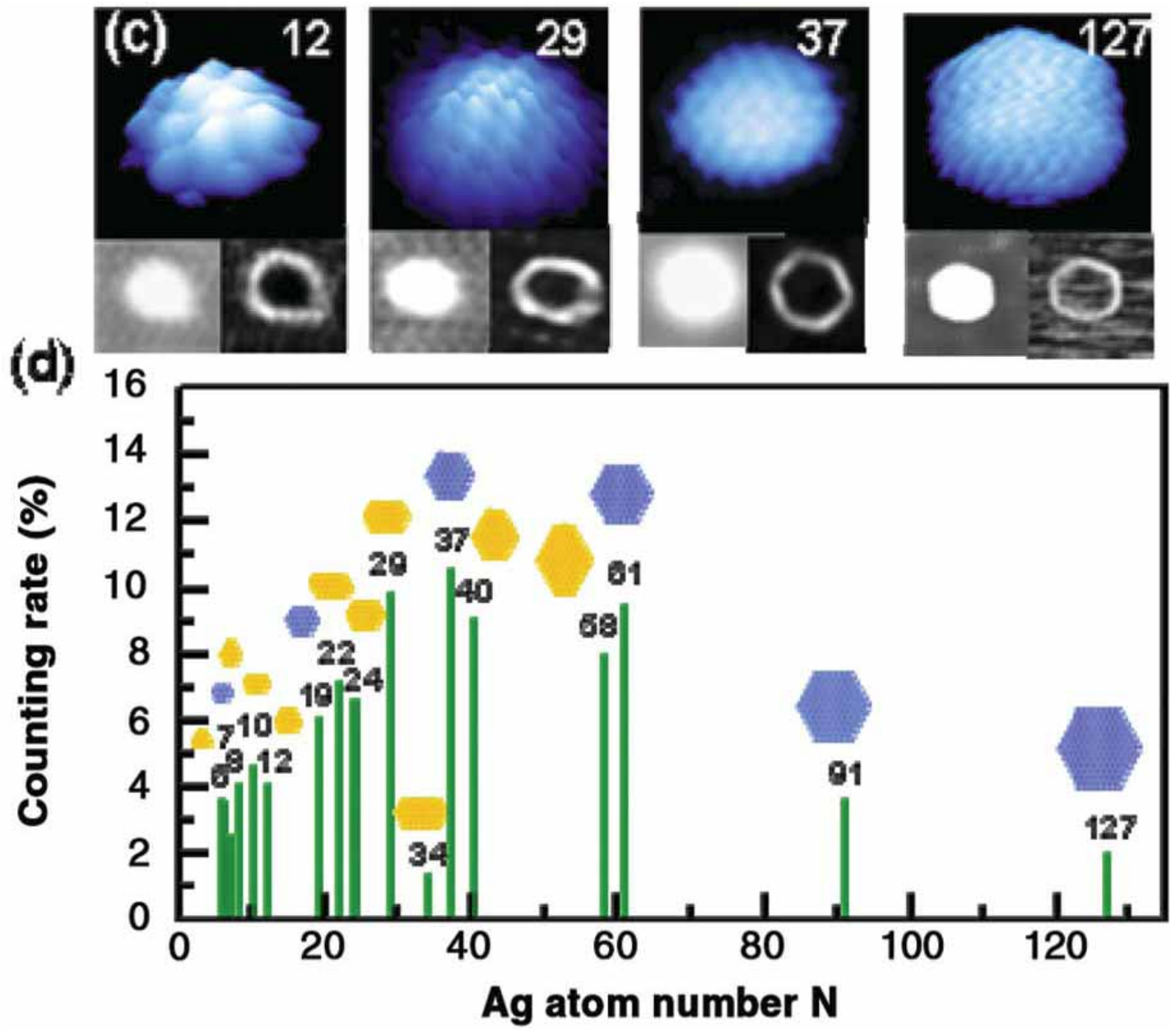

PRL **97,** 165504 (2006)

Stability of Ag nanopucks

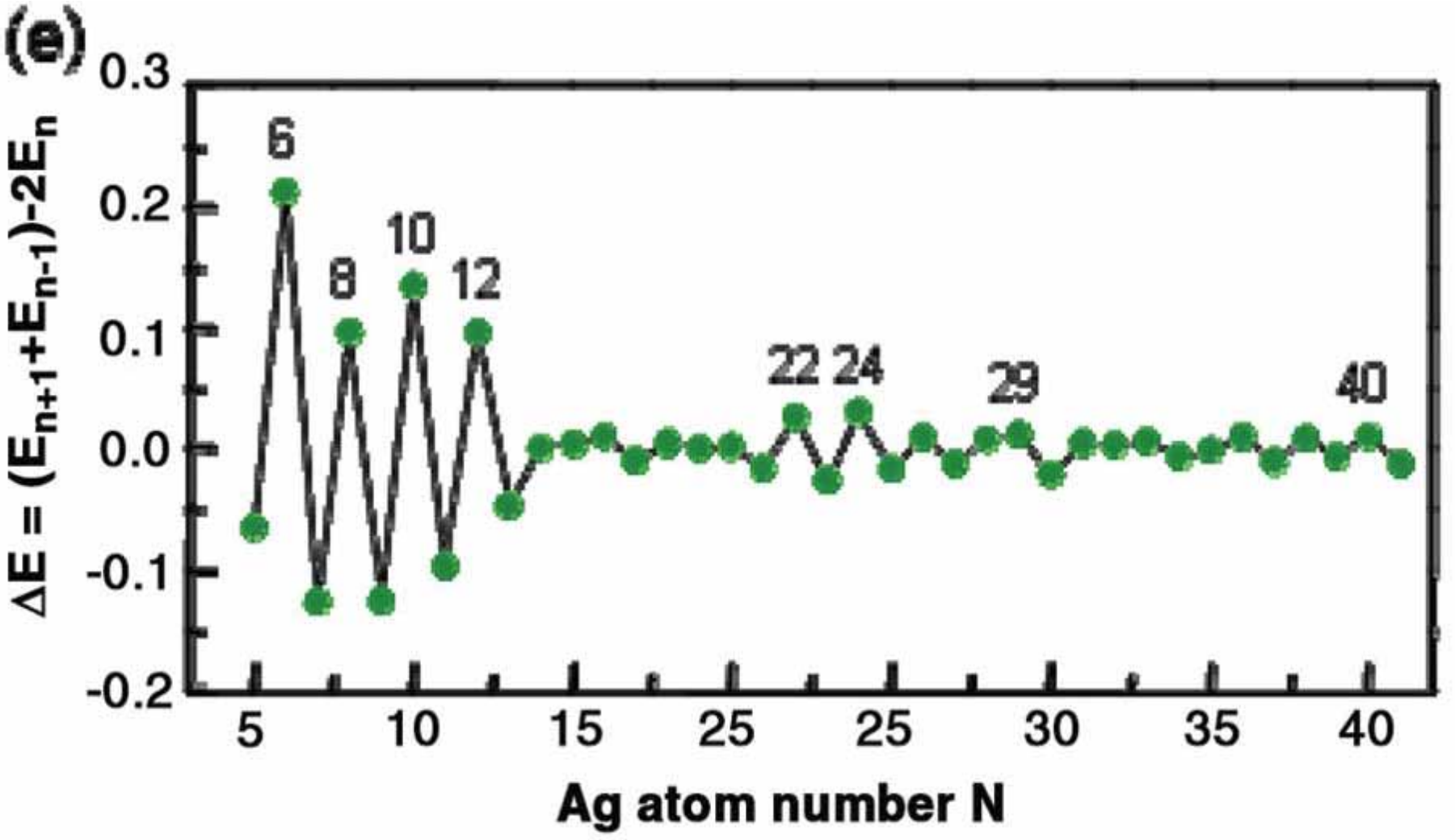

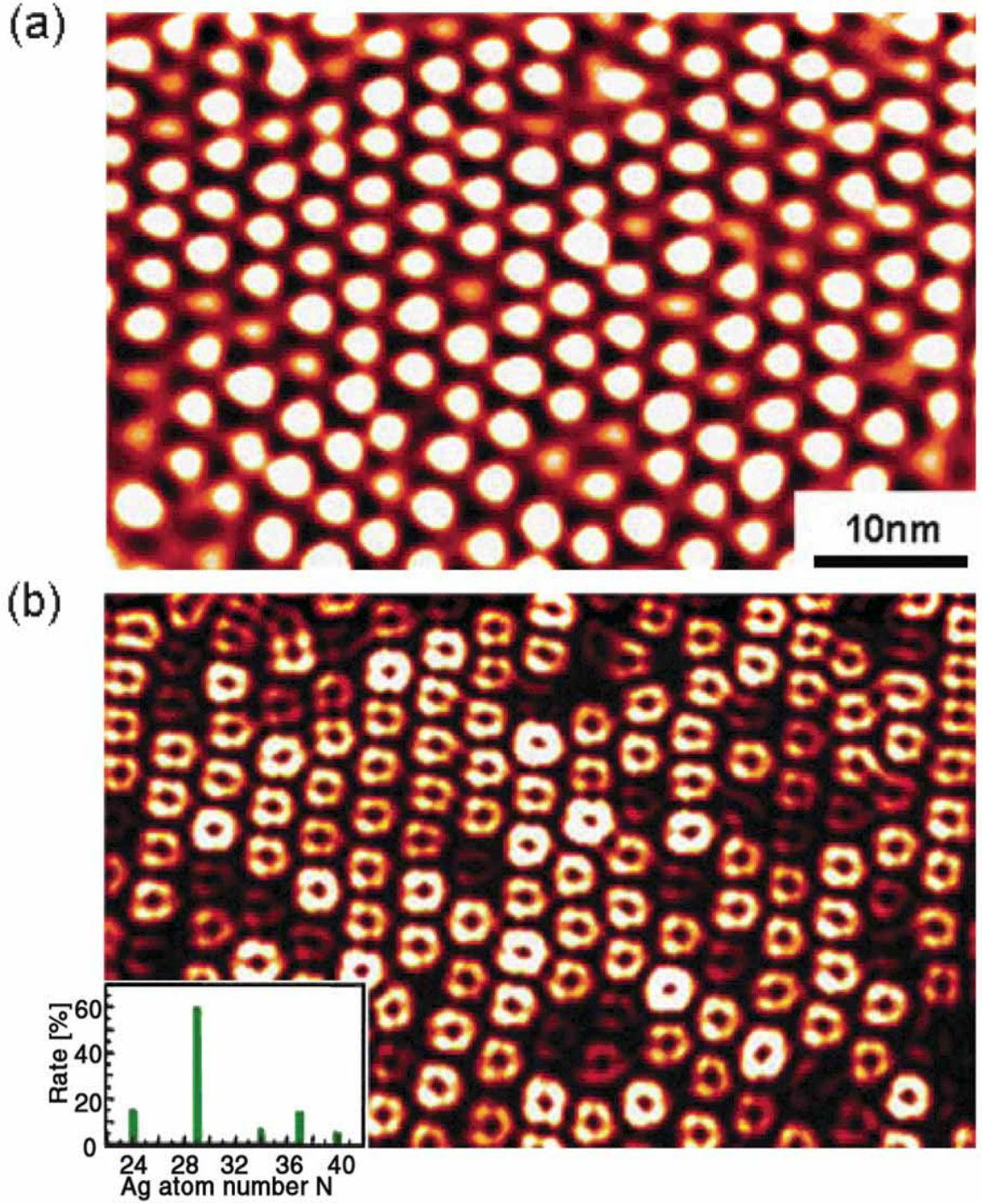
(a)
10nm
(b)
Rate [%]
60
40
20
0
24
28
32
36
40
Ag atom number N

Reversible Surface Phase Transition

Pb/Si(111) 1×1 ↔ √7 × √3

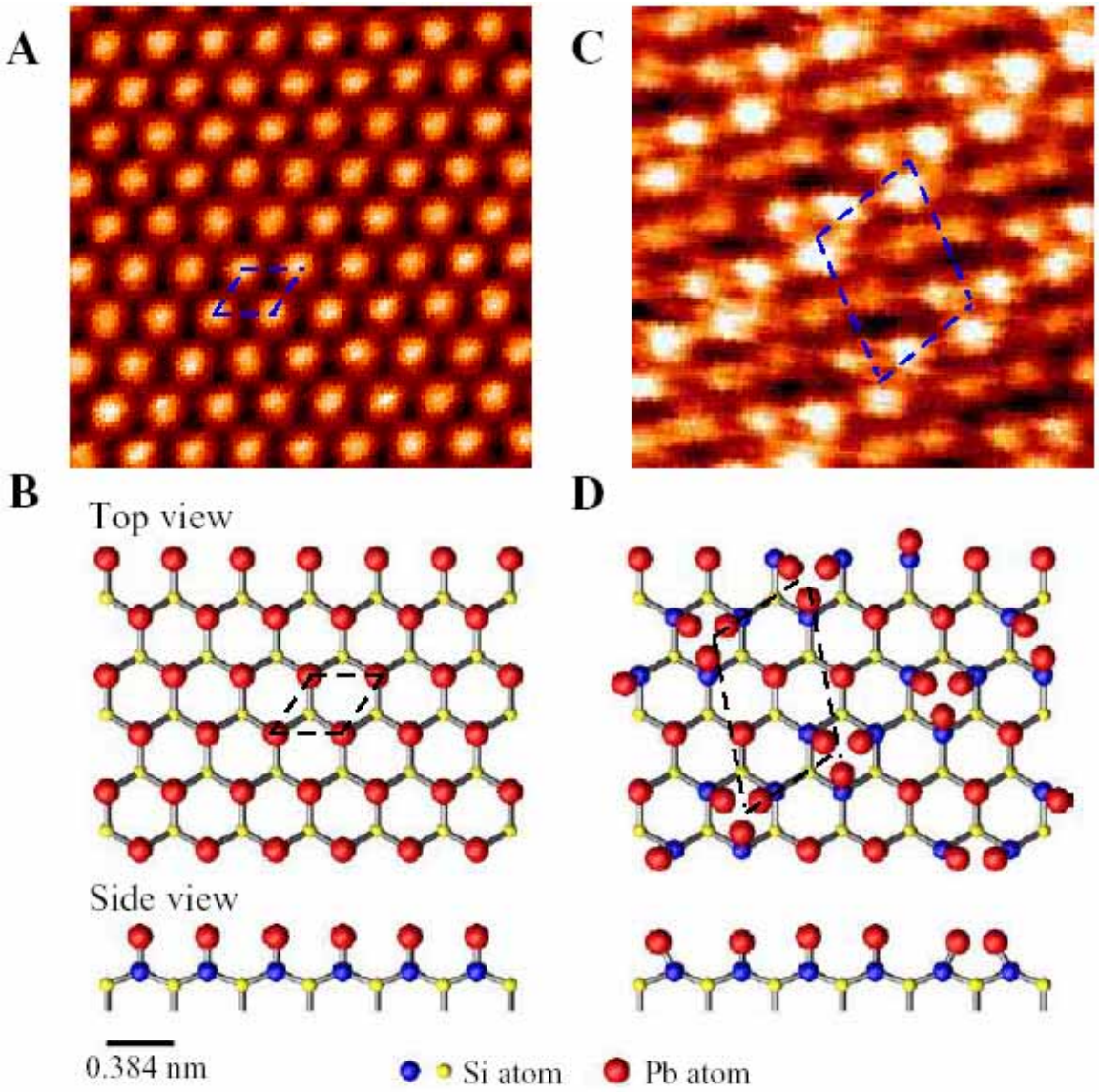

Size Effects on the Pb-Covered Si Islands

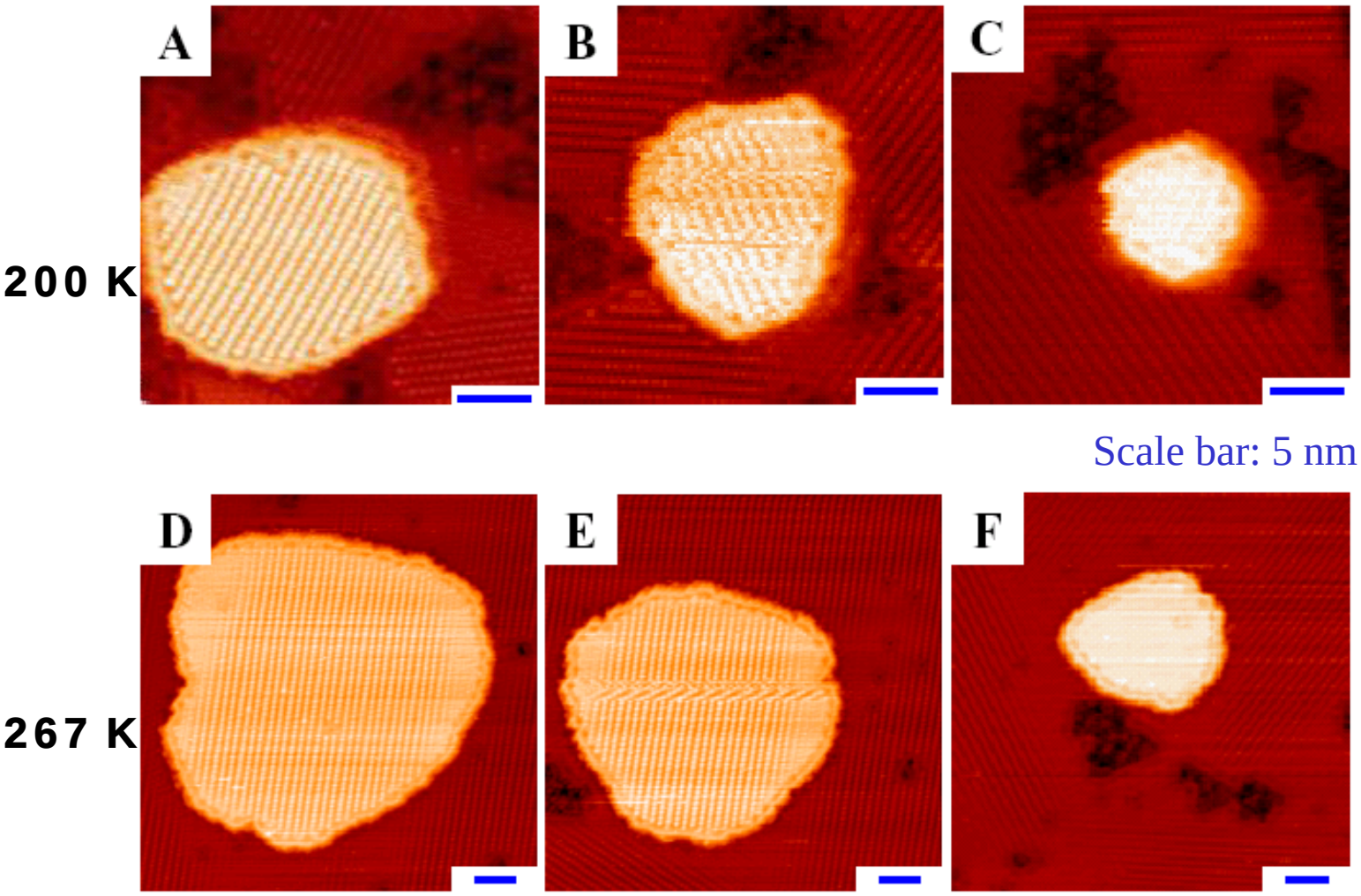

I.S. Hwang, et al., Phys. Rev. Lett. **93**, 106101 (2004)

Transition Temperature vs. Size

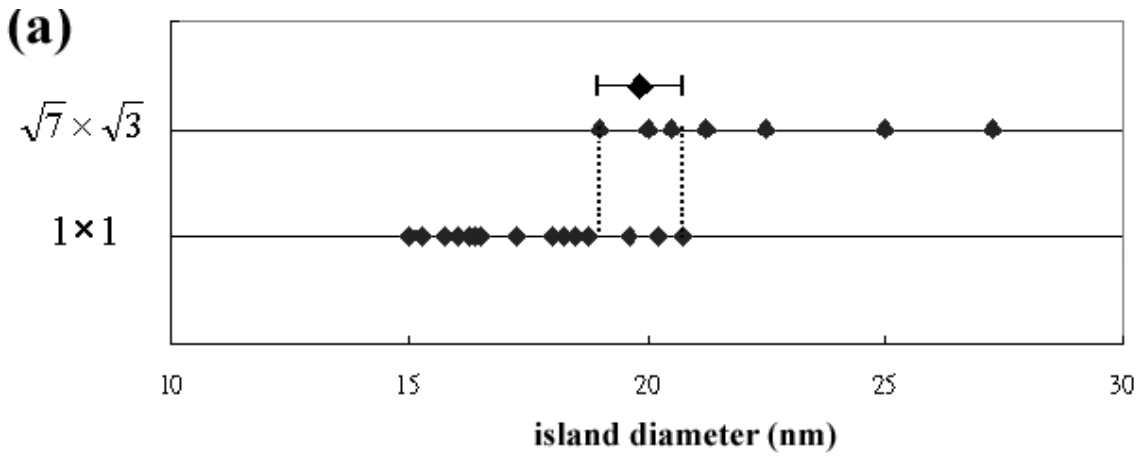

199 K

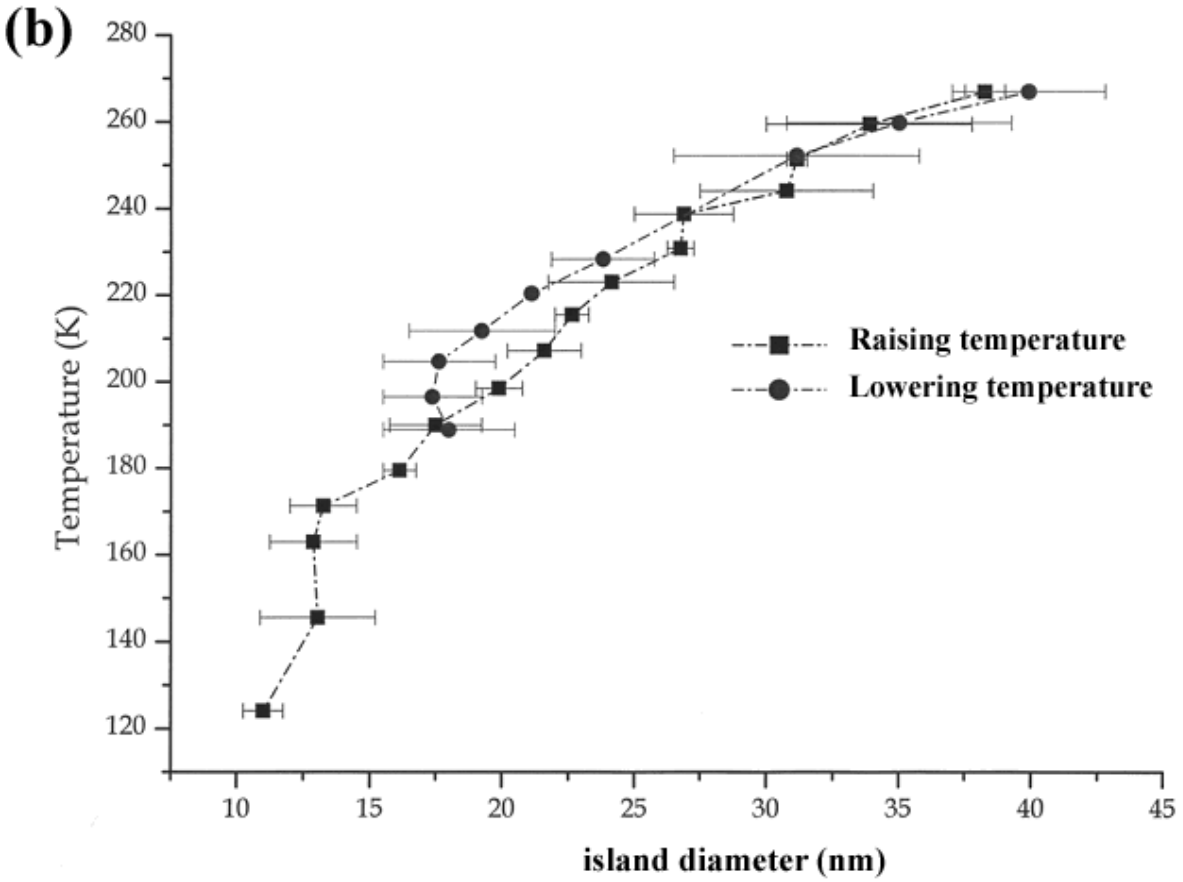

Temporal Fluctuations Near the Transition Temperature

Slow scan direction

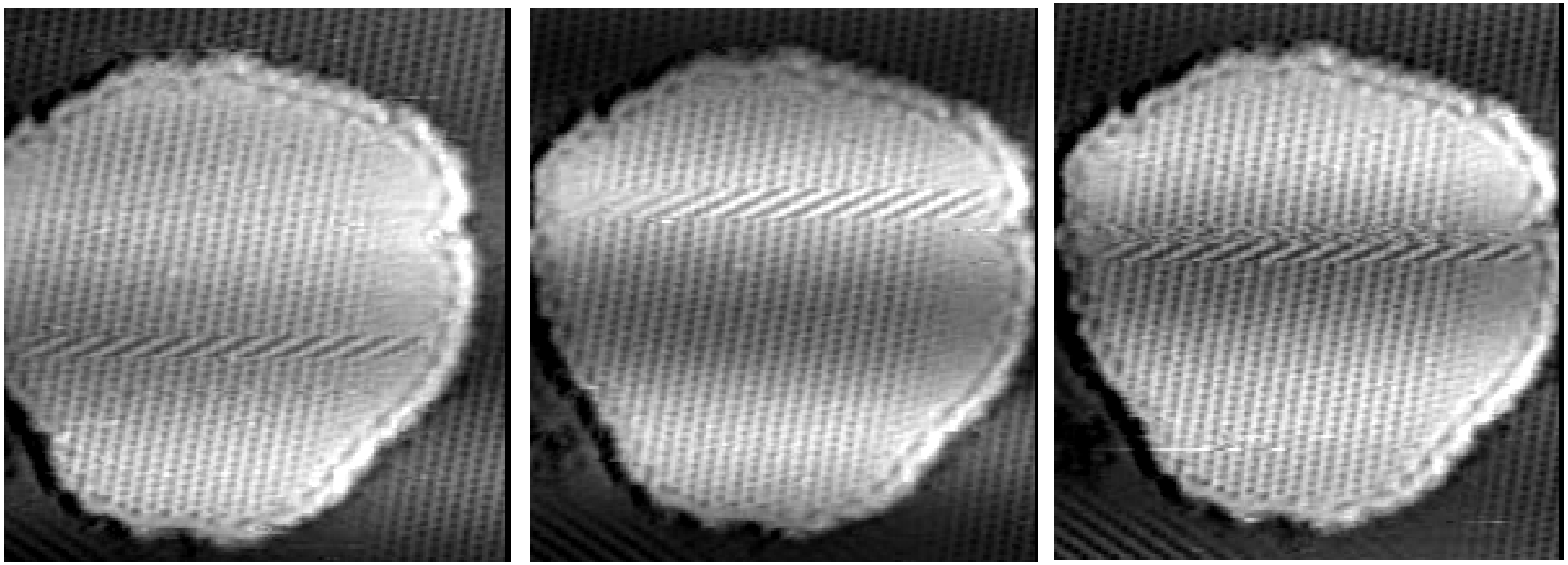

Image size: 34 nm × 38 nm

266 K

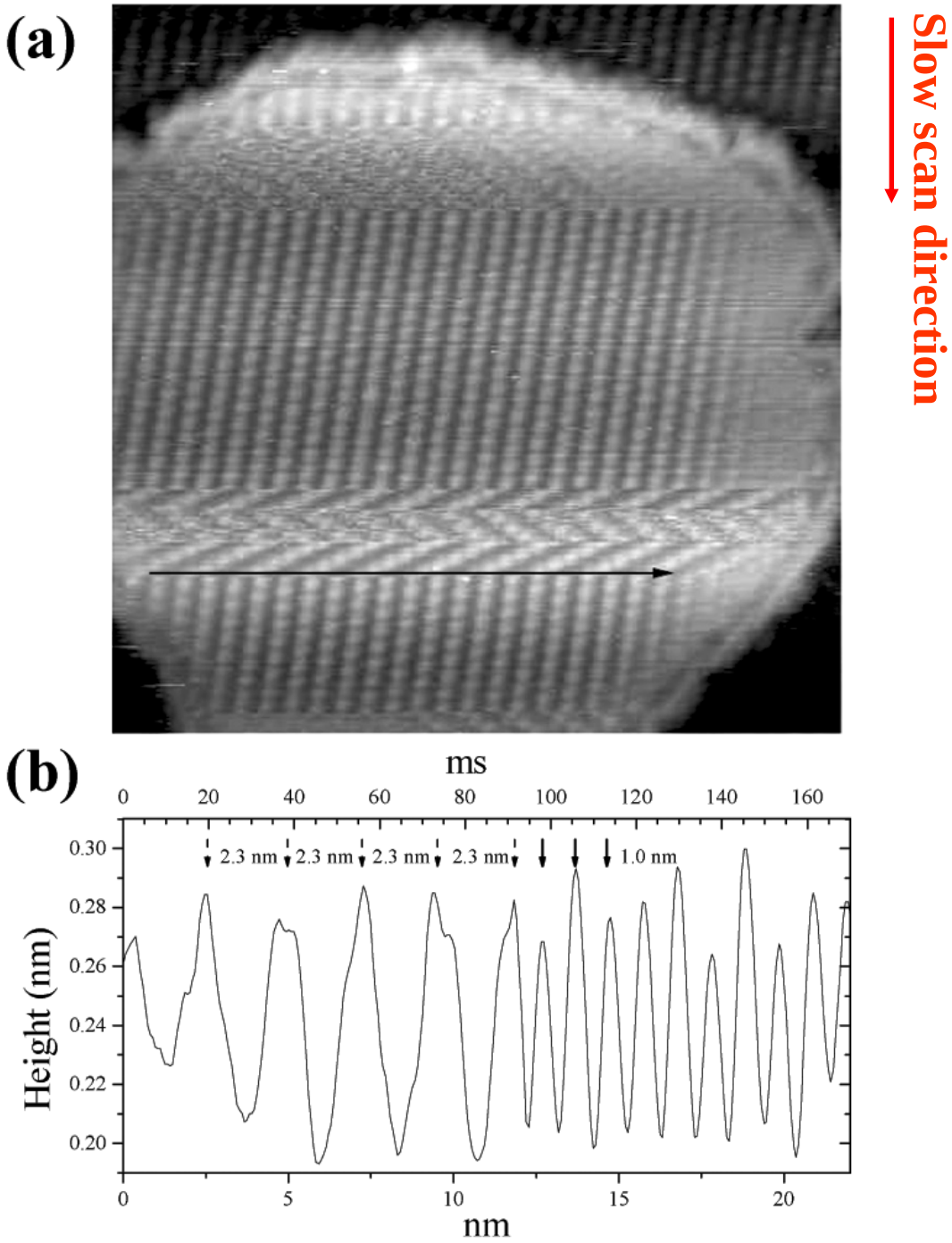
(a)
Slow scan direction
(b)
ms
0
20
40
60
80
100
120
140
160
2.3 nm
2.3 nm
2.3 nm
2.3 nm
1.0 nm
Height (nm)
0.30
0.28
0.26
0.24
0.22
0.20
0
5
10
15
20
nm

Temporal Fluctuations Near the Transition Temperature

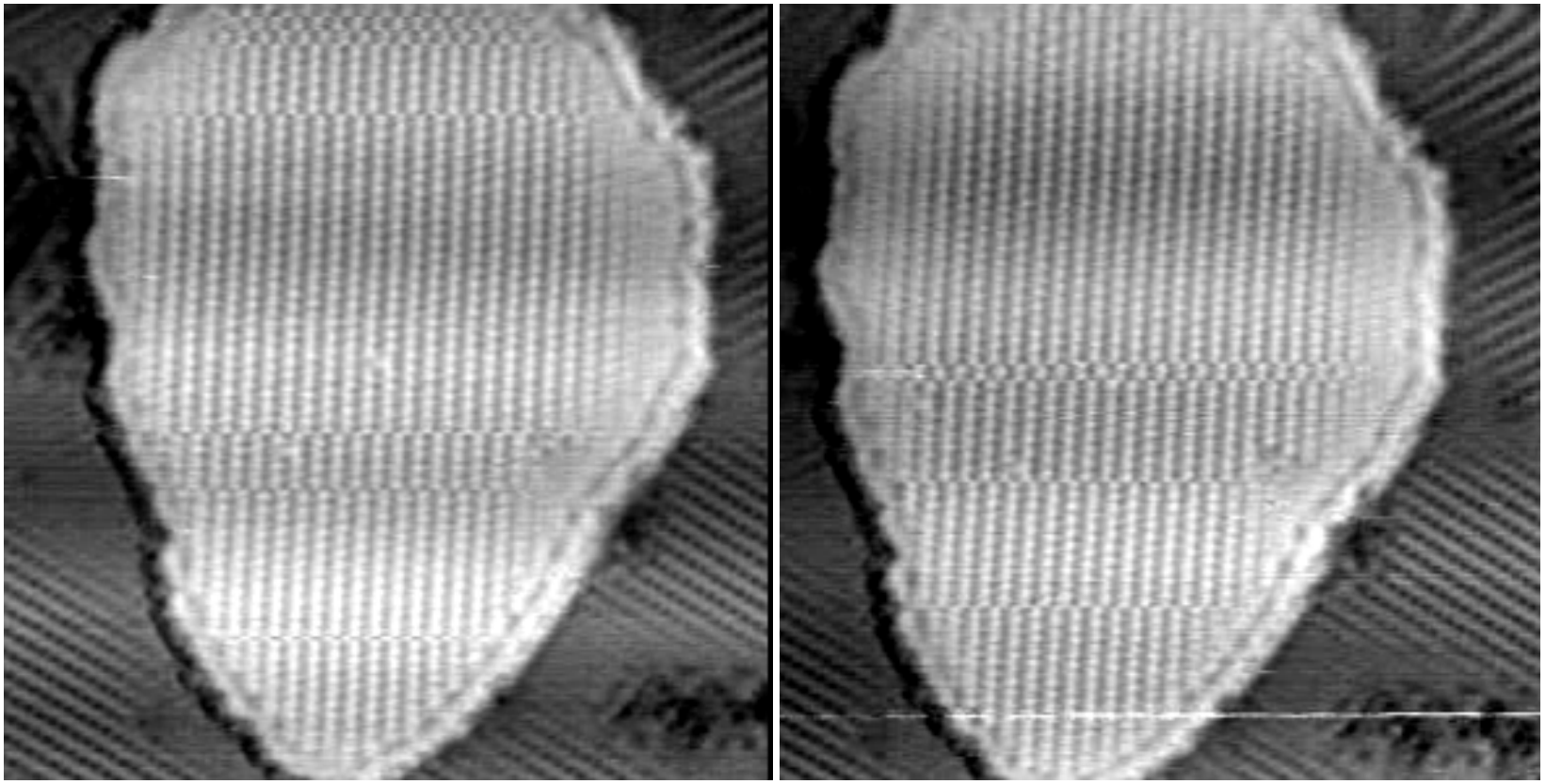

260 K

Image size: 40 nm × 40 nm

Electrochemical Scanning Tunneling Microscopy

Angew. Chem. Int. Ed. 40, 1162 (2001).

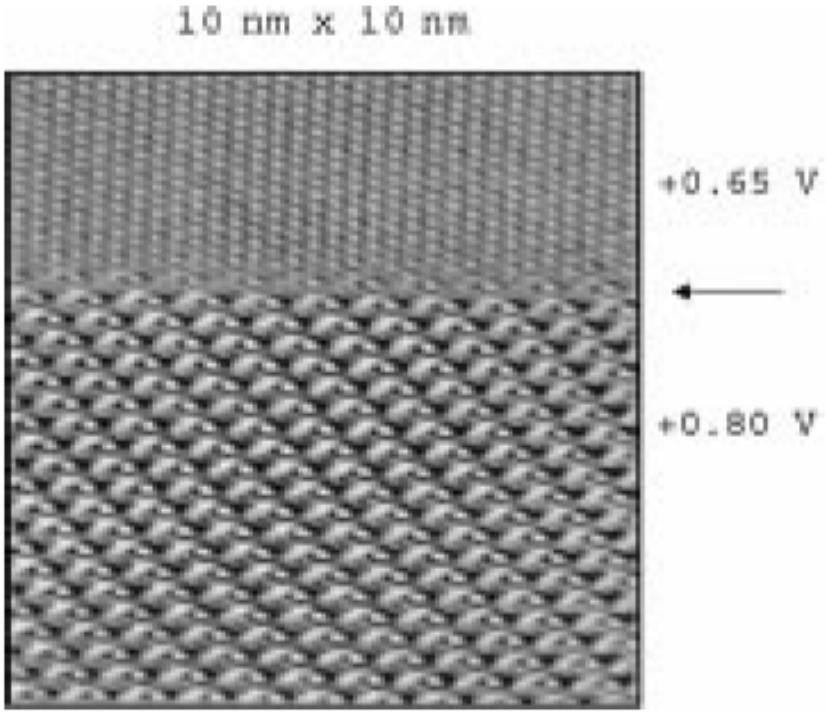

Figure 12. High-resolution STM image of Au(111) in 0.1M H_2SO_4. The upper part shows the Au(111) surface, atomically resolved, at +0.65 V versus SCE; the lower part shows the ordered adlayer of sulfate, formed by a potential step to +0.80 V versus SCE.